Synthesis of Polydentate Ligands and the Formation of Heterometallic and Circular Helicates

Martina Whitehead M(Sci)

Thesis submitted in partial fulfilment of the requirements for the Degree of Doctor of Philosophy

Department of Chemical and Biological Sciences

The University of Huddersfield

September 2010

Contents

List of Abbreviations 6
Acknowledgements 8
Abstract 9
1. Introduction 12
1.0 Supramolecular Chemistry 12
1.1 Origin of Supramolecular Chemistry 12
1.2 Supramolecular Interactions 13
1.2.2 Dipole-Dipole interactions 14
1.2.3 Hydrogen Bonding 14
1.2.4 p-p Stacking 15
1.3 Host-guest chemistry 15
1.3.1 Crown Ethers 16
1.4 Metallosupramolecular Chemistry 19
1.4.1 Grids 20
1.4.2 Cages 21
1.4.3 Racks 22
1.4.4 Ladders 23
1.5 Helicates 24
1.5.1 Helicate Nomenclature 25
1.5.2 Homoleptic Helicates 26
1.5.3 Heteroleptic Helicates 26
1.5.4 Unsaturated Helicates 27
1.5.5 Directional Helicates 28
1.5.6 Heteronuclear Helicates 29
1.5.7 Enantioselective and Diastereoselective Helicates 30
1.5.8 Meso Helicates 34
1.6 Ligand Recognition 34
1.6.1 Ligand Programming 36
1.7 Allosteric Interactions 39
1.7.1 Ditopic Ligands 43
1.8 Circular Helicates 44
2. Metal Ion Recognition in Bi- and Tri- Metallic Helicates 49
2.1 Ligand synthesis 50

2.1.1 Synthesis of L^1 50
2.1.2 Synthesis of L^2 52
2.1.3 Synthesis of L^3 53
2.2 Coordination Chemistry 55
2.2.1 Complexes of L^1 with Zinc (II) 55
2.2.2 Complexes of L^2 with Zinc(II) 58
2.2.3 Complexes of L^2 with Mercury(II) 59
2.2.4 Complexes of L^2 with Mercury(II) and Zinc(II) 59
2.2.5 Solution State Characterisation of HH-$[HgZn(L^2)_2]^{4+}$ 64
2.2.6 Complexes with L^3 68
2.3 Conclusion 70
3. Control of Metallosupramolecular Assemblies by Metal Ionic Radii 72
3.1.1 Synthesis of L^4 72
3.2 Coordination Chemistry 73
3.2.1 Complexes of L^4 with Cadmium (II) 73
3.2.2 Complexes of L^4 with Zinc(II) 75
3.3 Solution Studies 79
3.3.1 Solution state characterisation of $[Cd_2(L^4)_2]^{4+}$ 79
3.3.2 Solution state characterisation of $[Zn_5(L^4)_5]^{10+}$ 82
3.4. Discussion 85
4. Head-to-tail and Heteroleptic Circular Helicates 89
4.1.1 Synthesis of L^5 89
4.1.2 Synthesis of L^6 90
4.2 Coordination Chemistry 90
4.2.1 Complexes of L^5 with Copper (II). 90
4.2.2 Heteroleptic complexes of L^6 with L^4 and Copper (II). 95
4.3 Solution Studies 101
4.3.1 Solution state characterization of $[Cu_5(L^5)_5]^{10+}$ 101
4.3.2 Solution state characterization of $[Cu_5(L^4)_3(L^6)_2]^{10+}$ 103
4.4 Conclusion 104
5. Formation of a Pyrene-Containing Tetranuclear Circular Helicate. 105
5.1.1 Synthesis of L^7 105
5.2 Coordination Chemistry 106
5.2.1 Coordination Chemistry of L^7 with Zinc(II) 106
5.3 Solution Studies 110
5.3.1 Solution state characterization of $[Zn_4(L^7)_4]^{8+}$. 110

5.4 Discussion....111
6. Conclusion....115
7. Experimental....117
7.1 Preparation of L^1, L^2 and L^3....117
7.1.1 Synthesis of bipyridine 1-N-oxide (2)....117
7.1.2 Synthesis of 2,2'-bipyridine-6-carbonitrile, (3)....118
7.1.3 Synthesis of 2,2'-bipyridine thioamide, (4)....119
7.1.4 Synthesis of py-py-tz tridentate ester, (5)....120
7.1.5 Synthesis of py-py-tz tridentate alcohol, (6)....121
7.1.6 Synthesis of py-tz-py tridentate ester, (8)....122
7.1.7 Synthesis of the py-tz-py tridentate alcohol, (9)....123
7.1.8 Synthesis of the py-tz-py tridentate chloromethyl, (10)....124
7.1.9 Synthesis of, (L^1)....125
7.1.10 Synthesis of, (L^2)....126
7.1.11 Synthesis of (11)....127
7.1.12 Synthesis of, (L^3)....128
7.2 Preparation of L^4....130
7.2.1 Synthesis of, (L^4)....130
7.3 Preparation of L^5 and L^6....131
7.3.1 Synthesis of py-tz-ph bidentate bromoacetyl, (14)....131
7.3.2 Synthesis of, (L^5)....132
7.3.3 Synthesis of, (L^6)....134
7.4 Preparation of L^7....135
7.4.1 Synthesis of 1,3-diacetyl pyrene, (16)....135
7.4.2 Synthesis of 1,3-dibromo-diacetyl pyrene, (17)....136
7.4.3 Synthesis of, (L^7)....137
7.5 Synthesis of complexes....138
7.5.1 Synthesis of the complex $[Zn_2(L^1)_2](ClO_4)_4$....138
7.5.2 Synthesis of the complex $[Zn_2(L^2)_2](ClO_4)_4$....138
7.5.3 Synthesis of the complex $[ZnHg(L^2)_2](ClO_4)_4$....138
7.5.4 Synthesis of the complex $[HgCuZn(L^3)_2](PF_6)_5$....138
7.5.5 Synthesis of the complex $[Cd_2(L^4)_2](ClO_4)_4$....139
7.5.6 Synthesis of the complex $[Zn_5(L^4)_5](CF_3SO_3)_{10}$....139
7.5.7 Synthesis of the complex $[Cu_5(L^5)_5](ClO_4)_2$....139
7.5.8 Synthesis of the complex $[Cu_5(L^4)_3(L^6)_2](CF_3SO_3)_{10}$....139
7.5.9 Synthesis of the complex $[Zn_4(L^7)_4](CFSO_3)_2$....140

References 141
Appendix 1: Crystal Data Tables 147
Table A1. Crystallographic data of L^1 complex $[Zn_2(L^1)_2]^{4+}$.[a] 148
Table A2. Crystallographic data of L^2 complex $[HgZn(L^2)_2]^{+}$.[a] 149
Table A3. Crystallographic data of L^4 complex $[Cd_2(L^4)_2]^{4+}$.[a] 150
Table A4. Crystallographic data of L^4 complex $[Zn_5(L^4)_5]^{10+}$.[a] 151
Table A5. Crystallographic data of L^5 complex $[Cu_5(L^5)_5]^{10+}$.[a] 152
Table A6. Crystallographic data of L^6 complex $[Cu_5(L^4)_3(L^6)_2]^{10+}$.[a] 153
Table A7. Crystallographic data of L^7 complex $[Zn_4(L^7)_4]^{8+}$.[a] 154
Appendix 2: Publications 155

List of Abbreviations

Å	Angstroms
Py	Pyridyl
Tz	Thiazole
DMSO	Dueterated dimethylsulphoxide
MS	Mass Spectrometry
DCM	Dichloromethane
ppm	Parts per million, δ (delta), chemical shift
^{1}H NMR	Nuclear Magnetic Resonance
COSY	Correlation Spectroscopy
DOSY	Diffusion Ordered Spectroscopy
NOESY	Nuclear Overhauser effect
THF	Thetrahydrofuran
*m*CPBA	*meta*-chloroperoxybenzoic acid
RT	Room temperature
TMS-CN	Trimethylsilyl cyanide
ESI-MS	Electrospray ionisation mass spectrometry
m/z	mass/charge
MHz	Megahertz
Hz	Hertz
α	Alpha
β	Beta
γ	Gamma
δ	Delta (chemical shift)
g	Gram
mg	Miligrams
ml	Mililitre

mol	Moles
mmol	Millimoles
M	Molar
s	Singlet
d	Doublet
dd	Doublet of doublets
t	Triplet
dt	Doublet of triplets
ddd	Doublet of doublets of doublets
m	Multiplet
(g)	Gas
(aq)	Aqueous
J	Coupling Constant
TLC	Thin Layer Chromotography

Acknowledgements

I would like to thank my supervisor Dr. Craig R. Rice for his excellent support and guidance throughout my PhD. My thanks also go to the past and present members of the Rice research group whom have all been a delight to work with.

I would also like to thank the University of Huddersfield for providing me with this great opportunity and for the funding that has also made this PhD possible.

Assistance has been given from the following people Dr. Lindsay Harding for providing Mass Spectrometry experiments and also the assistance with interpretation of results, Dr. Neil McLay for the assistance with NMR experiments and software, Alexandria Rogerson for providing DOSY experiments and assistance with interpretation of results and Dr. Thomas Riis-Johannessen for the determination of crystal structures, all of whom I would also like to thank.

Most importantly I would like to thank my parents William and Patricia for all their support both emotionally and financially. Without their constant and unconditional support none of my achievements would have been possible.

Lastly, I would like to thank the rest of my family and friends who have supported me throughout my PhD.

Abstract

Described herein, is the synthesis and coordination chemistry of seven novel ligands **L**^{1} - **L**^{7}. These ligands form metallosupramolecular assemblies upon coordination of transition metal ions resulting in heterodi- and hetreotri-metallic double helicates and penta- and tetranuclear cyclic helicates.

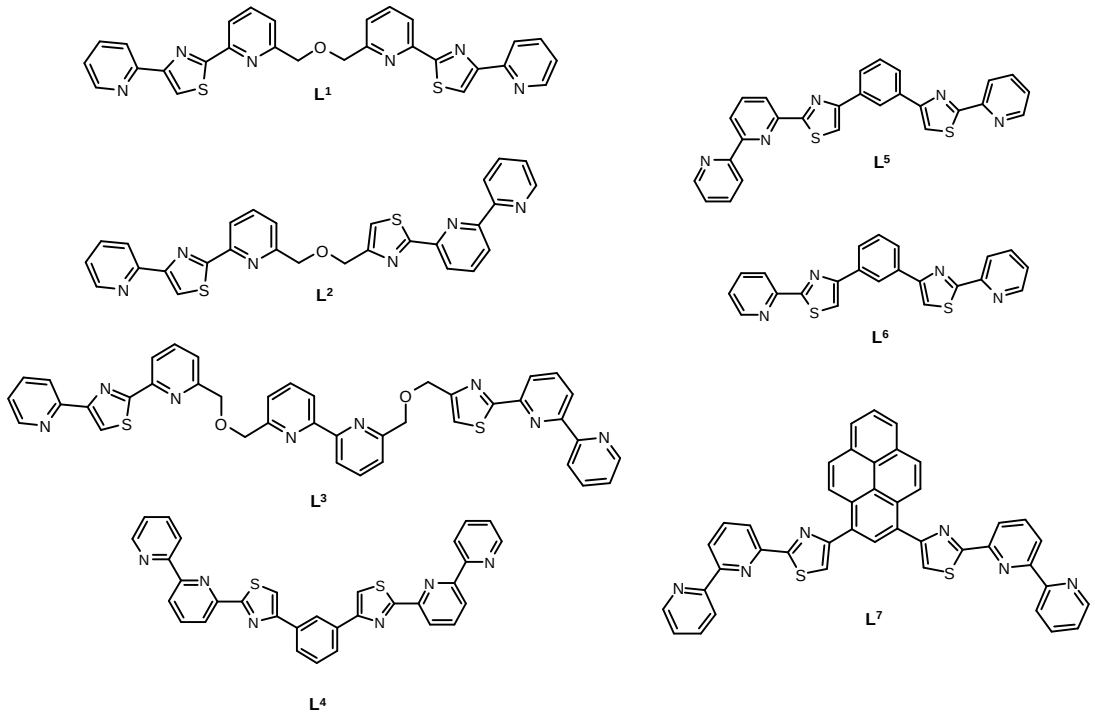

Described in Chapter 2 is a new class of ditopic segmental pyridyl-thiazole (py-tz) N-donor ligands **L**^{1} - **L**^{3}. Reaction of **L**^{1} with Zn^{II} ions results in the formation of a dinuclear double helicate $[Zn_2(\mathbf{L}^{1})_2]^{4+}$. Reaction of **L**^{2} with either Zn^{II} or Hg^{II} results in the formation of the **L**^{2}-containing dinuclear double helicates $[Zn_2(\mathbf{L}^{2})_2]^{4+}$ and $[Hg_2(\mathbf{L}^{2})_2]^{4+}$. However, reaction with both Zn^{II} or Hg^{II} results in the sole formation of the heterodimetallic helicate $[HgZn(\mathbf{L}^{2})_2]^{+}$. Both metal ions are 6-coordinate but the Hg^{II} ion is coordinated by the two py-tz-py units whereas the Zn^{II} ion is coordinated by the py-py-tz domain. The reason that these isomeric sites have different preferences for each of the metal ions is due to the position of the thiazole unit within the terdentate domains, as in the central position the thiazole unit increases the “bite angle” of the donor unit making it more suitable for the larger Hg^{II}. Conversely the py-py-tz

domain has a smaller bite angle and it more suited to the smaller Zn^{II} ion. Reaction of **L^3** with Zn^{II}, Hg^{II} and Cu^{II} results in the formation of a heterometallic trinuclear double helicate $[HH\text{-}[HgCuZn(\mathbf{L^3})_2]^{5+}$. In a similar fashion to **L^2**, the Zn^{II} ion coordinated by the terdentate py-py-tz domain and the Hg^{II} coordinated by the py-tz-py domain. The central bipyridine unit coordinates the tetrahedral Cu^{II} ion resulting in the first reported example of a heterotrimetallic double helicate.

Described in Chapter 4 is a potentially hexadentate N-donor ligand **L^4**, which upon reaction with Cd^{II} results in the formation of a dinuclear double helicate $[Cd_2(\mathbf{L^4})_2]^{4+}$. In this structure the ligand partitions into two tridentate tz-py-py domains each of which coordinate a different metal ion. However, reaction of **L^4** with Zn^{II} results in the formation of a pentanuclear circular helicate $[Zn_5(\mathbf{L^4})_5]^{10+}$, with all the five zinc ions adopting a octahedral coordination geometry arising from the coordination of the two tridentate tz-py-py domains from two different ligand strands. This difference in structure is attributed to unfavourable steric interactions which prevent the formation of $[Zn_2(\mathbf{L^4})_2]^{4+}$ but these unfavourable interactions are not present with the larger Cd^{2+} ion.

Described in Chapter 5 are the potentially pentadentate and tetradentate ligands **L^5** and **L^6**, respectively. The ligand **L^5** contains both a bidentate and tridentate binding site separated by a phenylene spacer unit. Reaction of **L^5** with Cu^{II} results in the formation of a pentanuclear circular helicate $[Cu_5(\mathbf{L^5})_5]^{10+}$. Each of the Cu^{II} ions adopts a 5-coordinate geometry formed by coordination of the bidentate domain of one ligand strand and the tridentate domain of a different ligand. As a result this gives a head-to-tail pentanuclear double helicate. Reaction of **L^6** and **L^4** (Chapter 4) with Cu^{II} results in the formation of a heteroleptic pentanuclear circular helicate $[Cu_5(\mathbf{L^4})_3(\mathbf{L^6})_2]^{10+}$. The cyclic array consists of five copper(II) ions, coordinated by three strands of **L^4** and two strands of **L^6**. In this species four of the Cu^{II} adopt a 5-coordinate geometry arising from coordination of a tridentate domain from **L^4** and a bidentate domain from **L^6**. The remaining copper ion is coordinated by two tridentate domains from **L^4** resulting in an octahedral coordination geometry.

Described in Chapter 6 is the potentially hexadentate N-donor ligand $\mathbf{L^7}$ which comprises of two identical tridentate py-py-tz N_3 binding domains separated by a pyrene unit. Reaction of $\mathbf{L^7}$ with Zn^{II} results in the formation of a tetranuclear circular helicate $[Zn_4(\mathbf{L^7})_4]^{8+}$ with all four zinc metal ions adopting a six-coordinate geometry arising from the coordination of two tridentate py-py-tz units from two different ligand strands. The formation of this lower nuclearity species (e.g. tetranuclear rather than pentanuclear) is attributed to the *p*-stacking between the pyrene unit and the py-py-tz domain.

1. Introduction

1.0 Supramolecular Chemistry

Supramolecular chemistry is currently one if the fastest growing areas of experimental chemistry. However, the field of supramolecular chemistry is difficult to define, as it encompasses a whole range of techniques and principles from various disciplines of chemistry, including biochemistry, organic, inorganic and physical chemistry.[1] This discipline has been defined by many chemists over the years; one definition by Jean-Marie Lehn described supramolecular chemistry as "chemistry of molecular assemblies and of the intermolecular bond".[2]

For many years, chemists have synthesised molecules and investigated their physical and chemical properties. The field of supramolecular chemistry has since been further defined as "chemistry beyond the molecule" and involves investigating new molecular systems in which the most important feature is that the components are held together reversibly by intermolecular forces and not by covalent bonds.[3]

1.1 Origin of Supramolecular Chemistry

Much of the foundations for supramolecular chemistry came from the developments in macrocyclic chemistry in the 1960's, particularly that of the development of macrocyclic ligands for metal cations. Following the work prepared by the groups of Curtis[4], Busch[5] and Jager[6], came a breakthrough by Charles J. Pedersen (1967) with the synthesis of crown ethers.[7,8] Researches such as Donald J. Cram, J-M. Lehn and Fritz Vogtle subsequently became active in shape- and ion-selective receptor synthesis.[9,10] Throughout the 1980's rapid growth of research within this area with concepts of mechanically-interlocked molecular architectures emerging. In 1987, D. J. Cram, J-M. Lehn and C. J. Pedersen received the Nobel Prize for their contributions within supramolecular chemistry, for the development of "host-guest" complexes, investigating three novel macrocyclic ligands for coordination with metal cations (Figure 1.1).

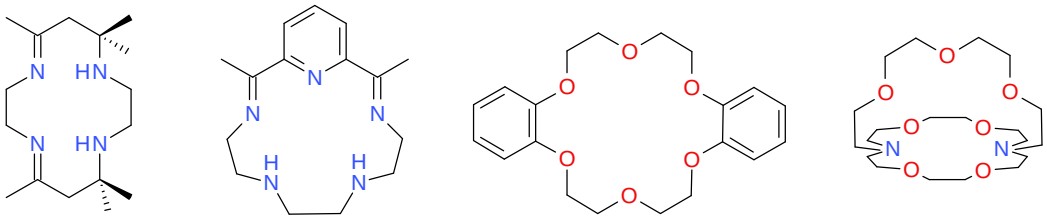

Curtis 1961 Busch 1964 Pedersen 1967 Lehn1969

Figure 1.1 Macrocyclic ligands.

1.2 Supramolecular Interactions

Supramolecular chemistry, in general, concerns noncovalent bonding interactions, sometimes described as 'glue' used by supramolecular chemists that holds the molecule together. The term 'noncovalent' includes a vast range of attractive and repulsive forces. In a supramolecular system it is crucial to consider the relationship of all these interactions and effects relating to that of both the host and guest as well as their surroundings such as solvation.[11] These interactions may include; electrostatic forces, hydrogen bonding and π-π stacking interactions.

1.2.1 Ion-dipole interactions

An ion-dipole force is an attractive force that results from the electrostatic attraction between an ion and a neutral molecule that has a dipole, they become stronger as either the charge on the ion increases, or as the magnitude of the dipole of the polar molecule increases. They are a highly - valued tool for achieving strong binding, a good example of this is where a crown ether and metal ion are involved (Figure 1.2). In this case, the positively charged metal cation attracts the polar lone pairs of the oxygen atoms in the crown ether receptor forming ion-dipole interactions.

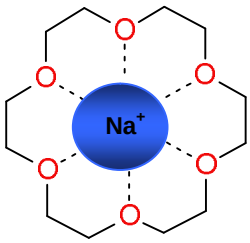

Figure 1.2 Ion-dipole interactions between that of the oxygen lone pairs from the crown ether and the positive metal cation.

1.2.2 Dipole-Dipole interactions

A dipole-dipole interactions occurs as the alignment of one dipole with another can result in a sizable attractive interaction between the pair of poles on adjacent molecules (Figure 1.3). The greater the number of electrons in a molecule the stronger these forces become, as regularly observed in organic carbonyl compounds.

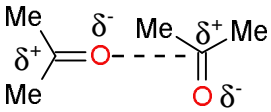

Figure 1.3 Dipole-dipole interaction.

1.2.3 Hydrogen Bonding

A hydrogen bond may be regarded as a specific kind of dipole-dipole interaction, in which a hydrogen atom attached to an electronegative atom (usually O, N or F), is attracted to a dipole of an adjacent molecule or functional group. Hydrogen bonds are found throughout nature and also play an important role in supramolecular chemistry due to the range of lengths, strengths and geometries, they are responsible for recognition or substrates by numerous enzymes and for the double helix structure of DNA.

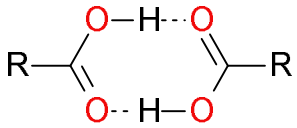

Figure 1.4 An example of hydrogen bonding.

1.2.4 p-p Stacking

π-π stacking forces occur between systems of aromatic rings, the intermolecular overlapping of the *p-orbitals* in the π-conjugated system become stronger as the number of π-electrons increase. Attractive interactions can occur either 'face-to-face' or 'edge-to-face' manner (Figure 1.5). π-π stacking interactions have a large influence on molecule-based crystal structures of aromatic compounds.

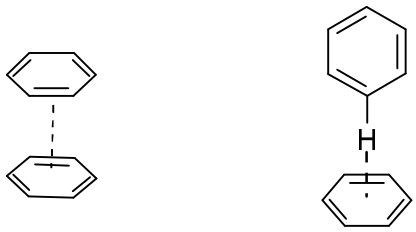

face-to face edge-to-face

Figure 1.5 π-π stacking interactions

1.3 Host-guest chemistry

In supramolecular chemistry, host-guest chemistry describes complexes that are composed of two or more molecules or ions that are held together in an exceptional structural relationship by forces other than those of covalent bonds. It encompasses the idea of molecular recognition and interactions via noncovalent bonding, which is vital in maintaining the three-dimensional structure of large molecules, such as proteins. Most people are familiar with the *'lock and key' principle* described in 1894 by Emil Fischer.[12] According to this theory the catalytic activity of enzymes stems from the fact that the substrate (the compound undergoing reaction), fits tightly into a 'pocket' in the surface of the enzyme. Once the substrate is inside this 'pocket' it is held in

close proximity to the reactant which converts it to its product. Great interest within this field had led to development of an entirely new field known as host-guest chemistry. Designing molecules that can 'recognise' each other and choose with which molecule they will form complexes, some mimicking the mode action of enzymes.

Jean-Marie Lehn and Donald J. Cram have subsequently each developed increasingly sophisticated organic compounds which when forming complexes leaves fissures and cavities where low molecular weight compounds with different types of geometry can be bound. According to Cram 'the host is a molecule or ion whose binding sites converge in the complex', common host molecules amongst others are cyclodextrins, calixarenes, crown ethers and carcerands. Furthermore, 'the guest component is any molecule or ion whose binding sites diverge in the complex', for example, if a metal cation is to be the guest, then its size (ionic radius), charge density and hardness are important.[13]

1.3.1 Crown Ethers

Crown ethers are among the simplest and most engaging macrocyclic ligands used in supramolecular chemistry as they act as a host cations, usually s-block metal cations. They are based on repeating $–OCH_2\text{-}CH_2\text{-}$ units. The fascinating discovery of crown ethers in 1967 by Pedersen was accidental, whist attempting to purify the expected target ligand. Unknown to Pedersen his starting material was contaminated, the resulting product was a mixture of his desired compound along with a small amount of dibenzo[18]crown-6 (0.4% yield). This unexpected compound dissolved sparingly in methanol, but addition of sodium salts significantly enhanced its solubility. The crystals that were characterised by both elemental analysis and mass spectrometry were found to be a macrocycle (Figure 1.6).[14]

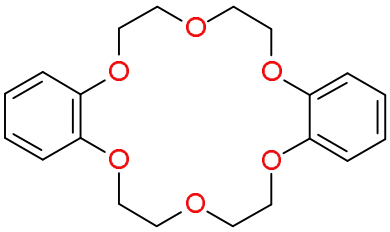

Figure 1.6 Structure of dibenzo[18]crown-6.

From this discovery, Pedersen observed via a space filling model that a sodium ion can assemble in the cavity of the crown, as the six oxygen donor atoms of the polyether ring hold the metal alkali cation by attractive electrostatic ion-dipole interactions. The initial result led to the rapid synthesis of a related macrocyclic species (Figure 1.7), to which Pedersen called 'crown ethers' due to their crown-like shape. Over recent years macrocycle developments have led to important roles in modern tools such as sensors,[15] molecular switches and dyes for spectrophotometric detection.[16]

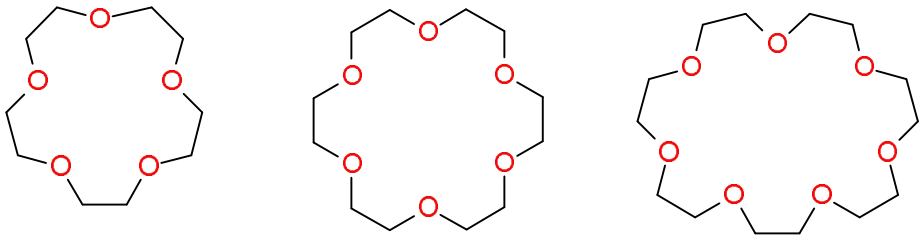

Figure 1.7 Structures of Crown Ethers

Crown ethers are a member of the *corand* family and are cyclic chemical compounds that comprise an array of ethylene glycol units –O-CH_2CH_2-O-, generating different sized cavities which are suitable to selectively binding with a guest species usually s-block metal cations. This established a relationship between cavity size, cationic radius and stability of the resulting complex (Table 1). [1]

Crown ether	Cavity diameter (Å)	Cation	Diameter (Å)
[12]crown-4	1.20-1.50	Li^+	1.36
[15]crown-5	1.70-2.20	Na^+	1.90
[18]crown-6	2.60-3.20	K^+	2.66
[21]crown-7	3.40-4.30	Cs^+	3.38
		Cu^+	1.92
		Ag^+	2.52
		Mg^{2+}	1.44
		Ca^{2+}	2.20
		La^{3+}	2.34
		Lu^{3+}	2.00
		Zr^{4+}	1.72

Table 1 Comparison of different crown ethers and compatible cation diameters

The better the spatial fit of the cation into the crown the stronger the complex formed. This concept is known as *optimal spatial fit*. Work by Frensdorff established the stability constants of various crown ethers with cations in methanol by potentiometry, the findings showed, for example, [21]crown-7 binds caesium more strongly whereas [18]crown-6, a smaller crown forms the most stable complexes with potassium cations. Structural evidence also shows this to be true, as the cavity size of [18]crown-6 is complementary for potassium, as it forms a 1:1 complex with the potassium metal ion sitting perfectly in the middle of the macrocycle.

Complimentarity is shown by size match between host and guest as a particular crown ether will form a stronger complex to a cation which is complementary to the host cavity. Cavity size can easily be changed by varying the number of O-donors or alkyl spacers within the macrocycle, by

changing the size of the cavity consequently changes the cation most suitable for coordination with the host. In fact, [18]crown-6 (internal cavity 2.60-3.20) is a reasonably good size match for all host cations, although it is optimum for potassium (diameter 2.66 Å), whereas caesium (diameter 3.22 Å) is not suitable for coordination to [18]crown-6.

Crown ethers can also be extended to *cryptands* and *lariat ethers* promoting three-dimensionality. In cryptands, metal ions could be encapsulated entirely with a crown-like host enhancing cation selectivity. Lariat ethers, regarded as a crown type macrocycle with a podland side arm, combining higher rigidity and preorganisation of the macrocyclic compounds with the addition of stability and flexibility of the podland complexation.

1.4 Metallosupramolecular Chemistry

The self-assembly process of metal complexes into highly organised architectures of grids[17], cages[18], racks[19] and ladder[20] represents one of the most important topics in supramolecular chemistry (Figure. Metallosupramolecular chemistry utilises the interaction of specific metal-binding domains with appropriate metal centres for the construction of complex functional structure. This term was introduced in 1994 by Edwin Constable to describe supramolecular assemblies that utilise the use of metal ion centres in order to self assemble structures.[21]

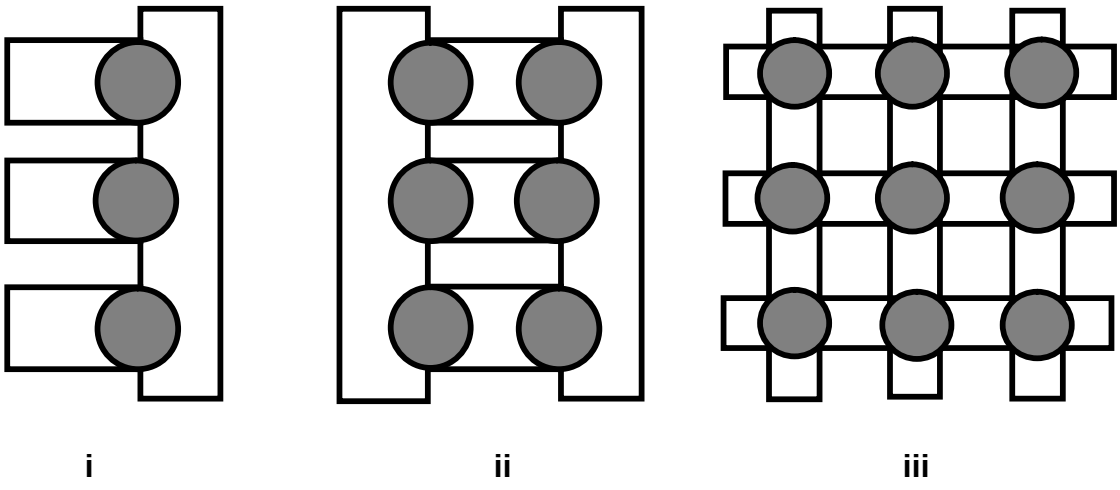

Figure 1.8 A schematic diagram of a molecular racks (i), ladder (ii), grid (iii).

Such metallosupramolecules have been synthesised and are assembled from the interaction of metal ions with the appropriate multifunctional ligands, this is a coded process, and systems are capable of spontaneously generating well-defined organised supramolecular molecules. The process of self-organisation may be directed via the molecular information stored in the covalent framework.[22] Self organisation is a fundamental process present in nature and has led to the generation of complex matter, the most familiar being that of DNA with its self-assembling double helical structure.

1.4.1 Grids

Metal-directed self-assembly has allowed the effective assembly of supramolecular entities with grid-like architectures. The molecular grid [*m x n*]*G* and consists of a square or rectangular-matrix array of metal centres. Square grids, [*n x n*]*G*, are based on metal ions with tetrahedral coordination geometry, such as Cu^{+}, Ag^{+}, and are constructed from *n-topic*, rigid rod-like ligands with tetrahedral coordination sites and n^2 metal ions. Although, polytopic ligands with octahedral coordination sites may generate grids by interaction with metal ions of octahedral geometry (Cu^{2+}, Ni^{2+}). The ligands are divided into two sets, one above and one below the plane of the metal ions. In order to achieve the desired grid structure the metallo-assembly is critically dependent on both the selection of metal ion and the organic component(s) employed. The great interest in such systems is motivated by their potential for molecular scale information storage and processing. Lehn and co-workers[23] have been major players with this particular area working on the preparation of individual systems and also the mechanistic aspect of the self-assembly process and important grid properties.

One of the first square grids was obtained by Lehn *et al,* combining a tritopic rigid ligand with tetrahedral Ag^{+} ions, the correct assembly of the 15–component reaction at one go, nine Ag^{+} ions and six, rigid linear 6,6'-bis[2-(6-methylpyridyl)-3,3'-bipyridazine ligands leads to a [3 x 3] grid.[24] G. S. Hanan and co-workers,[25] demonstrated the direct synthesis of [2 x 2]-grid-type coordination arrays of octahedrally coordinated metal ions. By preparing a potentially hexadentate ligand (**L**$^{\mathbf{a}}$), comprising of a central pyrimidine ring with a bipyridyl unit either side, allowing the ligand to partition into two bis-

terdentate domains. Upon reaction with an equimolar amount of cobalt acetate, analysis indicated a 1:1 ligand-to-metal ratio. The complex cation that formed consisted of four ligand strands and four cobalt cations arranged in a [2 x 2]-grid-type structure (Figure 1.9). Each of the metal centres displays a distorted octahedral coordination to two perpendicularly orientated ligand fragments. Further results also show that this [2 x 2]-grid type coordination can also be applied to other metal ions favouring octahedral coordination geometry generating grids of Ni^{2+}, Zn^{2+}, Cd^{2+} and Cu^{2+}.

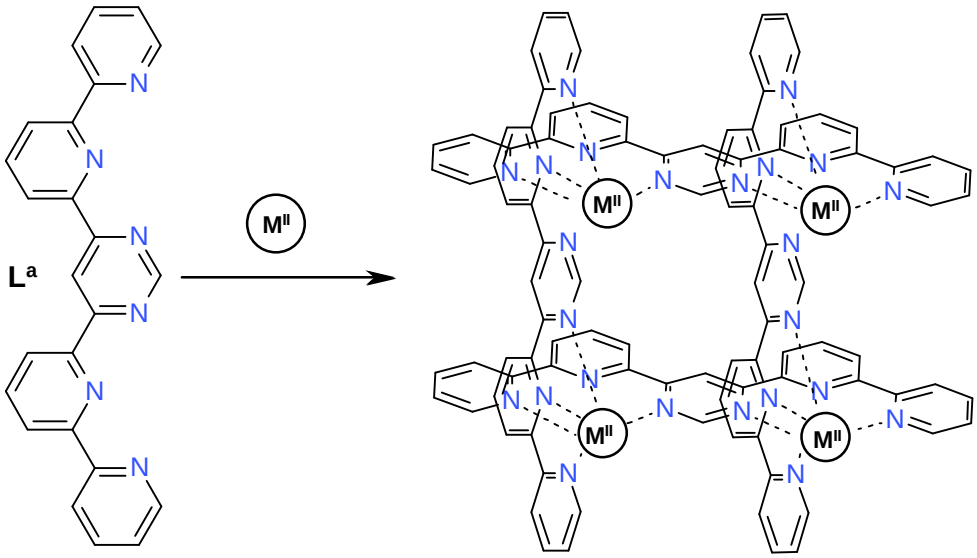

Figure 1.9 Formation of [2 x 2] grid structure.

1.4.2 Cages

Cage structures are similar yet more complex to that of grids. They are formed spontaneously by metal directed assembly of ligand strands producing many elaborate examples of three-dimensional structures with a central cavity.[26,27] Such cage structures have polyhedral or prismatic structures and tend to feature significant internal space, hence their a highly topical area not only for the self-assembly processes which lead to their formation, but also for the host-guest chemistry associated with their large central cavities which are suitable for coordination with a variety of guest species, some acting as templates to direct the cage assembly and they can often also contain counter-ions and solvent molecules.[28] Cages can be designed by exclusive positioning of binding domains on a ligand altering the size and shape of the

central cavity. Modifications are also possible by functionalising the ligands and using specific metal ions in order to change the shape and size of the cage.

M. Fujita and co-workers in recent years have demonstrated how well designed molecules are spontaneously organised into functional molecular systems with the preparation of many complex cage structures.[29, 30] The simple arrangement of transition metal geometry with well-designed bridging ligands gives rise to quantitative self-assembly of discrete organic framework that is nanosized. A particular example obtained a M_6L_4 octahedral assembly (Figure 1.10). An ethylenediamine-protected Pd(II) complex was prepared and successfully incorporated with **L**^{b} in a 3:2 ratio. **L**^{b}, is a triangular molecular panel consisting of three binding sites. In this complex the four triangular panels are linked together at the corners of the triangles, in a way such that every alternate face of the octahedron contains a molecular panel. The resulting cage complex is able to bind with various organic guest molecules within the cavity.

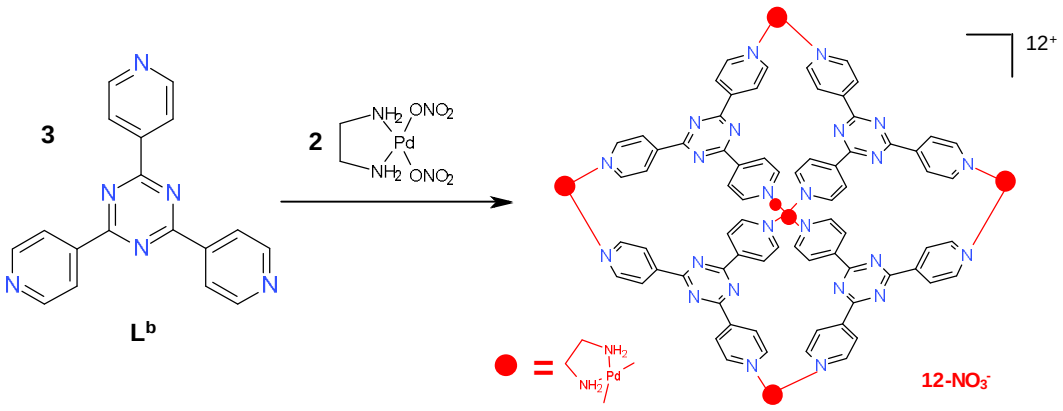

Figure 1.10 Formation of cage complex M_6L_4

1.4.3 Racks

Molecular racks ([*n*]*R*), are constructed from linear-*n-topic* ligands which connect *n* metal ions in a linear arrangement, as well as from ancillary ligands attached to the metal ions, playing the role of platforms. These would be formed by the complexation of several metal ions to rigid, linear sequence of binding sites. If the polytopic ligand contains octahedral coordination's sites

(tridentate moieties), then the ancillary ligand must also be tridentate, in order to fulfil the octahedral stereochemistry of the metal ion.

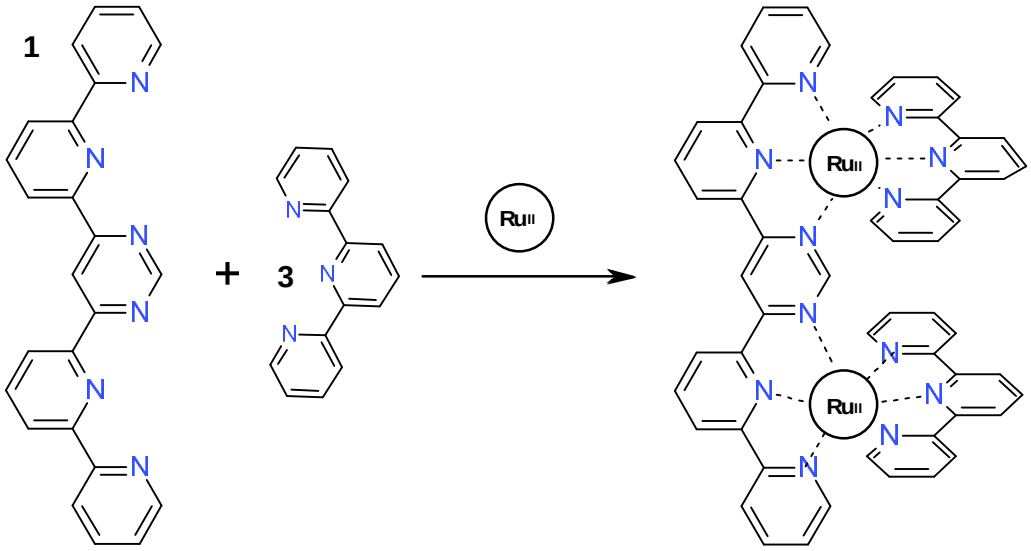

Figure 1.11 Formation of a rack type complex $[Ru^{II}_2(\mathbf{L}^{a})(typ)_2]^{4+}$

The first dinuclear and trinuclear racks (Figure 1.11), were reported by Lehn and co-workers[31] and were obtained by the coordination of linear ligands by octahedral coordination. The potentially hexadentate ligand ($\mathbf{L}^{a}$), comprising of a central pyrimidine ring with a bipyridyl unit either side, allowing the ligand to partition into two bis-terdentate domains upon reaction with $Ru^{II}(tpy)Cl_3$, resulting in the formation of the rack complex. Each metal centre occupies a distorted octahedral coordination geometry formed by the two terdentate domains. Rack type architectures can also be assembled from tetrahedral metal ions e.g. Cu^{+}, with polytopic ligands that have tetrahedral coordination sites and bidentate ligands such as phenanthroline or 2,2'-bipyridine.

1.4.4 Ladders

Ladder structures may result from the complexation of linear ligands with tetrahedral metal centres and are similar to the complexes observed in the formation of grids. The ladder topology [*2n*]*L*, can be obtained by using two linear polytopic ligands, such structures were obtained serendipitously rather than intentionally. Many examples of ladders have been reported over recent years.[32,33] One example in particular by Lehn and co-workers demonstrates ladder type complex formation by using a multidentate bridging ligand $\mathbf{L}^{c}$.

Reaction of the multidentate bridging ligand with equimolar amounts of the diotopic bipyridinium ligand **L^{d}** and copper(I) ions (Figure 1.12). The bipyridinium ligand is coordinated both sides by different copper(I) metal ions, as each metal ion occupies a distorted tetrahedral coordination geometry along with a bidentate binding domain from the multidentate ligand. The result is the formation of a ladder type complex.[34]

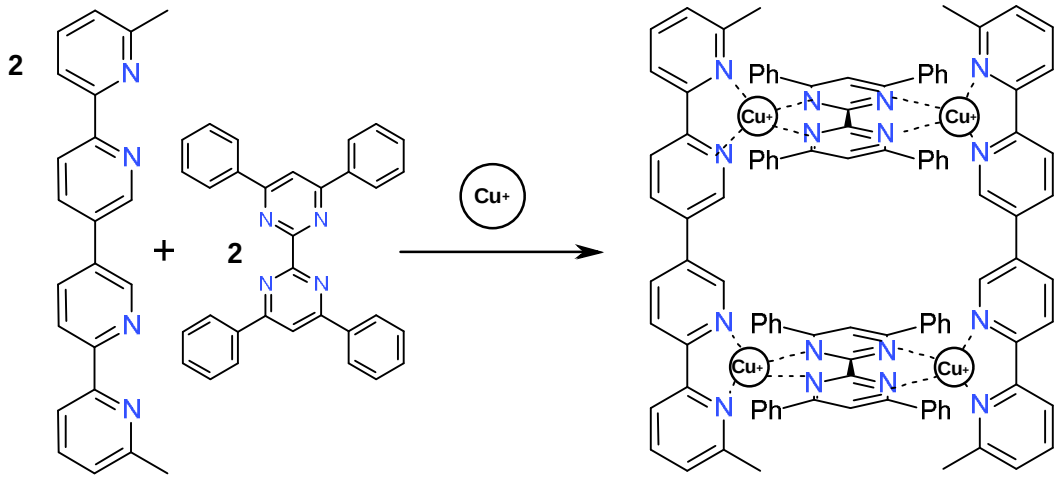

Figure 1.12 Formation of a ladder complex.

1.5 Helicates

Self-assembly and self-organisation have rapidly grown into a main theme of supramolecular chemistry. Inspiration within this area has been provided by the self-assembling double helical structure of DNA, where the two right-handed polynucleotide chains wind around a central axis defined by the hydrogen bonded complementary nucleic acids.[35] Current interest is in the ability of metal ions to control the arrangement of organic ligands in the use of metal ions to direct molecular topology.[36,37] For inorganic chemistry, self-assembly is expressed by the spontaneous formation of a double- and triple helical multinuclear complexes. Helicates are oligonuclear coordination compounds in which linear organic oligodonor ligands wrap around two or more metal centres. The term *helicate* was introduced by Lehn and co-workers in 1987, used to describe a polymetallic helical double strand .[38] An alternative description is that a helix is characterised by a helical axis, in a

screw like sense, as a compound that possesses chirality about a fixed axis. The pitch of the screw is the distance between the turns of the helix (rate of axially linear to angular properties), hence, helicity is a special case of chirality.[1]

A key factor in the assembly of helicates is how a flexible multidentate ligand becomes partitioned into distinct metal binding sites. In many cases ligands are constructed to contain several bi- and tridentate domains, so each site binds to a separate metal ion rather than chelating to a single metal ion. However, the formation of a helicate is dependent on the design of the ligand yet also the metal ion to be used.[39]

1.5.1 Helicate Nomenclature

Due to the vast amount of helicates species possible the classification can become quite complex. In order to differentiate between helicates certain aspects need to be taken into account; (a) the number of ligands, (b) the number of metal centres and (c) the number of binding sites. Therefore, a simple helicate will be named in terms of the number of metal centres and the number of ligand strands involved, for example *mononuclear*, *dinuclear*, *trinuclear*, *tetranuclear*…etc., refer to; one, two, three and four metal centres respectively. Next, the helicate can be made up from two ligand strands resulting in a *double helicate* or three ligand strands resulting in a *triple helicate*. Assembly of helicate strands is also an important factor, identical coordinated strands are termed *homostranded* helicates and a helicate consisting of different strands leads to a *heterostranded* helicate also termed *homoleptic* and *heteroleptic*, respectively. Isomeric forms also exist within the subject of helicates and two key types exist; the first type coordinates ligand strands possessing a sequence of similar binding units along the strand with similar built-in informations resulting to *homotopic* helicates. The second type coordinates ligand strands possessing different binding units leading to directionality within the strand resulting to *heterotopic* helicate and exist in two isomeric forms according to the orientations of the coordinated binding units head-to-head (*HH*) and head-to-tail (*HT*). Each category is further divided into *saturated* helicate when the stereochemical requirements of the metal ions are fulfilled by the donor atoms of the strands and the term *unsaturated*

helicate when the stereochemical requirements of the metal ions have an incomplete filling of the coordination spheres by the ligand strands leading to the combination of ligand strands and supplementary anions or solvent molecules. A ligand strand may be coordinated in a 'side-by-side' fashion and not a helicating fashion these are termed *meso-helicates* (*non-chiral*) or *mesocates* (*chiral*).

1.5.2 Homoleptic Helicates

Homoleptic helicates have been studied extensively[40,41] and are assembled from identical helicate strands. A particular example has been reported by Rice and co-workers[42] with $\mathbf{L^c}$ (Figure 1.13). This potentially hexandentate ligand contains two pyridyl-thiazole-pyridyl binding domains and an external crown ether binding site that bridges the 3,3'-positions of the central bipyridyl unit. They demonstrated that upon reaction of $\mathbf{L^c}$ with an equimolar amount of Zn(II) ions results in the formation of the homoleptic dinuclear double helicate $[Zn_2(\mathbf{L^c})_2]^{4+}$. Each of the Zn(II) centres has distorted octahedral geometry formed by the coordination of one tridentate pyridyl-thiazole-pyridyl N-donor unit from each ligand.

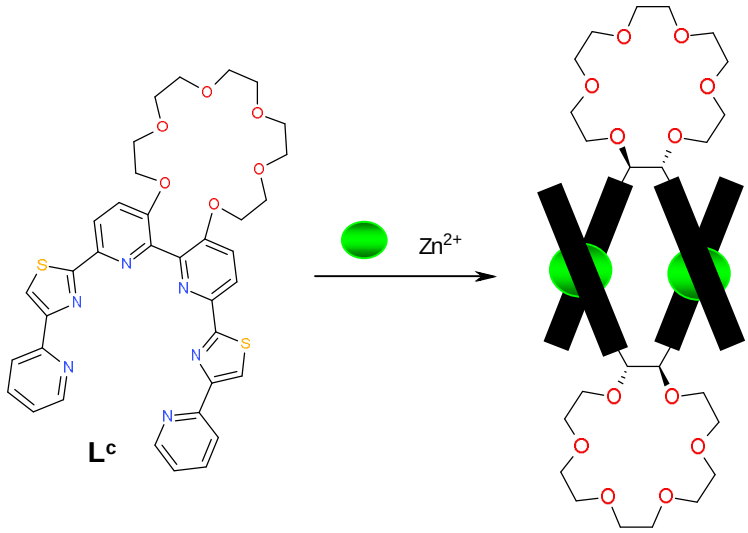

Figure 1.13 Formation of a homoleptic double helicate $[Zn_2(\mathbf{L^c})_2]^{4+}$ upon reaction with Zn(II) ions.

1.5.3 Heteroleptic Helicates

Most helicates that have been prepared within recent years are homoleptic as previously discussed. However, heteroleptic double-stranded helicates

composed of different strands have been reported.[43,44] Examples by Cohen and co-workers[45,46] demonstrated how structurally related ligands **L**^{d} and **L**^{e} are not 'sufficiently instructed' to avoid a cross reaction between ligands resulting in the formation of a heterotopic ligand. **L**^{d} consists of three 2,2'-bipyridine units linked via methylene spacer units, **L**^{e} consists of two 2,2'-bipyridine units at either side of 1,10-phenanthroline linked via methylene spacer units. Hence, upon reaction of a mixture of **L**^{d} and **L**^{e} with Cu(I) ions, resulted in the formation of both homoleptic and heteroleptic helicates. Each Cu(I) centre occupies a distorted tetrahedral coordination geometry formed by the two bidentate binding domains, one from each ligand strand, in a trinuclear double helical arrangement.

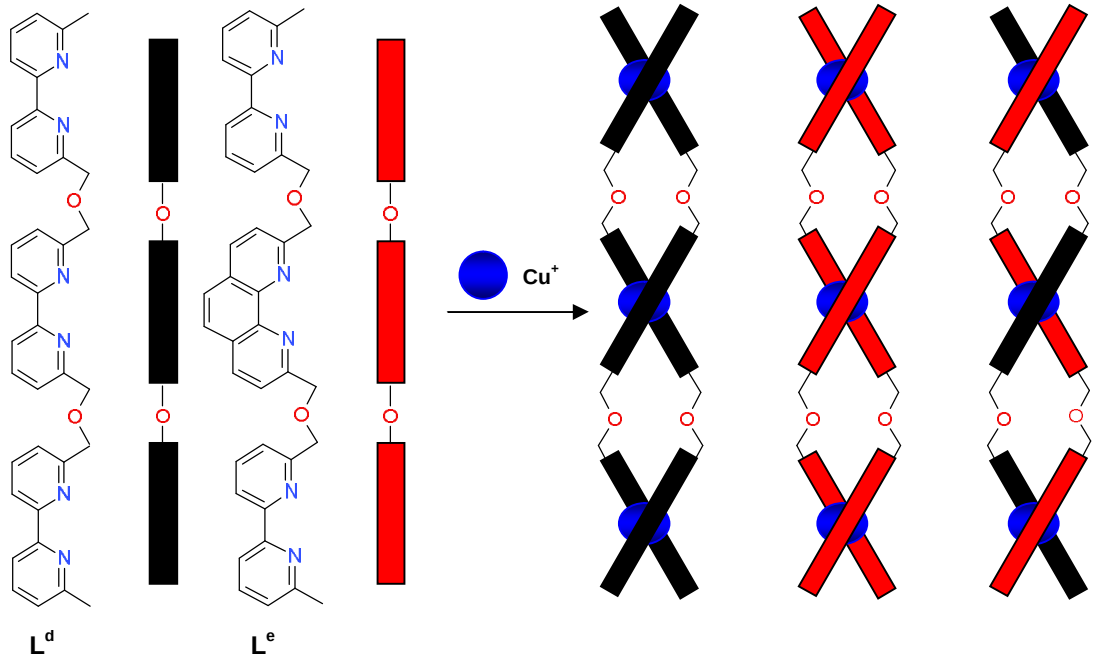

Figure 1.14 Illustration representation of the formation of homo- and heteroleptic helicates upon reaction of **L**^{d} and **L**^{e} with Cu(I) ions.

1.5.4 Unsaturated Helicates

Unsaturated helicates occur as a result of the disparity between the built-in information encoded in the components and therefore does not lead to the systematically elaborate mixtures of complexes yet selectively well defined self-assembled helicates. The result of this may be from; (a) partial use of the binding domains of the strands and (b) incomplete filling of the coordination spheres of the metal ion by the ligand strands, in order to fulfil the

stereochemical requirements of the helicate binding with supplementary ligands, anions or solvent molecules takes place.[46, 47] The most studied unsaturated helicates are those derived from the quinquepyridine ligand. An example of this has been demonstrated by Constable and co-workers,[48] the quinquepyridine ligand strand partitions into a bipyridine and terpyridine subunits adopting a head-to-head assembly (*HH*)-$[Cu_2(\mathbf{L^f})_2(OAc)]^{3+}$ when reacted with Cu(II) acetate hydrate (Figure 1.15). One copper(II) centre is pseudooctahedrally coordinated by the two face-to-face terpyridine units and the second Cu(II) is five-coordinate by the two bipyridine units together with a monodentate acetate anion.

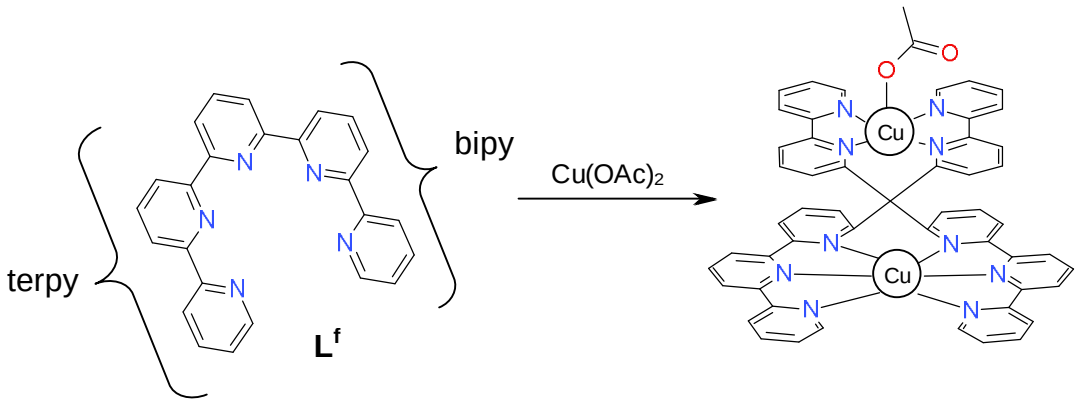

Figure 1.15 Formation of the saturated helicate (*HH*)-$[Cu_2(\mathbf{L^f})_2(OAc)]^{3+}$

1.5.5 Directional Helicates

The target of directional helicates encompasses the assembly of two like directional helicand ligands.[49,50] For a double stranded helicate, two different orientations must be considered; (a) head-to-head (*HH*) where the identical binding units of each strand are coordinated to the same metal ion and (b) a head-to-tail arrangement (*HT*) corresponding to the coordination of the different binding units of each strand to the same metal. An example of this by Constable and co-workers demonstrates how two new asymmetrically substituted 2,2':6,2'':6'',2'''-quaterpyridine ligands $\mathbf{L^g}$ and $\mathbf{L^h}$, comprising of a methyl unit and a *tert*-butyl unit, respectively show selectivity for the two possible conformations.[51] Upon reaction with Cu(I) ions $\mathbf{L^g}$ results in a 1:1 mixture of HH and HT conformation isomers in $[Cu_2(\mathbf{L^g})_2]^{2+}$, however in $\mathbf{L^h}$ this

results in the formation of only the HH isomer $[Cu_2(\mathbf{L}^{h})_2]^{2+}$. In both helicates the Cu(I) metal ion centres occupy a distorted tetrahedral coordination geometry as each ligand strand partitions into two bidentate binding domains.

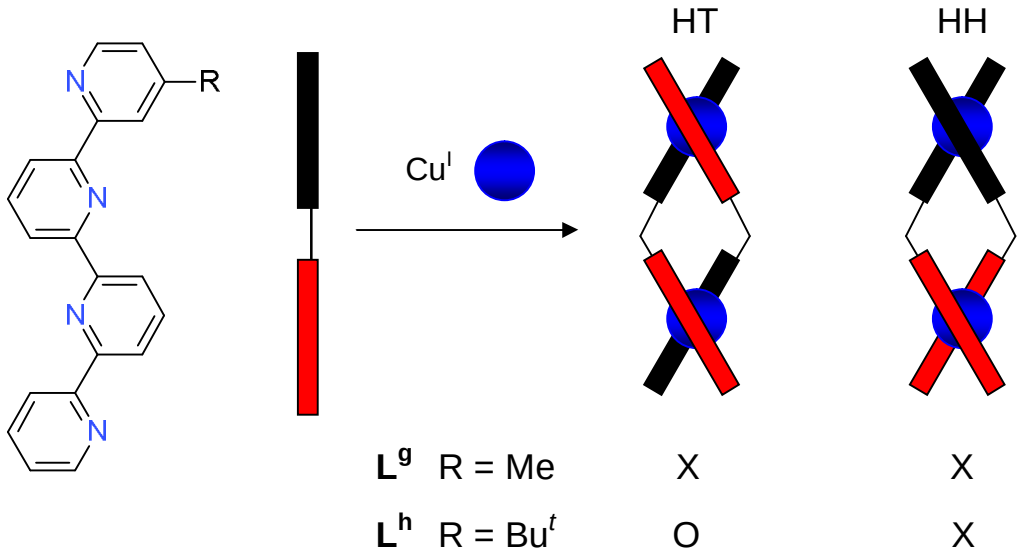

Figure 1.16. Formation of *HH*- and *HT*-$[Cu_2(\mathbf{L}^{g})_2]^{2+}$ and *HT*-$[Cu_2(\mathbf{L}^{h})_2]^{2+}$.

The directional specificity in these systems is subtle, yet the preferential formation of the *HH*-$[Cu_2(\mathbf{L}^{h})_2]^{2+}$ isomer arises from the short contacts between the *tert*-butyl substituents in the HT isomer.

1.5.6 Heteronuclear Helicates

Constable and co-workers have introduced various substituents able to form heteronuclear helicates with the basic quaterpyridine motive [52, 53], as it is possible for the helicate species to undertake self-assembly processes with metal ions that vary in coordination geometry. An excellent example of this has been demonstrated by Constable and co-workers with the pentadentate ligand quinquepyridine,[54] generating a heteronuclear helicate as it is able to adopt an unsymmetrical bidentate-tridentate binding system. Reaction of the quinquepyridine ligand $\mathbf{L}^{i}$ with equimolar amounts of Co(II) and Ag(I) produced the formation of the heteronuclear double helicate $[CoAg(\mathbf{L}^{i})_2]^{3+}$. $\mathbf{L}^{i}$ partitions into both bidentate and tridentate binding domains enabling the ligand to coordinate metals of different coordination geometries in a double

helical arrangement. Specifically, the ten N-donors of the two quinquepyridine strands can accommodate a six-coordinate metal ion Co(II) and a four-coordinate metal ion Ag(I) (Figure 1.17)

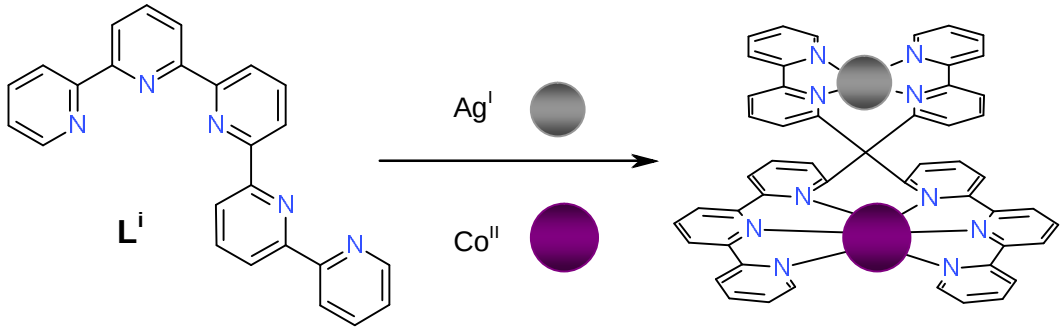

Figure 1.17 Formation of the heteronuclear helicate $[CoAg(\mathbf{L}^{i})_2]^{3+}$.

1.5.7 Enantioselective and Diastereoselective Helicates

Self-assembly, self-recognition and replication may entail chiral components. Chirality is expressed on both molecular and supramolecular levels, like a molecule, a supermolecule may exist in enantiomeric or diastereomeric forms. This research is of particular importance because many biologically and medically important molecules exist as enantiomers. As discussed previously a helix is characterised by a helical axis, a screw sense i.e. its chirality and a pitch, the rate of axially linear to angular properties. Helicity is a special case of chirality. In geometric terms, a helix is the figure generated by the motion of a point around and along a line, the helical axis. It may be right-handed (plus, P) or left-handed (minus, M) according whether the rotation is clockwise or anticlockwise.

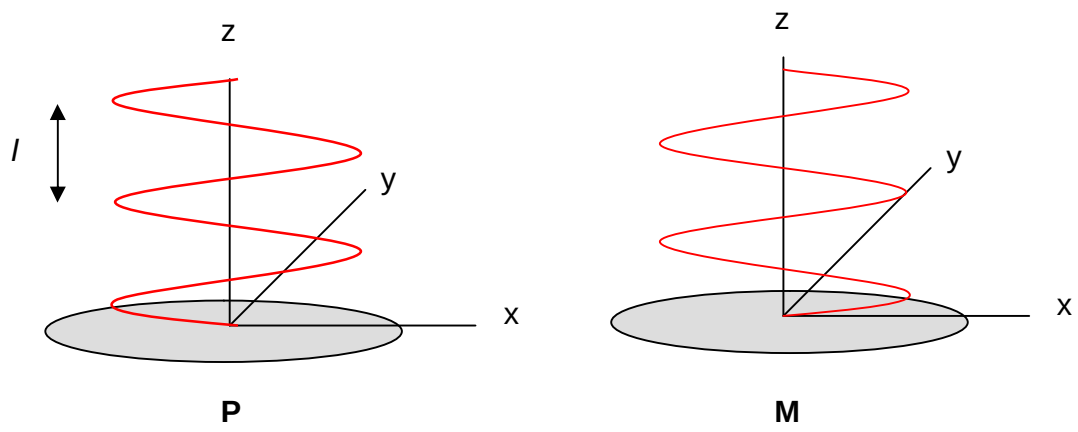

Figure 1.18 Illustration showing both right-handed (plus, P) and left-handed (minus, M) . L is the pitch and z is the helical axis.

The ability to selectively form P or M helicates requires additional stereochemical information within the system. With chiral ligands the P and M helicates are related as diastereoisomers, in contrast to that of enantiomers, diastereoisomers have different chemical and physical properties and will not necessarily be formed in equivalent amounts. However, if it is the stereochemistry of the metal centres that are different then side-by-side helicates (*meso*-helicates) are formed.[39]

Most studies have focussed on double- or triple-stranded helicates, however single stranded helicates are also inherently chiral. Kwong and co-workers have reported stereoselective formation of a single-stranded helicate.[55] The chiral quaterpyridine $\mathbf{L}^{j}$, reacts with Pd(II) ions to form a chiral single-stranded helical binuclear palladium complex. Each Pd(II) metal ion centres occupy a distorted square-planar coordination geometry. The ligand strand partitions into two bidentate domains, this small helical twist of the bridging ligand results in the formation of the complex *M*-$[Pd(\eta^3\text{-}C_3H_5)_2(\mathbf{L}^{j})]^{2+}$ due to shorter Pd-Pd bond observered.

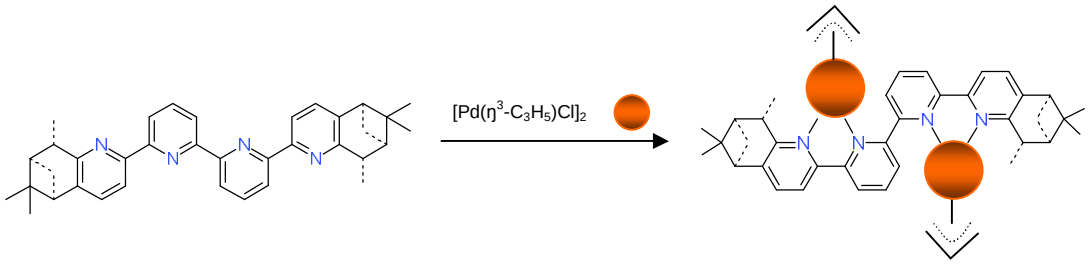

Figure 1.19. Stereoselective formation of single-stranded helicate *M*-[Pd(η^3-C_3H_5)$_2$(**L**^{j})]$^{2+}$

Constable and co-workers[56] have demonstrated how quaterpyridine (**L**^{k}) and sexipyridine (**L**^{l}) both form stereoselective double-helicates. Reaction of **L**^{k} with an equimolar amount of Cu(I) results in the formation of the dinuclear double-helical complex [Cu_2(**L**^{k})$_2$]$^{2+}$. As seen previously, the four N-donor ligand strand partitions into two bidentate binding domains with the Cu(I) metal ions occupying a distorted tetrahedral coordination geometry. Reaction of **L**^{l} with an equimolar amount of Co(II) also results in the formation of a dinuclear double-helical complex [Cu_2(**L**^{l})$_2$]$^{4+}$, the six N-donor ligand strand partitions into two tridentate binding domains with the Co(II) metal centres occupying a distorted octahedral coordination geometry.

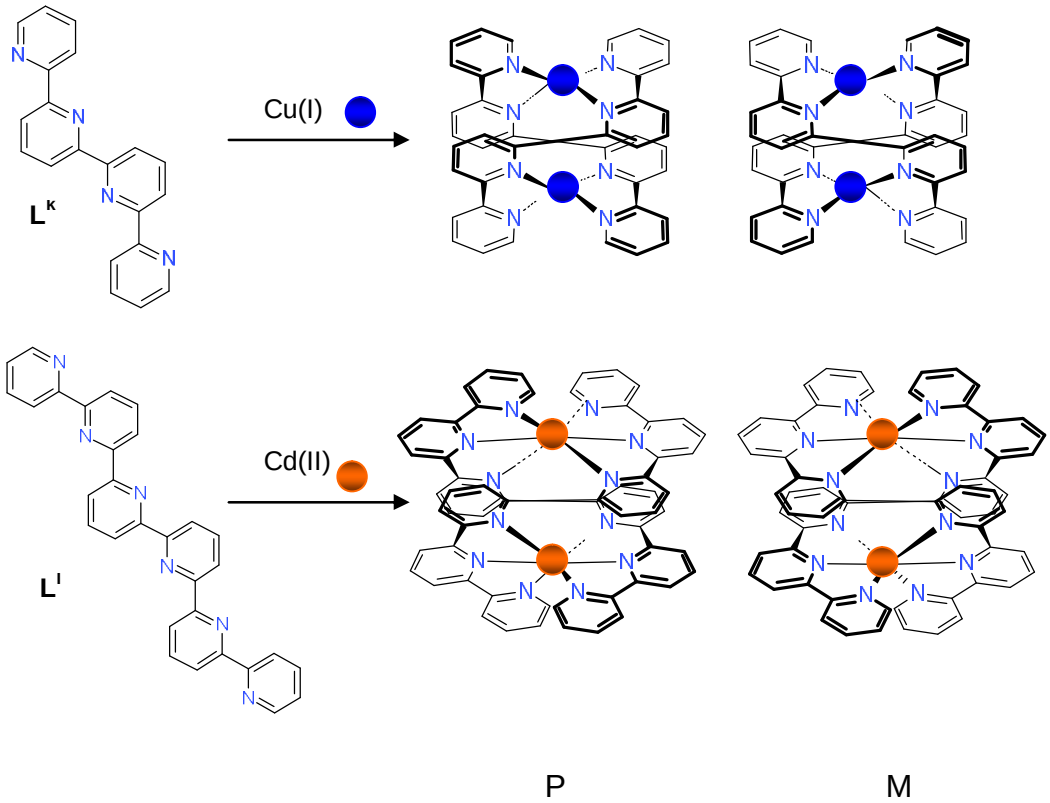

(Figure 1.20).Figure 1.20. Stereoselective complexes (i) [Cu_2(**L**^{k})$_2$]$^{2+}$ and (ii) [Cu_2(**L**^{l})$_2$]$^{4+}$.

The groups of Von Zelewsky[57] and Constable[58, 59] have designed ligands which gives a predictable structure with a given metal ion and predetermine the configuration of the inherently chiral molecules by synthesising oligopyridine species with the incorporation of pinene units (Figure 1.21). Pinene-based chirality can be easily combined with 2,2'-bipyridine metal-binding domains with such ligands undergoing stereoselective reactions with transition metal ions and maybe used as enantioselective building block in supramolecular chemistry. The great advantage of the pinene-based systems is the stability of the chiral auxillary, making it extremely unlikely for the system to be further manipulated.

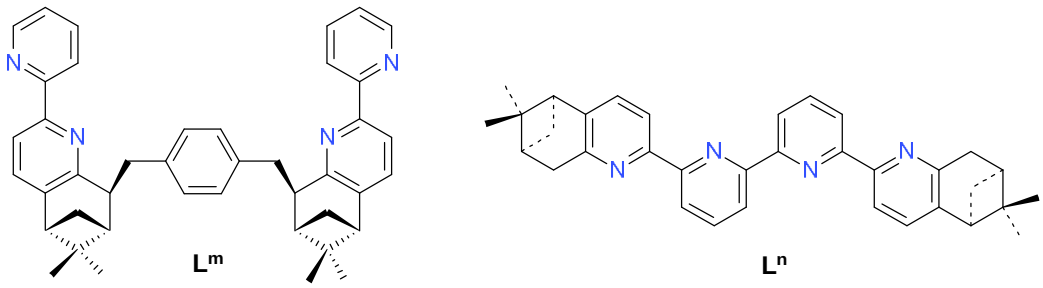

Figure 1.21. Pinene-based chiral oligopyridines structures of Von Zelewsky $\mathbf{L^m}$ and E. C. Constable $\mathbf{L^n}$.

Von Zelewsky demonstrated that upon reaction of either the (+)- and (-)-$\mathbf{L^m}$ enantiomers with either Cd(II) and Zn(II) metal ions (ratio L:M, 2:3) resulted in the formation of a dinuclear triple helicate preferential of one stereoisomer. Constable and co-workers[60] demonstrated the stereoselective self-assembly of double helicates in high diastereomeric excess from chiral oligopyridines with either formation of the (S,S) or (R,R) enantiomers. Reaction of $\mathbf{L^n}$ with an equimolar amount of Cu(I) ions resulted in the formation of the complex (*P*)-$[Cu_2(\mathbf{L^n})_2]^{2+}$. Such stereoselectivity arises from interactions between the chiral auxillaries and the oligopyridine strands.

1.5.8 Meso Helicates

There has been much interest for the study of metal-ligand assembly and recognition processes which lead to the formation of what is seen as the conventional helicate. In all but few cases helicates are homoleptic with all ligands being the same, however, related achiral assemblies where two ligands are 'side-by-side' instead of being twisted around one another are expressed as meso-helicates. Ward and co-workers demonstrated an unusual example of a mixed-ligand mesocate complex.[61] The ligands $\mathbf{L^o}$ and $\mathbf{L^p}$ both have bidentate N,O-donor pyrazolylphenol at terminal ends of the ligand strands with different spacers separating them. A 1:1 mixture of $\mathbf{L^o}$ and $\mathbf{L^p}$ were reacted with Zn(II) metal ion resulting in the formation of complex $[Zn_2(\mathbf{L^o})(\mathbf{L^p})]^{4+}$. Confirmation of the complex structure was achieved by single crystal X-ray diffraction studies showing the structure to be an achiral mesocates with the two ligand strands in a 'face-to-face' arrangement. The Zn(II) metal ion centres occupy a distorted tetrahedral coordination geometry (Figure 1.22).

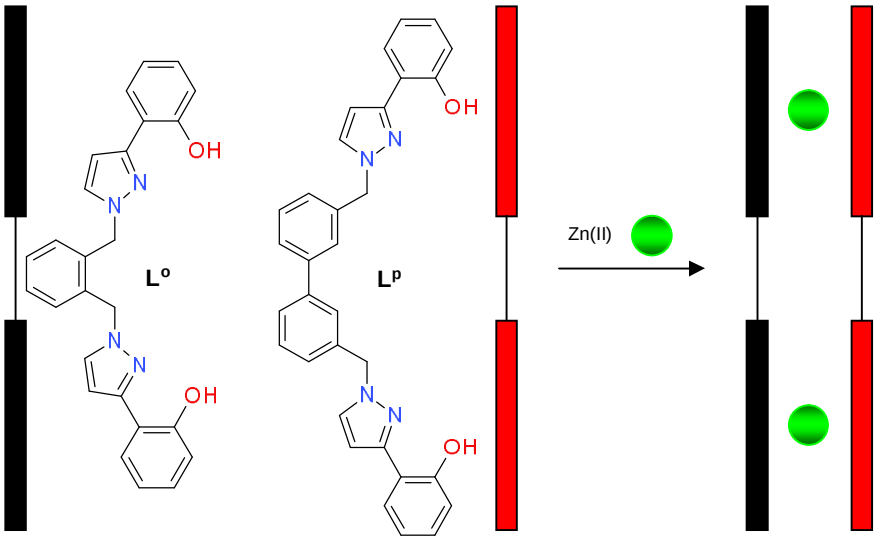

Figure 1.22. Formation of heteroleptic mesocates $[Zn_2(\mathbf{L^o})(\mathbf{L^p})]^{4+}$.

1.6 Ligand Recognition

Self-assembly and self-organisation have rapidly grown into a main theme of supramolecular chemistry and now widespread research activities are

directed towards the preparation and self-organisation of supramolecular metallohelicates. Most helicates that have been prepared to date are homoleptic helicates, consisting of identical strands. One such example along with the importance of self-recognition within the area of self-assembly of helicates was demonstrated by Lehn and co-workers.[62] They demonstrated that strands of oligo(2,2'-bipyridine) of different lengths do not form heteroleptic double stranded helicates upon addition with Cu(I) ions, however result in the spontaneous formation of only homoleptic helicates (Figure 1.23).

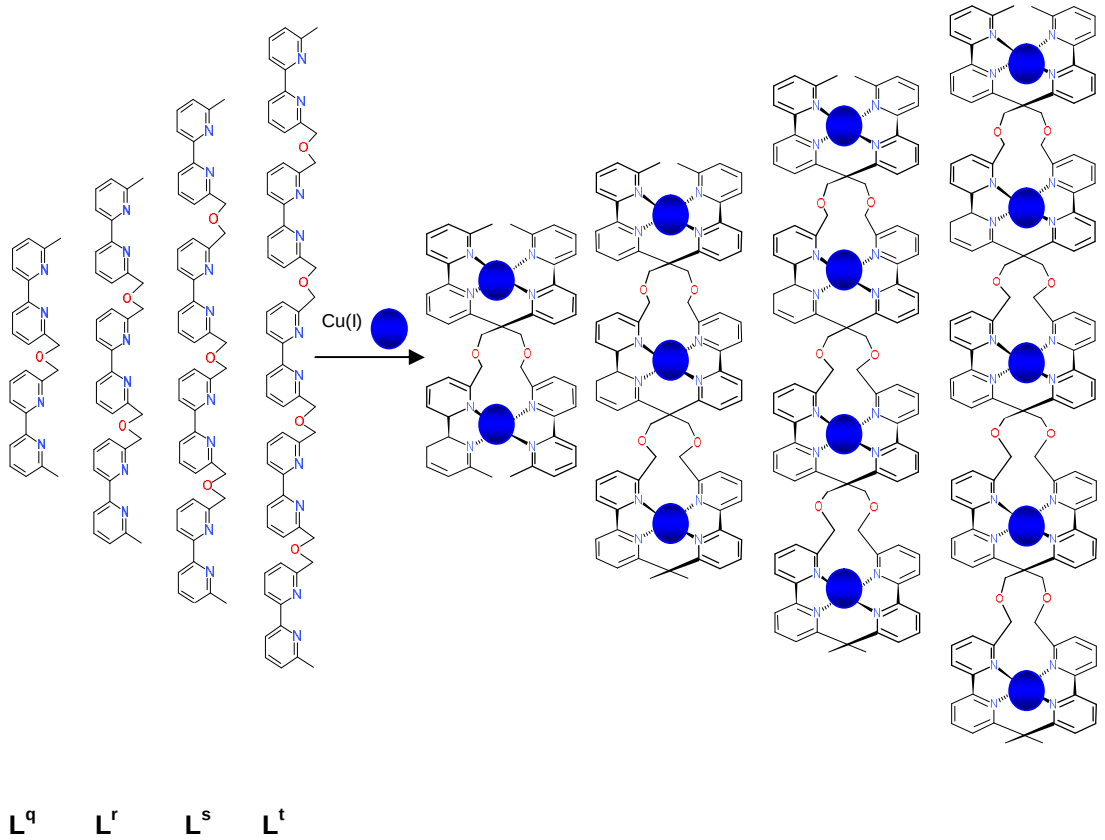

Figure 1.23. Self-recognition in the self-assembly of the double helicates from a mixture of oligopyridine ligands $\mathbf{L^q}$-$\mathbf{L^t}$ with Cu(I) ions.

Further to this, Lehn and co-workers were able to demonstrate ligand recognition between two ligand strands $\mathbf{L^r}$ and $\mathbf{L^u}$. Each of the tri-bidentate ligands consist of bipyridine units separated by different spacer. Reacting stoichiometric amounts of both ligands with Cu(I) and Ni(II) resulted in the formation of only the homoleptic species $[Cu_3(\mathbf{L^r})_2]^{3+}$ and $[Ni_3(\mathbf{L^u})_3]^{6+}$, demonstrating the recognition of the tetrahedrally coordinating Cu(I) ions by

the 6'6'-linked tritopic bipyridine ligand $\mathbf{L^r}$ and of the octahedrally coordinated Ni(II) ions by the 5,5'-linked tris(bipyridine) of $\mathbf{L^u}$ (Figure 1.24).

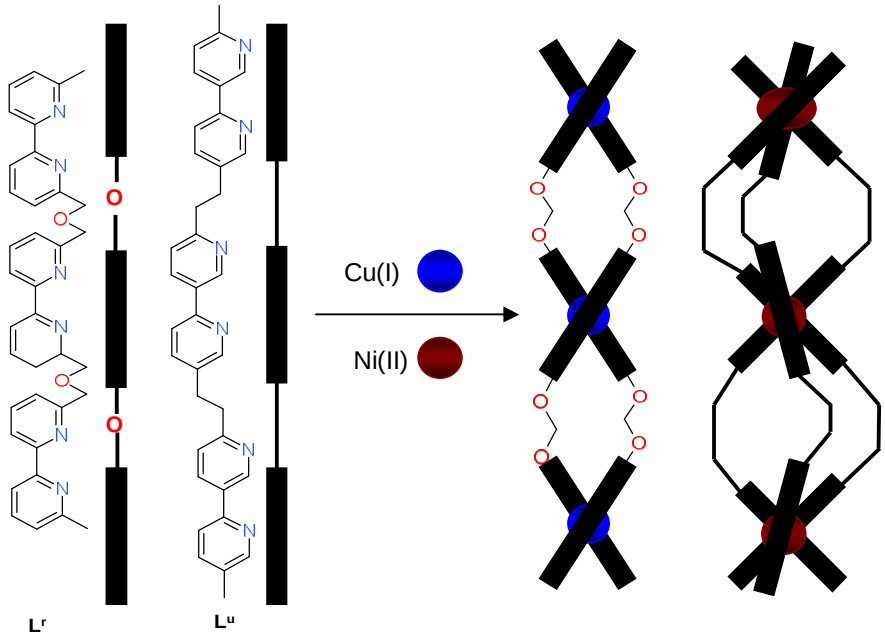

Figure 1.24. Self-recognition in the self-assembly of the double helicate $[Cu_3(\mathbf{L^r})_2]^{3+}$ and triple helicate $[Ni_3(\mathbf{L^u})_3]^{6+}$ from a mixture of oligobipyridine strands $\mathbf{L^r}$ and $\mathbf{L^u}$ with Cu(I) and Ni(II) ions.

In both of the self-assembly experiments self-recognition allows for the generation of desired products from a mixture of starting molecules.

1.6.1 Ligand Programming

Extensive work has gone into the development of preprogrammed systems, in which small readily prepared molecular components automatically join to produce much greater and more complicated aggregate. In the term '*preprogramming*' understanding of the chemical system in which the very nature of the molecular building blocks (such as size, shape, symmetry, and electronic properties of their binding sites) contains all the necessary information in order to selectively produce the desired superstucture.[1] Ligand programming involves the incorporation of instruction into molecular components leading to a generation of desired supramolecular architecture, the supramolecular complex assembles itself. The presence and operation of molecular information has become the basic and crucial tenet of

supramolecular chemistry, specifically designed to contain binding domains with various metal ions of a preferred geometry.

An example by Constable and coworkers[63, 64] of research in the development of coordination chemistry of higher oligopyridines as the organic component of helical supramolecular arrays. An example of this is the research undertaken with 2,2':6',2'':6'',2''':6''',2'''':6'''',2''''':6'''''-sexipyrindine ligand (spy) with a range of different metal ions possessing different electronically imposed preferences for their coordination geometry.[65, 66] The potentially hexandentate ligand spy $\mathbf{L^I}$, forms double-helical binuclear complexes with first, second and third row transition metals, however the reaction of spy with lanthanide cation Eu(III) results in the formation of helical 1:1 complex $[Eu(\mathbf{L^I})(NO_3)_2]^+$. $\mathbf{L^I}$ acts as a hexandentate ligand and adopts a helical twist about an equatorial plane forming a mononuclear helicate with the Eu(III) metal ion centre . Upon reaction of $\mathbf{L^I}$ with Cd(II) metal ion forms a dinuclear double-helical complex $[Cd_2(\mathbf{L^I})_2]^{4+}$, as the divalent transition metal ion binds to the terdentate tpy functionality, one from each ligand strand. The Cd(II) metal ion centres adopt a distorted octahedral coordination geometry. Upon reaction of $\mathbf{L^I}$ with Cu(I) metal ion forms a trinuclear double-helical complex $[Cu_2(\mathbf{L^I})_2]^{4+}$. The Cu(I) metal ion binds to two (py-py) bidentate domain, one from each ligand strand as the ligand partitions giving the Cu(I) metal ion centre distorted tetrahedral coordination geometry (Figure 1.25).

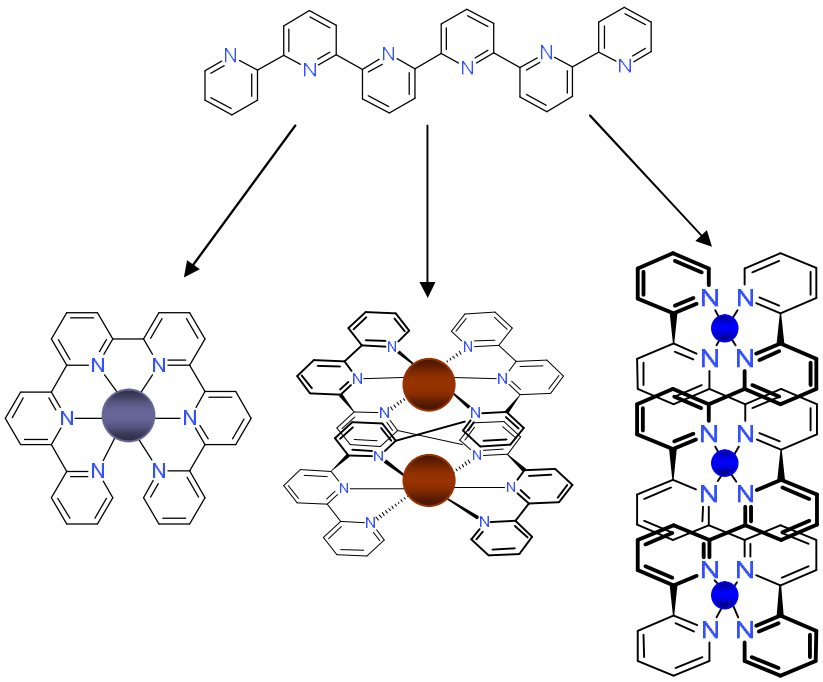

Figure 1.25. Possible complexes of spy derivatives to metal ions.

Rice and coworkers have established the synthesis and coordination chemistry of a series of polydentate *N*-donor ligands based on pyridyl and thiazole donors, preparing a new class of ligand for the assembly of helicates.[67, 68] The inclusion of the five-membered thiazole unit into the backbone of the chain results in a natural partitioning of the ligand strand into separate binding domains (Figure 1.26).

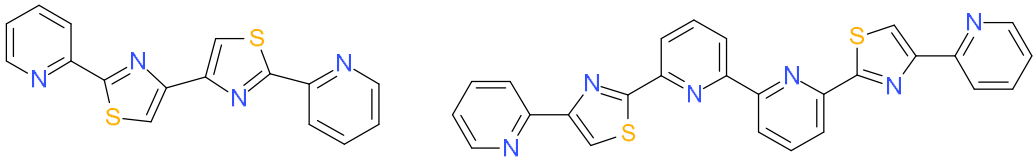

L^{v} **L^{w}**

Figure 1.26. Pyridyl-thiazole ligands produce by Rice *et al*.

The two pyridyl-thiazole ligands **L^{v}** and **L^{w}** both contain py-tz units differing as a bidentate pyridine unit has been inserted between the two thiazole rings of **L^{v}**. **L^{v}**, although potentially a tetradentate chelate, partitions into two bidentate py-tz units by twisting about the central C-C bond, as the two thiazole units cannot coordinate to the same metal ion.[69, 70] This is a geometric effect that arises from the presence of the adjacent five-membered

heterocyclic rings, leading to the formation of dinuclear triple helicates with Cu(II), Zn(II) and Co(II) ions. All three complexes are very similar to each other as all metal centres are of distorted octahedral coordination geometry. Although $\mathbf{L^w}$ is potentially a hexadentate chelate it does not act in this manner as it is able to coordinate in one of three different modes dependent of the metal ion. Upon complexation with Cu(II) and Zn(II) metal ions, a dinuclear double helicate is formed as the acts as a bis-bidentate py-tz chelate noticeably the central bipyridyl unit is uncoordinated. Upon reaction with Ni(II) a double helicate is also formed however, in this case the ligand is partitioned into two terdentate py-tz-py domains. Upon coordination with Cd(II) the ligand partitions into terdentate py-tz-py and bidentate py-tz coordination domains with the terminal pyridyl units not coordinated.

1.7 Allosteric Interactions

Self-assembly and self-organisation require molecular components containing two or more interaction sites, allosteric interactions are vital to this behaviour. Allostery occurs when the occupation of a given site leads to a change in the binding features of other site(s) making binding either easier or more difficult.[2] Allosteric effects play an important role in biology, for example in an enzyme the conformational changes induced by the binding effector and regulating the activity. For supramolecular architectures the ability of ligands to partition into different binding domains is active for the formation of transition-metal complexes, thus ligands are designed and synthesised to contain binding sites of differing nature and number.[71, 72] Therefore, by reaction of such ligand with metal ions a particular disposition of binding sites is achieved resulting in the target supramolecular assembly. Rebek *et al* first demonstrated allosteric effect with macrocyclic polyethers, these structures incorporate two remote but independent sites showing that the transport of alkali metal ions by the crown ether site was subject to the simple control by binding a transition metal at the bipyridyl site.[73, 74] Within the macrocyclic polyether (Figure 1.27) two binding sites are present, the

crown ether for the binding of alkali or ammonium ions and the 2,2'-bipyridyl unit for the binding of transition metal ions.

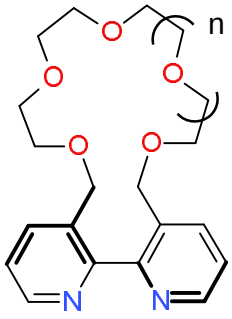

L^x

Figure 1.27. Rebek *et al*. macrocyclic polyether **L^x**.

Although these sites are separate they are not expected to behave independently, however chelation of transition metal ions at the bipyridyl unit forces the benzylic hydrogens toward each other lowering the dihedral angle to near 0°, consequently directing the benzylic oxygens away from each other in such manner that they both cannot be part of the ether cavity. Binding of the crown ether to an alkali metal bring the oxygen atoms closer together fixing the position of the benzyl hydrogen atoms with a dihedral angle *ca.* 90° (Figure 1.28).

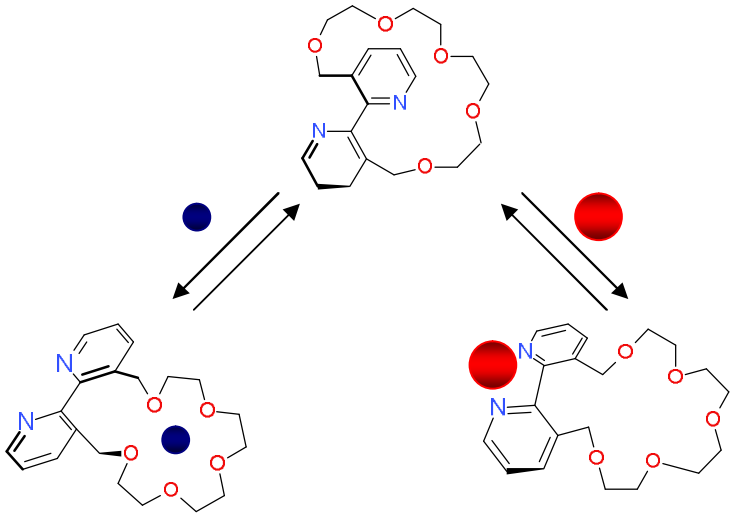

Figure 1.28. Binding induced conformation changes adopted by **L^x**.

Rice and coworkers have since investigated allosteric interactions demonstrating the formation of helicate species can also be controlled by such factors.[75, 76] Designing novel ditopic pyridine-thiazole (py-tz) based helicates. $\mathbf{L^y}$ is contains a potentially tetradentate ligand chain with a remote crown ether receptor spanning the 3,3' –position of the bipyridyl unit (Figure 1.29).[77, 78]

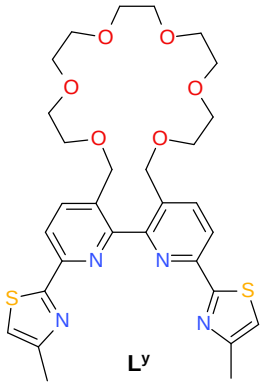

Figure 1.29. Novel Ditopic ligand $\mathbf{L^y}$.

Reaction of $\mathbf{L^y}$ with an equimolar amount of Hg(II) ions results in the self-assembly of a dimercury double stranded helicate $[Hg_2(\mathbf{L^y})_2]^{4+}$. The ligand partitions into two *bis*-bidentate binding domains by increase of the the bipyridyl interannular dihedral angle allowing each ligand to bridge the two Hg(II) centres. Each of the Hg(II) centres has a distorted tetrahedral coordination geometry formed by coordination of two py-tz bidentate N-donor units, one from each ligand, each ligand is twisted about the central bond bond between the two pyridine rings. An excess of Na(I) cation was reacted with the Hg(II) complex resulting in the formation of $[Hg_2(\mathbf{L^y})_2Na_2]^{6+}$. Both crown ethers partially coordinate the Na(I) ions, the inability of the Na(I) ions to coordinate all of the oxygen atoms from the crown ether is expected as the crown-6 type section is known to be too big to optimally coordinate the Na(I) cation. In contrast to this, when $[Hg_2(\mathbf{L^y})_2]^{4+}$ is reacted with excess Ba(II) ions a mononuclear complex is formed $[Hg(\mathbf{L^y})Ba]^{+}$. The ligand is almost planar with a shallow twist displayed due to the unfavourable steric interactions between the methylene substituents on the central bipyridyl core. The barium is ten-coordinate and strongly bonded to all six oxygen atoms

from the crown ether , with oxygen atoms of two perchlorate anions acting as bidentate O-donor ligands. All the oxygen atoms from the crown ether moiety form bonds to Ba(II) demonstrating good size match between the ion and the crown-6 section (Figure 1.30).

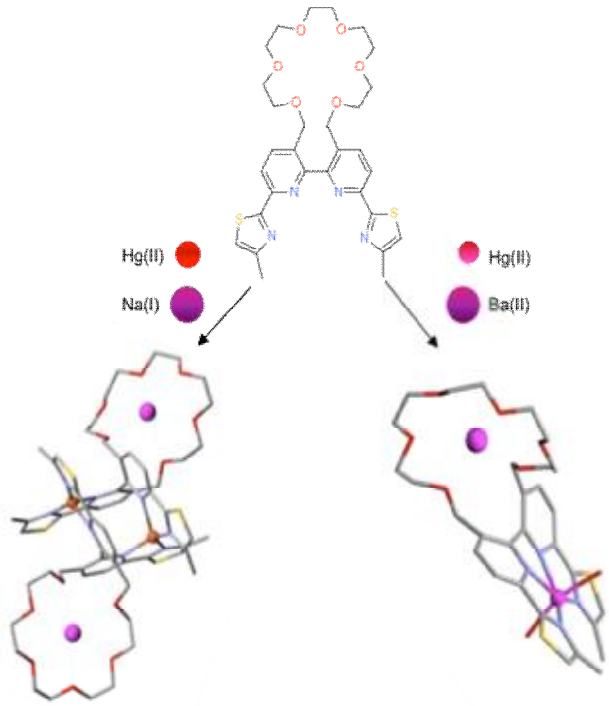

Figure 1.30. Allosteric reprogramming of **L^{y}.**

Such control of self-assembly for each complex can be attributed to one of two factors. Firstly, an electrostatic effect as coordination of barium to the helicate leads to a higher charged 8+ ion. Consequently, unassembly of the mononuclear species lowers the electrostatic repulsion increasing the entropy of the system, yet this change in structure may also be attributed to an allosteric effect. In summary, demonstrating how ligand-binding domains can be changed or '*reprogrammed*' by a combination of electrostatic and allosteric effects.

1.7.1 Ditopic Ligands

A ditopic ligand possesses two guest binding sites that are capable of coordinating various or specific guests. Ditopic ligands have gained considerable attention in recent years with synthesis and characterisation of a vast range of examples reported.[79, 80] In most cases they contain a macrocyclic unit attached to another metal-ion binding site.

Beer and coworkers[81] reported the synthesis of a novel allosteric bis crown ether ligand **L^z**, containing a 2,2'-bipyridyl fragment whose binding of a diquat dication substrate is dependent upon the absence of a cobound transition metal guest at the bipyridyl site. Results demonstrated that the presence of a transition metal ion at the bipyridyl nitrogen sites of **L^z** leads to a rigid conformation of the two benzo-crown ether units, when the N-donor units are uncoordinated the ligand possesses a degree of conformational freedom (Figure 1.31). Coordination of the two benzo-crown ether units with $[Ru^{II}(bipy)_2]PF_6$ unit causes the bipyridyl unit to approach near planarity therefore restricting the conformational freedom of the crown ether group, so coordination of the dication in between the two benzo-crown ethers units is unfavourable as they are now in close proximity, cofacial to one another disfavouring the intercalation of the planar diquat dication but favouring the formation of intramolecular sandwich complexes with spherical alkali metal cationic guest such as sodium.

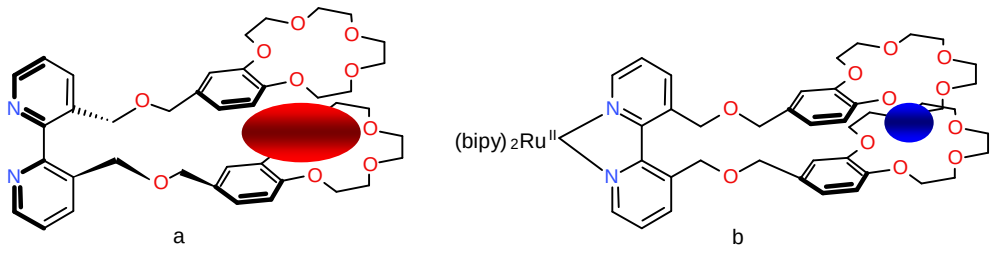

Figure 1.31. Conformations adopted by **L^z** (a) upon reaction with the diquat dication, (b) upon reaction with $[Ru^{II}(bipy)_2(PF_6)$ and Na^+ ions.

M. D. Ward and coworkers reported a well-designed yet simple example of a ditopic ligand,[82] preparation of a series of ligands in which a phenanthroline binding site is attached to a adjacent crown ether unit of various sizes. This new series of ditopic phenanthroline-crown ethers ligands contain two metal

binding sites of which are directly fused. The NN chelating site of the phenanthroline is capable of coordinating transition metal cations, and the pendant crown ether fragment capable of binding group I and II metal ions.

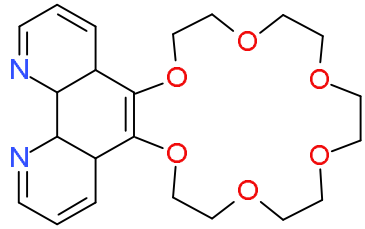

Figure 1.32. Ditopic ligand $\mathbf{L}^{\mathbf{aa}}$.

Reaction of $\mathbf{L}^{\mathbf{aa}}$ with $[Ru^{II}(bipy)_2Cl_2]\cdot 2H_2O$ resulted in a range of complexes of $[Ru^{II}(bipy)_2(\mathbf{L}^{\mathbf{aa}})][PF_6]_2$. The redox properties of the ruthenium complex $[Ru^{II}(bipy)_2(\mathbf{L}^{\mathbf{aa}})]^{2+}$ were investigated upon addition of barium ions. $[Ru^{II}(bipy)_2(\mathbf{L}^{\mathbf{aa}})][PF_6]_2$ shows the typical redox properties of a $[Ru(bipy)_3]^{2+}$ derivative, with a Ru(II)/Ru(III) couple at -0.89 V *vs.* ferrocene/ferrocenium (Fc/Fc^+), and three ligand centred couples at -1.74, -1.93 and -2.17 V vs. Fc/Fc^+ in MeCN. Upon addition of Ba^{2+} to the solution, the ligand centre becomes broader, but the Ru(II)/Ru(III) couple undergoes a gragual positve shift to +0.94 V. Demonstrating clearly that the barium ions are coordinated by the crown ether unit causing slight electrostatic destabilisation of the Ru(III) state.

1.8 Circular Helicates

The rational design of polynuclear helicates is one of the major achievements of metallosupramolecular chemistry. These linear structures formed by self-assembly and consist of two or more multidentate ligand strands that are helically wrapped about a central array of metal cations. Not only can polynuclear double-, triple-, and quadruple-stranded helicates now be made in a predictable fashion, they can also be programmed to express certain structural features of higher order complexity. This goal may be achieved by elaborating on the basic design principles that govern helicate formation itself, such as, careful consideration of ligand topology and metal stereoelectronic

preferences and, amongst others, can entail: 1) directional control over ligand alignment, 2) selective incorporation of different metal cations, and 3) selective incorporation of different ligand strands within a helical array. However, the formation of the helicates' higher nuclearity cousin, the cyclic helicate, is conversely less well understood. One of the major problems in the formation of these higher nuclearity assemblies is that the design principles that apply to helicate formation, *i.e.* using a ligand that contains two binding domains that coordinate *different* metal ions, equally apply to the formation of cyclic helicates. For the larger cyclic species to preside in solution, the formation of the entropically favoured dimer has to be prevented and this can be achieved by intermolecular interactions (*e.g.* templation by anions) or by intramolecular interactions which stabilise the formation of the cyclic species relative to its double-stranded alternative.

A striking example has been demonstrated by Lehn and coworkers[83], using tris-2,2'-bipyridine ligand $\mathbf{L_{bb}}$ and $FeCl_2$ resulting in a pentanuclear circular helicate. The pentanuclear circular helicate has a pentagonal shape and encloses a strongly bound chloride anion that tightly fits into its central cavity (Figure 1.33).

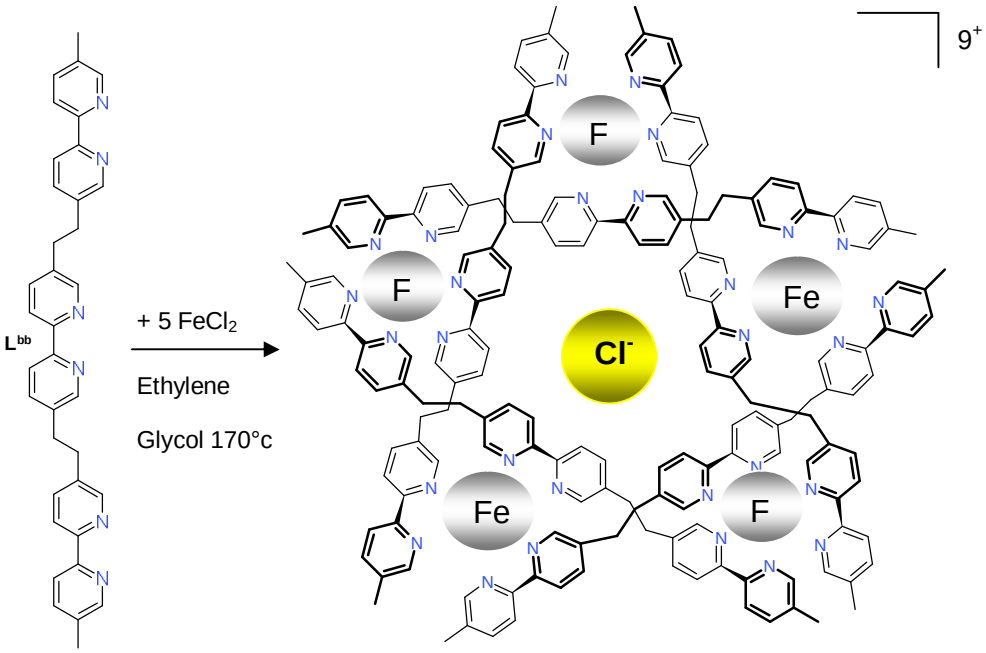

Figure 1.33. Self assembly of the pentanuclear circular helicate from five $\mathbf{L_{bb}}$ ligand strands and five Fe(II) ions in the presence of chloride anions.

Due to the short linkers between bipyridine units the terminal and the central bipyridine cannot be arranged around the same metal ion. Therefore, each Fe(II) ion is complexed by three bipyridine units, one from each of three different ligand strands. The chloride anion bound in the centre of the helicate cannot be exchanged for other anions such as PF_6^- or $CF_3SO_3^-$ demonstrating the selectivity of the circular helicate for Cl^-. To build upon this result, it was of interest to Lehn and coworkers to investigate the features controlling the self-assembly of such circular helical architecture or in the metal salt. If another iron salt is used within this reaction, such as $Fe(BF_4)_2$, the pentanuclear circular helicate structure does not form, instead the resulting structure is a hexanuclear circular helicate. In presence of the smallest anion, Cl^-, the self-assembly forms a pentanuclear circular helicate. However, with larger anions, such as SO_4^{2-}, BF_4^- and SiF_6^{2-}, the resulting structure is the hexanuclear circular helicate and with Br^- anion which if of an intermediate size yields a mixture of the pentanuclear and hexanuclear circular helicates. The charge of the anion has a little influence on the structure formed, as in the hexanuclear circular helicate is obtained with both mono- and divalent anions. The structure depends on the size of the anion to be included in the circular helicate formation, clearly demonstrating the role played by the chloride anion in templating the assembly of the pentanuclear circular helicate.

An elegant example by Ward[84] and coworkers demonstrates the coordination chemistry of a tetradentate ligand consisting of two pyrazole-pyridine arms that are connected by a 1,8-naphthalenediyl spacer, $\mathbf{L^{cc}}$. Reaction of $\mathbf{L^{cc}}$ in a ratio 1:1 with $[Cu(MeCN)_4](OTf)$ or $[Ag(MeCN)_4](BF_4)$ in acetonitrile resulted in mononuclear complex, in which both pyrazole-pyridine arms of $\mathbf{L^{cc}}$ coordinate to the sole metal ion. The Cu(I) metal centre is of an intermediate coordination geometry between that of planar and tetrahedral, there is no evidence of close contact between the Cu(I) centre and the triflate anions. The $[Ag(\mathbf{L^{cc}})](BF_4)$ is similar, with exception that the two ligand arms are essentially coplanar, providing a planar array of four N-donor around the Ag(I) ion (Figure 1.34).

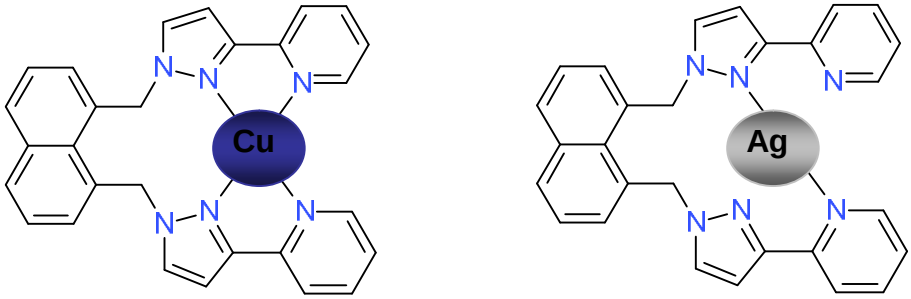

Figure 1.34. Structures of the complex cations of [Cu($\mathbf{L}^{cc}$)]OTf and [Ag($\mathbf{L}^{cc}$)](BF_4).

With electrospray mass spectrometry (ESMS) the spectra of these complexes in solution showed the presence of strong ions corresponding to both the monocations $[M(\mathbf{L}^{cc})]^+$. For [Cu($\mathbf{L}^{cc}$)](OTf) there was no evidence for the formation of higher-nuclearity species. However, for [Ag($\mathbf{L}^{cc}$)](BF_4) the spectra contained weak signals corresponding to traces of oligmers $\{Ag_2(\mathbf{L}^{cc})_2(BF_4)\}^+$, $\{Ag_3(\mathbf{L}^{cc})_3(BF_4)_2\}^+$ and $\{Ag_4(\mathbf{L}^{cc})_4(BF_4)_3\}^+$, these are minor components and only appear for [Ag($\mathbf{L}^{cc}$)](BF_4) and not [Cu($\mathbf{L}^{cc}$)](OTf), suggesting a templating role played by the tetrafluoroborate anion. To see if the tetrafluoroborate could act as a template for circular helicates, Ward and coworkers then prepared in the same way a complex of $\mathbf{L}^{cc}$ with [Cu(MeCN)$_4$](BF_4), resulting in the formation of $[Cu_4(\mathbf{L}^{cc})_4][BF_4]$. The four ligand strands and four metal cations assemble in a cyclic helical array, the Cu(I) ions are of four coordinate from the pyrazole-pyridine units, with the tetrafluoroborate anion occupying the central cavity. The circular helicate structure is a result of the four ligand strands having an “over and under” conformation (Figure 1.35).

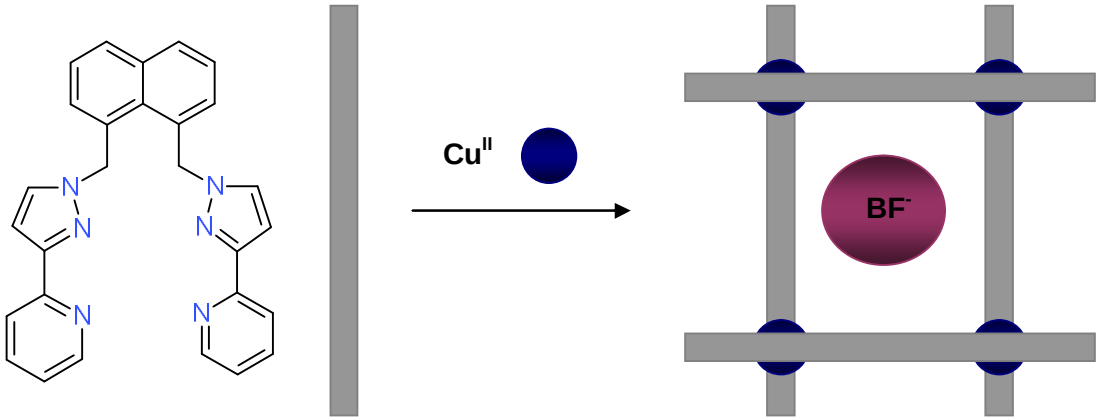

Figure 1.35. Cartoon representation showing complex cation of $[Cu_4(\mathbf{L}^{cc})_4](BF_4)$.

An elegant example of circular helicates has been demonstrated by Gloe and coworkers[85], who prepared a series of bis-bidentate ligands containing bis-pyridylimine, differing from each other in the linking element (-S-, -CH_2-, -O-) (Figure 1.36).

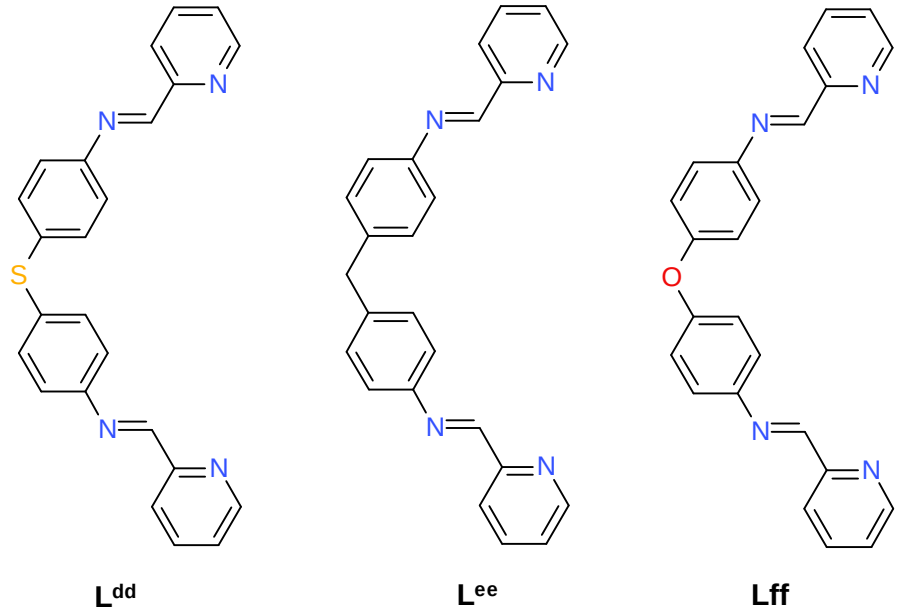

$\mathbf{L^{dd}}$ $\mathbf{L^{ee}}$ $\mathbf{Lff}$

Figure 1.36. Bis-pyridylimine ligands, $\mathbf{L^{dd}}$, $\mathbf{L^{ee}}$ and $\mathbf{L^{ff}}$, respectively.

Reaction of $\mathbf{L^{dd}}$-$\mathbf{L^{ff}}$ with $CuSO_4{\cdot}5H_2O$ in a MeOH/H_2O/MeCN mixture (v/v 2:1:2) afforded crystal complexes with one independent $[Cu\mathbf{L^{(dd\text{-}ff)}}(SO_4)]_6$. Each Cu(II) ion has distorted octahedral coordination environments involving interactions with two bidentate pyridylimine strands of different ligands and one bidentate sulfate ion, leading to a neutral hexanuclear circular helicate. Clearly, the coordinating sulfate anions play a key role in formation of the hexanuclear *meso*-helicates as upon reaction with different anions such as SO_4^{2-}, ClO_4^- or NO_3^- only the cationic, non-cyclic triple helicate $[Cu_2(\mathbf{L^{ee}})_3]^{4+}$ was produced under the same conditions, demonstrating in this case, how topological control of the assembly process is clearly associated with the bidentate coordination of the sulfate anions, directing the formation of a double rather than a triple-stranded structure around the octahedrally coordinated Cu(II) metal in centres. The significant changes of the linking angle of the pyridylimine strands by variation of the linking element, however, has little influence on the resulting structures.

2. Metal Ion Recognition in Bi- and Tri- Metallic Helicates

Described in this chapter is the synthesis and coordination chemistry of a new class of ditopic segmental pyridyl-thiazole (py-tz) N-donor ligands which demonstrate an alternative strategy for selectively introducing different metals into polynuclear arrays. These particular ligands comprise of isomeric N-donor domains via a flexible oxo-propylene bridge. The simplest of these ligands **L**^{1}, contains two identical tridentate pyridyl-thiazole-pyridyl N_3 binding domains linked by an oxo-propylene bridge. The ligand **L**^{2} is very similar to **L**^{1}, however, the tridentate N_3 domains are structural isomers of one another with one of the units comprising of a pyridyl-thiazole-pyridyl N_3 binding domain and the other containing a thiazole-pyridyl-pyridyl domain. The ligand **L**^{3} contains the two isomeric domains in a similar fashion to **L**^{2} but these units are separated by a central bipyridine unit. Insertion of a bidentate bipyridyl fragment into the middle of the chain of **L**^{2} leads to a tritopic ligand **L**^{3} (Figure 2.1).

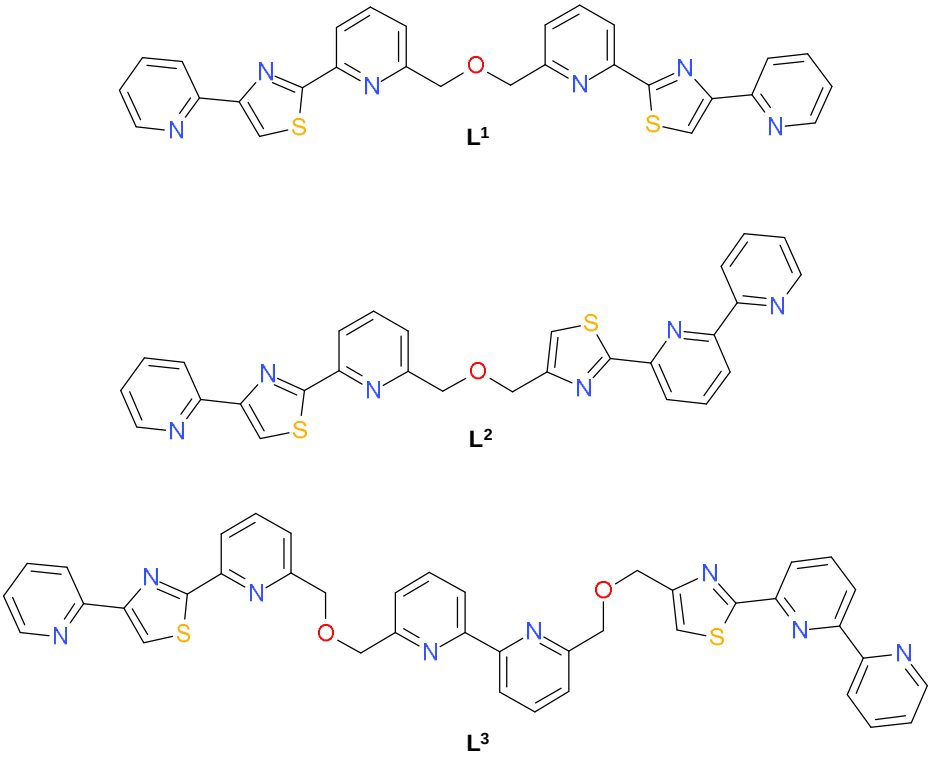

Figure 2.1. The new class of ditopic segmental pyridyl-thiazole N-donor ligands **L**^{1}, **L**^{2} and **L**^{3}.

2.1 Ligand synthesis

The three polydentate pyridyl-thiazole-containing ligands **L^1**, **L^2** and **L^3** were synthesised in an analogous fashion via a multi-step synthetic route.

2.1.1 Synthesis of L^1

The synthesis of ligand, **L^1**, was achieved by the Williamson ether synthesis reaction of its hydroxy-methylene and chloro-substituted py-tz-py constituents. A solution of methyl picolinate-6-thioamide (1) and the hydrobromide salt of α-bromoacetyl pyridine was refluxed for 6 hours, the solution was left to stand overnight during which time a precipitate formed, which was isolated by filtration giving the tridentate ester (2) as a tan solid. Reduction of the ester (2) to the alcohol (3) was achieved by addition of $NaBH_4$ to a solution of (2) in EtOH. Formation of the primary alcohol was confirmed by the appearance of a singlet at 3.67 ppm corresponding to the $–CH_2OH$ group and the disappearance of the signal at 4.05 ppm corresponding to the methyl ester. Reaction of the alcohol (3) with thionyl chloride and Na_2CO_3 in DCM resulted in the chloro derivative (4) after work-up and purification by column chromatography. The final step in the formation of **L^1** involved the reaction of the alcohol (3) and the chloromethylene derivative (4) in anhydrous THF with an excess of NaH and a catalytic amount tetraethylammonium iodide. The solution was then refluxed and monitored by TLC until all of the chloro-derivative was consumed. Aqueous work-up and purification by column chromatography gave **L^1** (Scheme 2.1). Conformation of the successful formation of the ether-containing ligand **L^1** was obtained by ^{1}H NMR which showed a total of 8 aromatic signals in the ^{1}H NMR spectrum as well as a singlet at 4.85 ppm corresponding to the four methylene protons. Furthermore an ion in the ESI-MS was observed at *m/z* 521 corresponding to ($L^1 + H^+$).

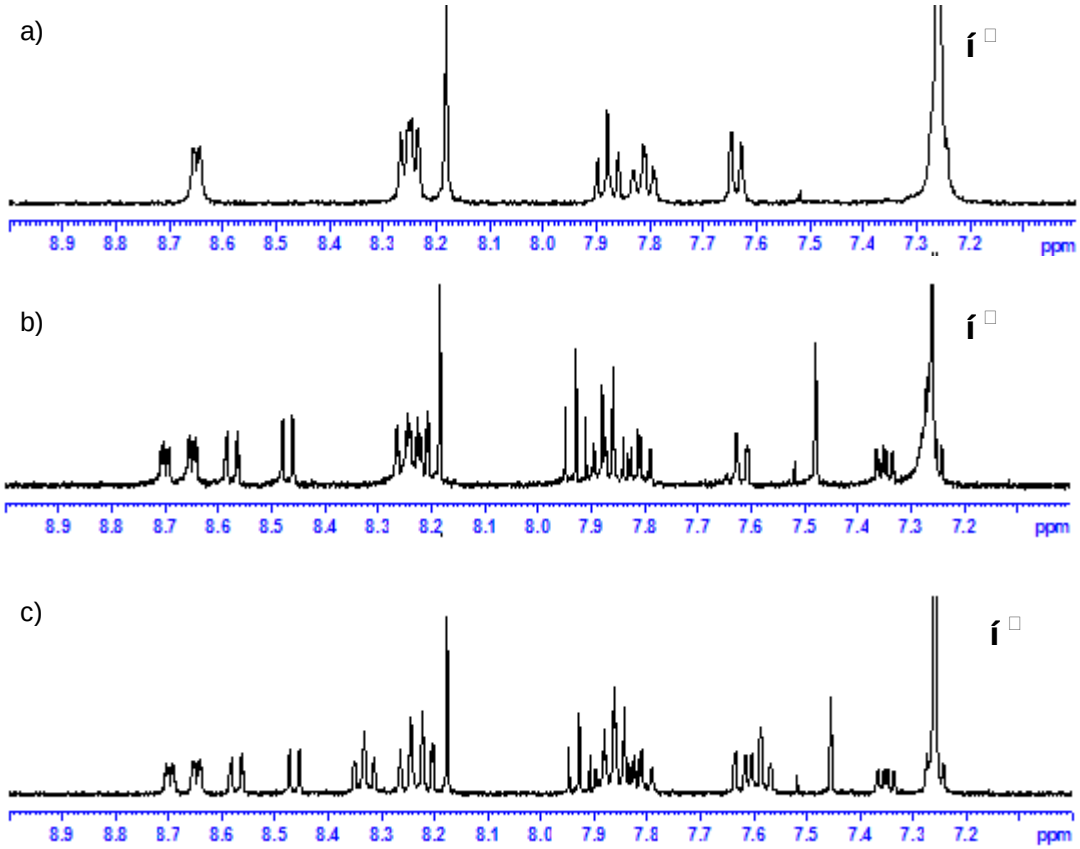

Figure 2.2. Aromatic regions in the ^{1}H NMR spectra ($CDCl_3$) of L^1 (a), L^2 (b) and L^3(c) (**í** indicates a signal overlapped by $CDCl_3$).

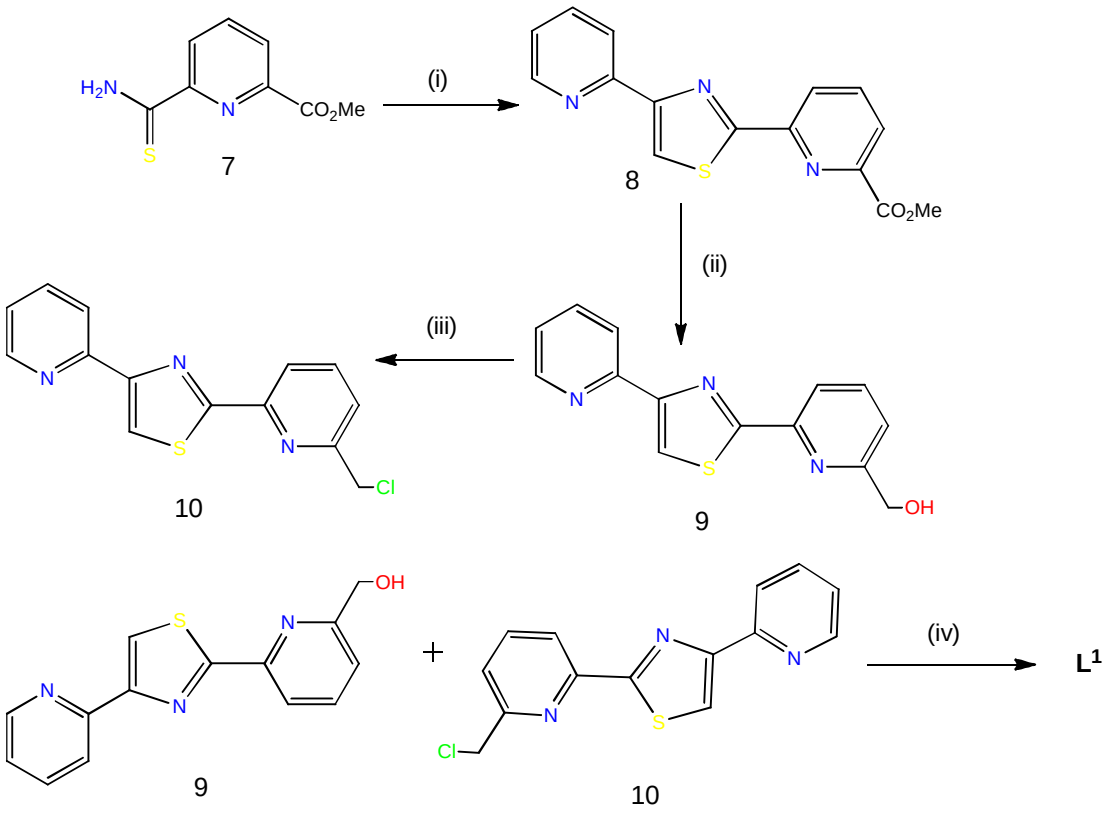

Scheme 2.1. Synthesis of $\mathbf{L^1}$. Reagents and conditions: (i) α-bromoactyl pyridine, EtOH, reflux (ii) $NaBH_4$, EtOH, reflux (iv) thionyl chloride, DCM, reflux (v) NaH, anhydrous THF, EtN_4I, reflux.

2.1.2 Synthesis of L^2

The synthesis of $\mathbf{L^2}$ is outlined in Scheme 2.2 and was carried out in a similar manner to that of $\mathbf{L^1}$. To a solution of 2,2'-bipyridine-6-thioamide in EtOH was added ethyl bromopyruvate and the reaction refluxed for 6 hours, resulting in the formation of pyridine-pyridine-thiazole ester (6). Reduction of the ester (6) to the alcohol (7) was achieved by addition of $NaBH_4$ to a solution of (6) in EtOH. A solution of the alcohol (7) and tetraethylammonium iodide in anhydrous THF, under dinitrogen, was added in excess of NaH. After 1 hour at 50°C a solution of one equivalent of the chloro derivative (4) in THF solution was added and the reaction refluxed. Purification by column chromatography gave $\mathbf{L^2}$. The ^{1}H NMR of this material is complex but it does show a total of 16 aromatic signals, consistent with the unsymmetrical nature of the ligand, although some are coincident. Furthermore, the two signals present at 4.85 and 4.82 ppm indicates there are two different methylene

groups, which would be expected in ligand L^2. An ion in the ESI-MS at *m/z* 521 ($L^2 + H^+$) confirms formation of the ligand.

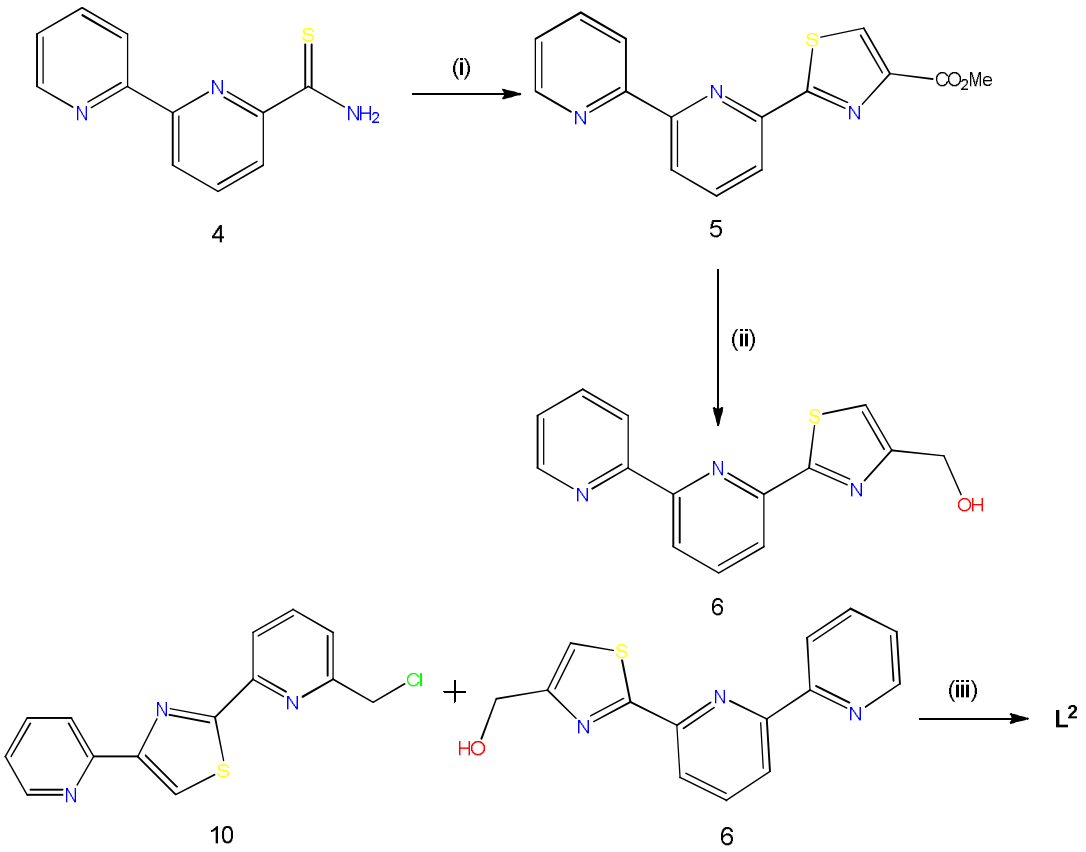

Scheme 2.2. Synthesis of **L²**. Reagents and conditions: (i) ethyl bromopyruvate, EtOH, reflux (ii) $NaBH_4$, EtOH, reflux (iii) NaH, anhydrous THF, EtN_4I, reflux.

2.1.3 Synthesis of L³

To a solution of py-tz-py tridentate alcohol (3) and tetraethylammonium iodide in anhydrous THF, under dinitrogen was added NaH and the reaction stirred at 50°C for 1 hour. To this was then added a solution of 2,2'-bipyridine-6,6'-dichloromethyl[86] in THF and the reaction was refluxed. The reaction was monitored by TLC and upon consumption of the dichloromethyl derivative the ligand was purified by column chromatography giving (8) as a colourless solid. Again analysis of this product by ^1H NMR is non-trivial but a total of 14 signals in the aromatic region is consistent with the suggested structure. However, the presence of three signals between 4.85 – 4.69 ppm confirms the presence

of an unsymmetrical oxo-propylene bridge and a chloromethylene unit. Further conformation was provided by ESI-MS with an ion present at *m/z* 486 corresponding to (8 + H^+). The final ligand was prepared by reaction of a solution of the alcohol (7), tetraethylammonium iodide and NaH in anhydrous THF, with one equivalent of the chloro derivative (4). Purification by column chromatography gave **L^3** as a colourless solid. Analysis by ^{1}H NMR spectroscopy revealed a highly complex spectrum, but careful analysis did show a total of 22 aromatic signals although some of these were coincident. The methylene region is more informative and shows a total of three different environments; signals at 4.92 and 4.91 ppm correspond to the methylene units attached to the terminal ligand domains. A signal at 4.90 ppm (corresponding to 4H) is attributed to the methylene groups of the central bipyridine unit which are sufficiently similar within the molecule to be coincident in the ^{1}H NMR. Analysis by ESI-MS supports formation of the ligand **L^3** with an ion present at *m/z* 718 corresponding to (L^3 + H^+).

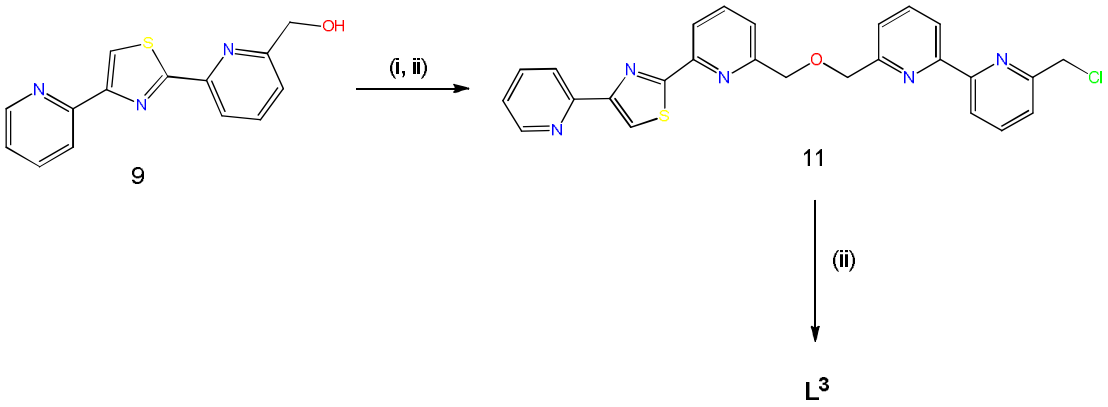

Scheme 2.3. Synthesis **L^3**. Reagents and Conditions: (i) 6,6'-dichloromethyl -2,2'-bipyridine (ii) NaH, anhydrous THF, EtN_4I, reflux.

2.2 Coordination Chemistry

2.2.1 Complexes of L^1 with Zinc (II)

The reaction of **L**^{1} with an equimolar amount of $Zn(ClO_4)_2 \cdot 6H_2O$ in acetonitrile produced a colourless solution. Analysis by ESI-MS gave an ion at m/z 1469 which corresponds to dinuclear double-stranded helicate complex $[Zn_2(\mathbf{L}^{1})_2]^{4+}$. The ^{1}H NMR studies are consistent with the formation of a helicate species with a total of 8 aromatic signals and one AB spin system (two doublets) corresponding to the diastereotopic methylene group. Slow diffusion of diethyl ether into the resulting solution afforded colourless crystals of X-ray quality. Single crystal X-ray crystallographic analysis confirmed the formation of the dinuclear double-stranded helicate $[Zn_2(\mathbf{L}^{1})_2]^{4+}$ (Figure 2.3).

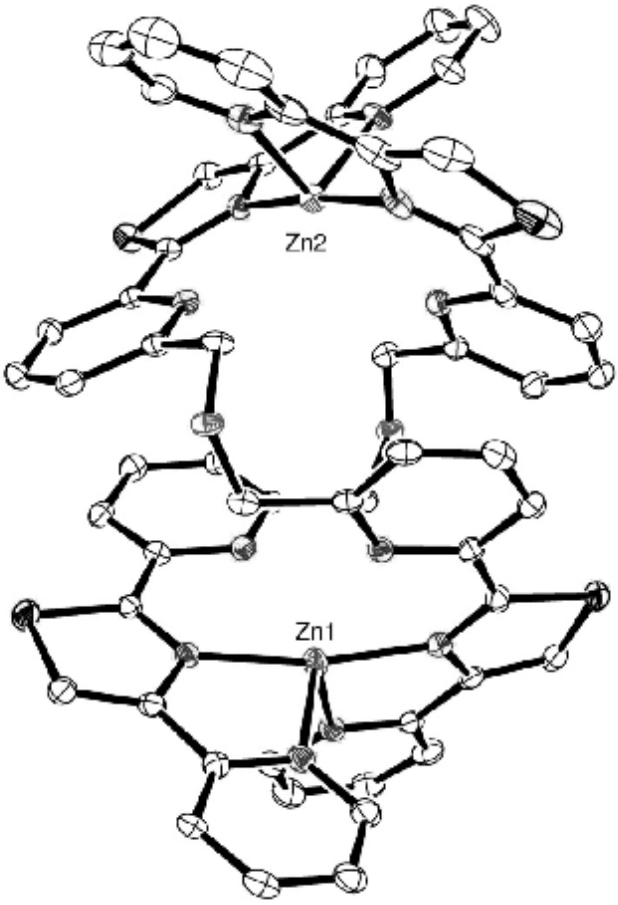

Figure 2.3. Solid state structure of the complex cation $[Zn_2(\mathbf{L}^{1})_2]^{4+}$.

The crystal structure confirms the formation of a dinuclear double helicate, with the ligand partitioning into two separated binding domains, each of which coordinates a different metal ion. However, the distance between the Zn^{2+} ion and the terminal thiazole-pyridyl domains (1.962(3) - 2.183(3) Å) is much shorter than distance to the central pyridyl unit (2.551(3) - 2.610(3) Å). As these are too long to be considered to be bonding interactions, the pyridyl-thiazole-pyridyl unit, although potentially tridentate, acts as a bidentate thiazole-pyridyl unit resulting in a distorted tetrahedral 4-coordinate metal ion.

Initially this would seem somewhat surprising and it would be expected that the domain acts a tridentate unit giving an octahedral 6-coordinate metal ion. However, the inclusion of a 5-membered thiazole unit in the *middle* of the ligand strand increases the bit angle of the donor unit such that the bite angle is too divergent for the domain to act as a tridentate unit.

Bond	Bond length **Å**
Zn(1)-N(11)	2.184(4)
Zn(1)-N(21)	1.972(3)
Zn(1)-N(71)	2.134(3)
Zn(1)-N(81)	1.986(3)
Zn(2)-N(51)	1.978(2)
Zn(2)-N(61)	2.160(3)
Zn(2)-N(111)	1.962(3)
Zn(2)-N(121)	2.136(4)

Table 1. Selected bond lengths (Å) for the complex cation $[Zn_2(\mathbf{L^1})_2]^{4+}$.

Bond	Bond angle (°)	Bond	Bond angle (°)
N(11)-Zn(1)-N(21)	77.4(1)	N(41)-Zn(2)-N(51)	70.7(1)
N(11)-Zn(1)-N(31)	146.6(1)	N(41)-Zn(2)-N(61)	148.3(1)
N(11)-Zn(1)-N(71)	109.3(1)	N(41)-Zn(2)-N(111)	108.5(1)
N(11)-Zn(1)-N(81)	108.7(1)	N(41)-Zn(2)-N(121)	81.5(1)
N(21)-Zn(1)-N(31)	70.4(1)	N(51)-Zn(2)-N(61)	77.7(1)
N(21)-Zn(1)-N(71)	109.4(1)	N(51)-Zn(2)-N(111)	172.4(1)
N(21)-Zn(1)-N(81)	168.5(1)	N(51)-Zn(2)-N(121)	108.4(1)
N(31)-Zn(1)-N(71)	89.9(1)	N(61)-Zn(2)-N(111)	102.8(1)
N(31)-Zn(1)-N(81)	101.7(1)	N(61)-Zn(2)-N(121)	110.0(1)
N(71)-Zn(1)-N(81)	78.3(1)	N(111)-Zn(2)-N(121)	78.7(1)

Table 2. Selected bond angles (°) for the complex cation $[Zn_2(\mathbf{L}^1)_2]^{4+}$.

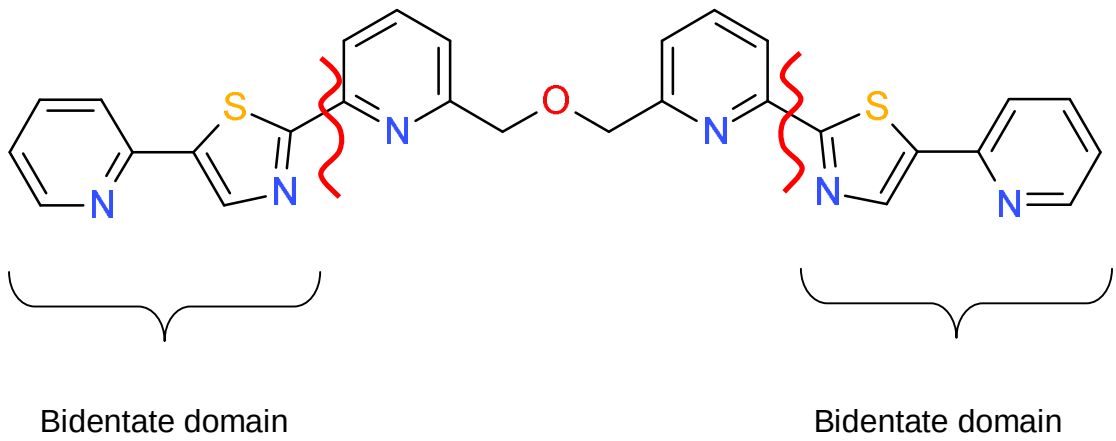

Figure 2.4. Structure of $\mathbf{L}^1$ showing partitioning of the ligand into two bidentate binding domains.

2.2.2 Complexes of L^2 with Zinc(II)

Reaction of **L^2** with one equivalent of $Zn(ClO_4)_2 \cdot 6H_2O$ in acetonitrile produced a colourless solution and ESI-MS studies confirmed the formation of the dinuclear complex with an ion at *m/z* 1469 corresponding to the dizinc(II) species $[Zn_2(\mathbf{L^2})_2(ClO_4)_3]^+$. In this ligand strand there are two different binding domains. One of the domains consists of a potentially tridentate pyridyl-thiazole-pyridyl unit and the other domain is an isomer of this with the 5-membered thiazole unit at the end of the tridentate unit (tz-py-py). Although we have no solid state characterization of this helicate species it would seem highly likely that the ligand partitions into two domains each of which will coordinate a different metal ion, in an analogous fashion to L^1. Again it would be expected that the pyridyl-thiazole-pyridyl domain coordinates the Zn^{2+} ion via the terminal bidentate thiazole-pyridyl as is observed in $[Zn_2(\mathbf{L^1})_2]^{4+}$. However, the other thiazole-pyridine-pyridine domain could possibly act as a tridentate unit as the thiazole is at the end of the ligand strand and in this position the 5-membered may not have such a marked effect on the divergent nature of the tridentate unit. Indeed, in previous reported work this thiazole-pyridine-pyridine does act as a tridentate donor unit with Zn^{2+}.[70] The 500 MHz ^1H NMR spectrum of the complex $[Zn_2(\mathbf{L^2})_2]^{4+}$ in CD_3CN features two major sets of resonances in addition to a third minor set which accounts for < 5 % of the total ligand (peak integration also suggests that one of the major species is in slight excess of the other). The most informative part of the spectra is the aliphatic region (4.1-3.1 ppm), which contains four AB spin systems (eight doublets Figure 2.5a). This indicates there are two complexes formed upon reaction of the ligand with Zn^{2+}. However, this is still consistent with the formation of the dinuclear double helicate as the ligand is unsymmetrical and helicate formation will result in both *HH*- and *HT*-isomers. In the head-to-head isomer the zinc ions will be coordinated by the same two donor units i.e. each metal centre will be either coordinated by two py-tz-py or two tz-py-py domains. In the head-to-tail isomer each of the zinc ions will be coordinated in an identical donor environment by a py-tz-py unit from one ligand and a tz-py-py domain from the other.

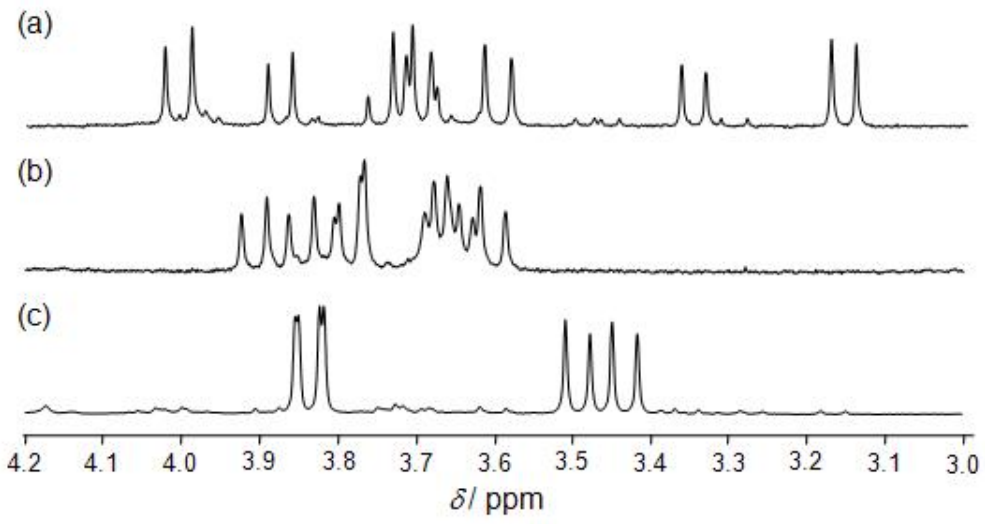

Figure 2.5. Methylene regions in the ^{1}H NMR spectra (CD_3CN) of (a) $[Zn_2(\mathbf{L^2})_2]^{4+}$, (b) $[Hg_2(\mathbf{L^2})_2]^{4+}$ and (c) $[HgZn(\mathbf{L^2})_2]^{4+}$.

2.2.3 Complexes of L^2 with Mercury(II)

Reaction of $\mathbf{L^2}$ with an equimolar amount of $Hg(ClO_4)_2{\cdot}4H_2O$ in acetonitrile gives a colourless solution and analysis by ESI-MS shows an ion at *m/z* 1741 corresponding to the dimercury(II) complex $[Hg_2(\mathbf{L^2})_2]^{4+}$. As with the other L^2-containing species $[Zn_2(\mathbf{L^2})_2]^{4+}$ this ligand would be expected to partition into two different binding domains and coordinate two different metal ions. The 500 MHz ^{1}H NMR spectrum of the complex $[Hg_2(\mathbf{L^2})_2]^{4+}$ in CD_3CN again shows eight diastereotopic methylene protons indicating the occurrence of both *HH*- and *HT*-isomers in approximately equal quantities (Figure 2.5b) as would be expected for a dinuclear double helicate.

2.2.4 Complexes of L^2 with Mercury(II) and Zinc(II)

Upon reaction of $\mathbf{L^2}$ with both $Hg(ClO_4)_2{\cdot}4H_2O$ and $Zn(ClO_4)_2{\cdot}6H_2O$ in the ratio 2:1:1 in acetonitrile produced a colourless solution. ESI-MS confirmed the formation of a dinuclear bimetallic double helicate with an intense ion peak at *m/z* 1605 for the perchlorate adduct $[HgZn(\mathbf{L^2})_2(ClO_4)_3]^+$ and only minor signals for the homodimetallic complexes (*m/z* 1469 corresponding to $\{Zn_2(\mathbf{L^2})_2(ClO_4)_3\}^+$ and *m/z* 1737 corresponding to $\{Hg_2(\mathbf{L^2})_2(ClO_4)_3\}^+$).

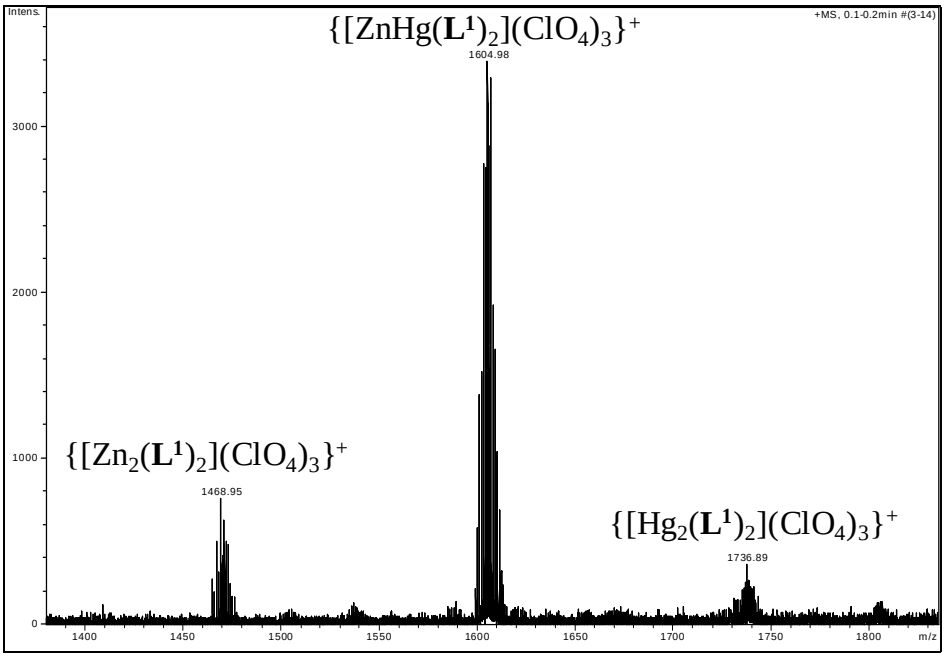

Figure 2.6. ESI-MS spectrum of the reaction of two equivalents of $\mathbf{L^2}$ with one each of $Hg(ClO_4)_2{\cdot}4H_2O$ and $Zn(ClO_4)_2{\cdot}6H_2O$.

Slow diffusion of diethyl ether into the resulting solution produced colourless crystals. Analysis by single crystal X-Ray diffraction confirmed the formation of the dinuclear bimetallic double helicate $[HgZn(\mathbf{L^2})_2(ClO_4)_3]^+$ (Figure 2.7).

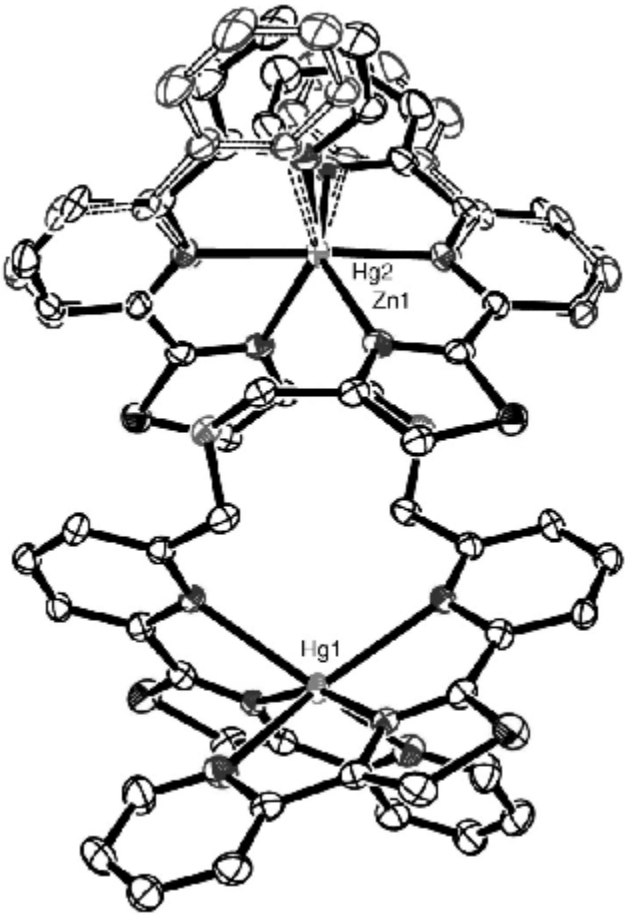

Figure 2.7. Solid state structure of the complex cation $[HgZn(\mathbf{L^2})_2(ClO_4)_3]^+$.

Bond	Bond length Å	Bond	Bond length Å
Hg(1)-N(41)	2.495(3)	Zn(1)-N(11A)	2.12(1)
Hg(1)-N(41')	2.495(3)	Zn(1)-N(11A')	2.12(1)
Hg(1)-N(51)	2.174(4)	Zn(1)-N(21A)	2.094(9)
Hg(1)-N(51')	2.174(4)	Zn(1)-N(21A')	2.094(9)
Hg(1)-N(61)	2.672(5)	Zn(1)-N(31)	2.32(1)
Hg(1)-N(61')	2.672(5)	Zn(1)-N(31')	2.32(1)

Table 3. Selected bond lengths (Å) for the complex cation $[HgZn(\mathbf{L^2})_2(ClO_4)_3]^+$.

Bond	Bond angle (°)	Bond	Bond angle (°)
N(41)-Hg(1)-N(51)	70.7(1)	N(11A)-Zn(1)-N(21A)	77.5(6)
N(41)-Hg(1)-N(61)	133.9(1)	N(11A)-Zn(1)-N(31)	150.5(8)
N(41)-Hg(1)-N(41)	109.2(1)	N(11A)-Zn(1)-N(11A)	97.3(7)
N(41)-Hg(1)-N(51)	122.3(1)	N(11A)-Zn(1)-N(21A)	105.6(7)
N(41)-Hg(1)-N(61)	79.6(1)	N(11)-Zn(1)-N(31)	90.4(6)
N(51)-Hg(1)-N(61)	67.1(1)	N(21A)-Zn(1)-N(31)	73.0(5)
N(51)-Hg(1)-N(41)	122.3(1)	N(21A)-Zn(1)-N(11A)	105.6(7)
N(51)-Hg(1)-N(51)	159.8(1)	N(21A)-Zn(1)-N(21A)	175.5(9)
N(51)-Hg(1)-N(61)	103.5(1)	N(21A)-Zn(1)-N(31)	103.9(7)
N(61)-Hg(1)-N(41)	79.6(1)	N(31)-Zn(1)-N(11A)	90.4(6)
N(61)-Hg(1)-N(51)	103.5(1)	N(31)-Zn(1)-N(21A)	103.9(7)
N(61)-Hg(1)-N(61)	127.4(1)	N(31)-Zn(1)-N(31)	96.9(6)
N(41)-Hg(1)-N(51)	70.7(1)	N(11A)-Zn(1)-N(21A)	77.5(6)
N(41)-Hg(1)-N(61)	133.9(1)	N(11A)-Zn(1)-N(31)	150.5(8)
N(51)-Hg(1)-N(61)	67.1(1)	N(21A)-Zn(1)-N(31)	73.0(5)

Table 4. Selected bond angles (°) for the complex cation $[HgZn(\mathbf{L^2})_2(ClO_4)_3]^+$.

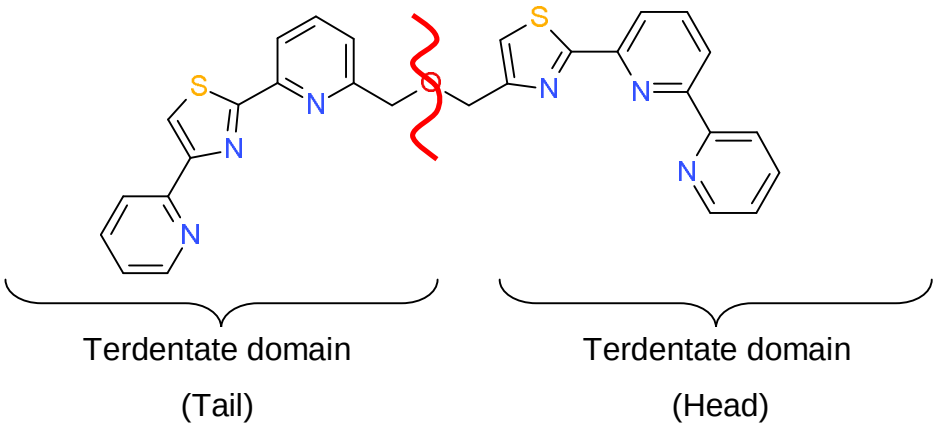

Figure 2.8. Structure of **L²** showing partitioning of the ligand into two terdentate binding domains.

As expected, in the solid state the complex cation is a helicate, with both strands of L^2 aligned in a *HH*-manner along the central metal axis. The Hg^{2+} ion is pseudo-octahedrally coordinated by two near orthogonal py-tz-py units. The Zn^{2+} ion is pseudo-octahedrally coordinated by the other isomeric py-py-tz domain. However, this domain is host for a Zn^{2+} ion in only *c.a.* 70 % of the crystal. For the remainder, this site complexes another Hg^{2+} ion. The partial site occupancies of the metals are well-defined and have been modelled in conjunction with disorder in the coordinating py-py-tz rings, which alternate between one of two positions (Figure 2.8). Not surprisingly, the terminal py rings move further away from the metal centre in the *c.a.* 30 % of the crystal containing only the dimercury(II) helicate. We note that an identical picture was obtained from two independent measurements on crystals grown from different solutions of *HH*-$[HgZn(L^2)_2]^{4+}$, despite the latter clearly being the predominant species present on both occasions. The metal/site scrambling observed in the solid-state is thus likely the result of kinetic resolution effects operating during the crystallisation process.

2.2.5 Solution State Characterisation of HH-[HgZn(L^2)$_2$]$^{4+}$

Further evidence for the formation of the head-to-head complex of *HH*-[HgZn(**L^2**)$_2$]$^{4+}$ was gained through ^{1}H and two-dimensional spin-spin (^{1}H-^{1}H COSY) and dipole-dipole (^{1}H-^{1}H NOSEY) NMR spectra of solutions of *HH*-[HgZn(**L^2**)$_2$]$^{4+}$ in CD_3CN (500 MHz, 298 K), shown in Figure 2.5c, 2.9 and 2.10, respectively, along with complete peak assignment for the aromatic protons of **L^2**.

In the ^{1}H NMR spectra there are a total of 16 signals in the aromatic region and 2 AB spin systems (four doublets) corresponding to the diastereotopic methylene protons. The four doublets in this region indicates that only one of the *HT* or *HH* isomers is present and it is probable that the isomer found in solution is the same as that observed in the solid state (i.e. *HH*). It is also worth noting that none of the signals correspond to the heterometallic helicates [Zn$_2$(**L^2**)$_2$]$^{4+}$ and [Hg$_2$(**L^2**)$_2$]$^{4+}$ and the only species in solution is HH-[HgZn(**L^2**)$_2$]$^{4+}$. The ^{1}H-^{1}H COSY NMR spectrum shows that the two thiazole protons (H^8 and H^{16}) appear as two well separated singlet's in the one-dimensional spectra. Proton H^8 is assigned the low frequency singlet (δ = 7.2 ppm) based on the observation that, in solid state this proton is held above the plane of an aromatic ring in the complementary ligand strand of *HH*-[HgZn(**L^2**)$_2$]$^{4+}$ and hence subject to shielding ring current anisotropies.

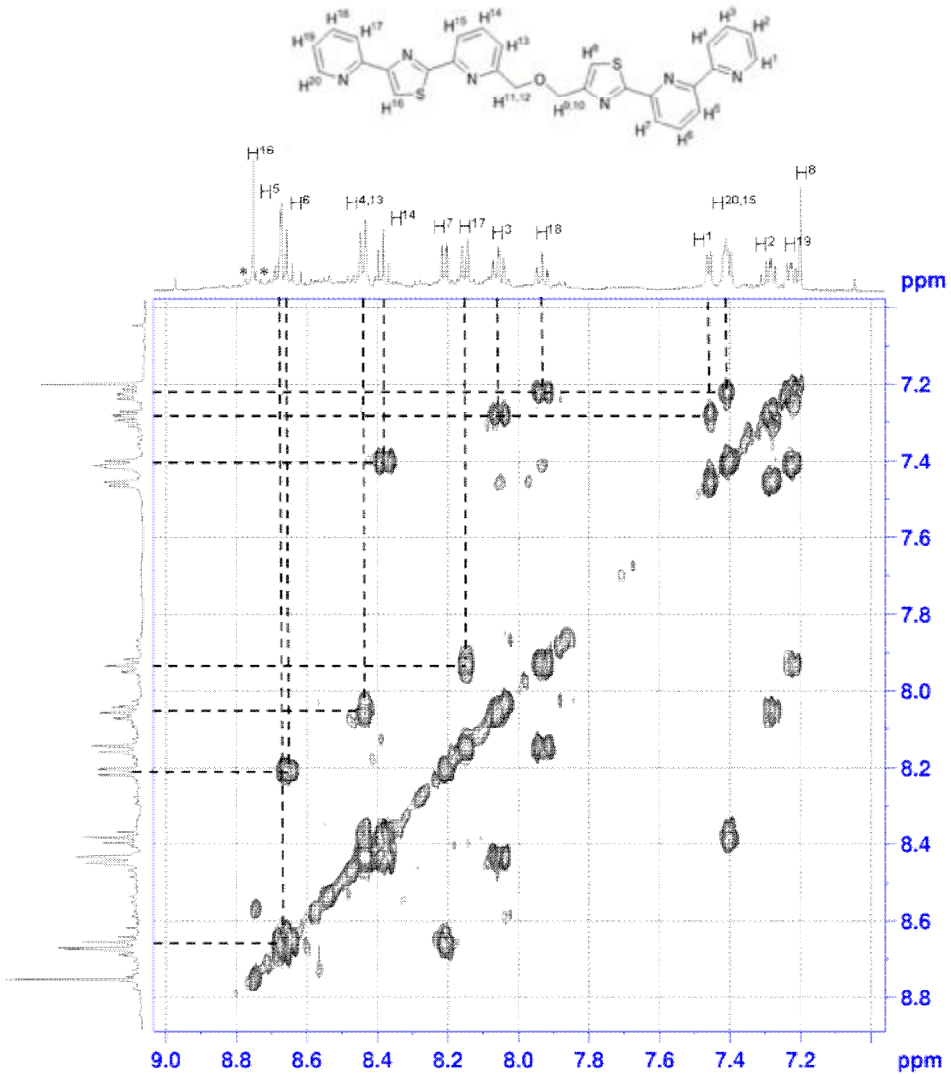

Figure 2.9. Aromatic region of the ^{1}H-^{1}H COSY spectrum of *HH*-[HgZn(**L**^{2})$_2$]$^{4+}$ in CD_3CN.

In the ^{1}H-^{1}H NOSEY spectrum of the complex *HH*-[HgZn(**L**^{2})$_2$]$^{4+}$ in CD_3CN, we observed through-space dipole-dipole interactions between proton pairs H^4/H^5 and H^{16}/H^{17} as a result of *trans- trans-* to *cic- cic*-conformational changes occurring on complexation of the terminal py-py and py-tz moieites, respectively, to the metals. However, there are few through-space interactions between protons on different ligand strands. Only a very low intensity off-diagonal peak present for the proton H^7/H^{13}, for which the non-bonded distance in the solid state is *ca.* 3 Å, noted that this is the shortest inter-strand proton-proton distance in the crystal structure of *HH*-[HgZn(**L**^{2})$_2$]$^{4+}$.

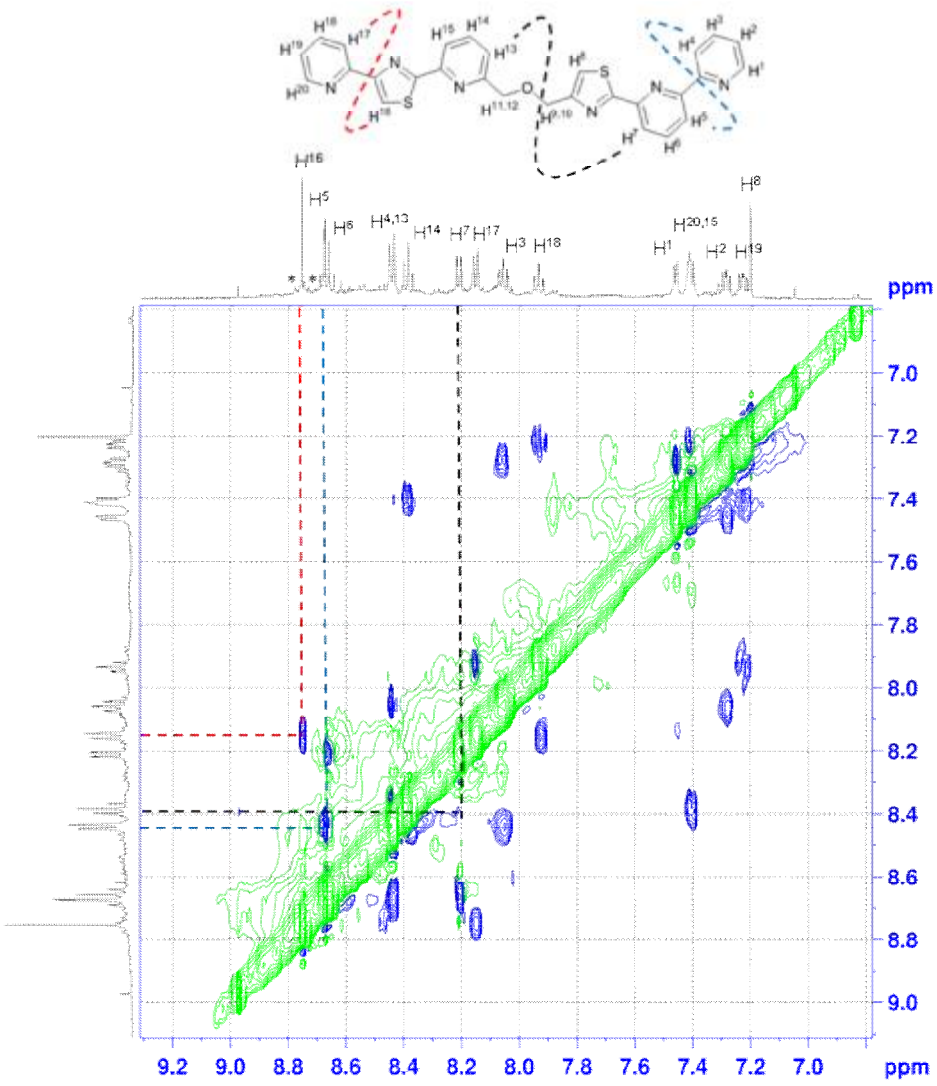

Figure 2.10. Aromatic region of the 1H-1H NOESY spectrum of *HH*-[HgZn($\mathbf{L^2}$)$_2$]$^{4+}$ in CD_3CN.

$\mathbf{L^2}$, contains two tridentate N_3 binding domains py-py-tz and py-tz-py linked by an oxo-propylene bridge. Self-assembly with equimolar amounts of either Hg^{2+} or Zn^{2+} ions gives numerous isomers of a dinuclear double-stranded complex in solution. However, combining $\mathbf{L^2}$ with both Hg^{2+} and Zn^{2+} ions in the ratio of 2:1:1 results in the formation of a strikingly different species in solution. The ^{1}H NMR (Figure 2.5c) shows the methylene groups are diastereotopic and the presence of only four such doublets points to the near exclusive formation of a hetero-bimetallic complex *HH*-[HgZn($\mathbf{L^2}$)$_2$]$^{4+}$. The high selectivity for *HH*-[HgZn($\mathbf{L^2}$)$_2$]$^{4+}$ in solution is quite notable, assuming that the self-assembly process gives only saturated helical conformers of first order complexity,[87] then the observed *HH*-[HgZn(L^2)$_2$]$^{4+}$ is one of *seven* species (additionally: a *HH*-[HgZn(L^2)$_2$]$^{4+}$ in which the metals are inversed,

HT-$[HgZn(L^2)_2]^{4+}$, *HH*-$[Hg_2(L^2)_2]^{4+}$, *HT*-$[Hg_2(L^2)_2]^{4+}$, *HH*-$[Zn_2(L^2)_2]^{4+}$ and *HT*-$[Zn_2(L^2)_2]^{4+}$) competing for L^2 when ligand, Zn^{2+} and Hg^{2+} are combined in a 2:1:1 ratio. In the absence of directing effects, symmetry considerations state that all seven species would form in a statistical 1:1:2:1:1:1:1 ratio, respectively. That *HH*-$[HgZn(L^2)_2]^{4+}$ clearly presides in solution therefore requires that it be disposed to stabilising contributions which are absent in the other complexes.

The solid-state structure of *HH*-$[HgZn(\mathbf{L^2})_2]^{4+}$ holds nothing to suggest that inter-ligand interactions are responsible for its high relative stability. Intermetallic interactions and pre-organisation effects could be of greater importance, however, we suspect that the main reason for *HH*-$[HgZn(\mathbf{L^2})_2]^{4+}$ being selected is that the two binding sites of $\mathbf{L^2}$ are structurally very different. By varying the position of the thiazole unit from terminal (in py-py-tz) to central (in py-tz-py) has a pronounced effect on the respective bite angles of the tridentate chelates (Figure 2.11).

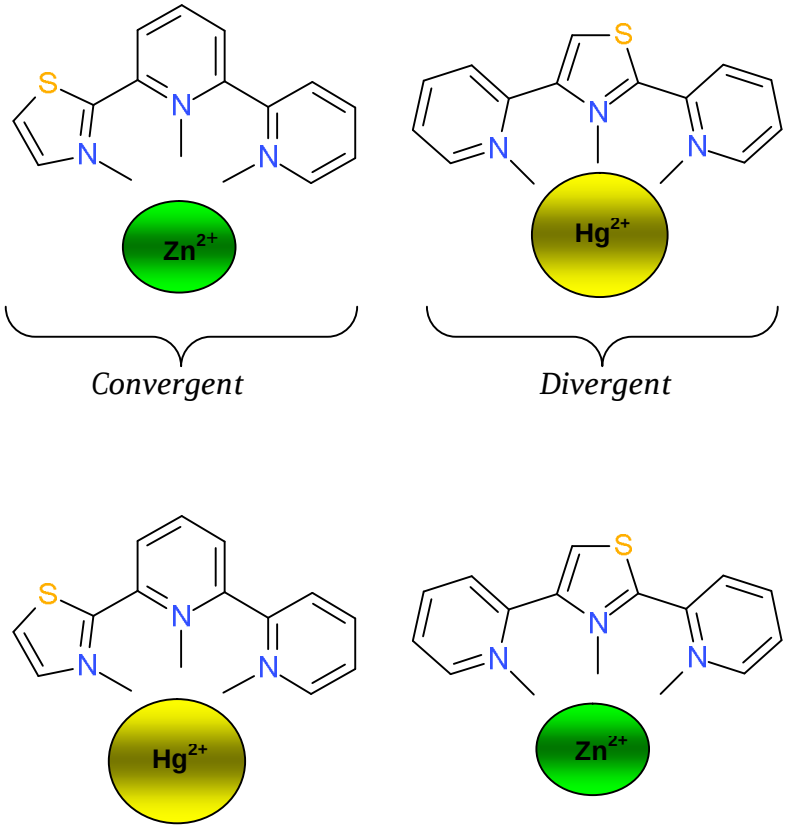

Figure 2.11. Illustration of respective bite angles of the tridentate chelates.

From the structural characterisation of $\mathbf{L^1}$ we can demonstrate that the py-tz-py unit can only coordinate Zn^{2+} via two of its N-donor domains, whereas from L^2 we show that Hg^{2+} can be coordinated by all three donor atoms within the tridentate py-tz-py domain. The difference in this ligands coordination behaviour is attributed to its divergent nature, which is more suitable for the diffuse Hg^{2+} ion (151 pm) which has a higher affinity for the geometrically more divergent py-tz-py unit, relative to the Zn^{2+} ion (134 pm). Previous work has shown that the isomeric tz-py-py domain can easily accommodate the zinc ion as the inclusion of the 5-membered thiazole unit at the *end* of the ligand chain does not produce a ligand as divergent as the py-tz-py domain which has a thiazole unit in the *middle* of the ligand chain. As a result a ligand that contains these two domains, upon reaction with transition metal ions of different size will result in each domain selectively coordinating different metal ions. As can be seen from the formation of *HH*-$[HgZn(\mathbf{L^2})_2]^{4+}$ these isomeric domains can be used to produce heterometallic self-assemblies.

2.2.6 Complexes with L^3

As we have shown that the different isomers of a unit containing two pyridine and one thiazole unit can differentiate between metals of different size we synthesized a ligand strand which will differentiate metal ions by both their size and coordination preference.

Reaction of two equivalents of $\mathbf{L^3}$ with one each of $Zn(ClO_4)_2{\cdot}6H_2O$, $Hg(ClO_4)_4{\cdot}4H_2O$ and $[Cu(MeCN)_4][PF_6]$ in CD_3CN gives an immediate orange colour in solution, typical of the metal-to-ligand charge transition of $[Cu(bipy)_2]^+$ -type chromophores. ESI mass spectrum shows peaks at *m/z* 2347 and 1101 for the hexafluorophosphate adducts $[HgCuZn(\mathbf{L^3})_2(PF_6)_4]^{4+}$ and $[HgCuZn(\mathbf{L^3})_2(PF_6)_3]^{2+}$, respectively, (Figure 2.12a and 2.12b), but the spectrum does contain a large number of other species are also clearly present. However, peaks for the latter diminish in intensity after tempering the solution at 60°C for a week, consistent with their being kinetic products. The 500 MHz ^1H NMR spectrum reflects these observations, as at early stages a complicated mixture of species is established in the spectra, whist only one set of peaks prevails on tempering the solution. The aliphatic region (4.1-3.1 ppm) (Figure 2.12c), clearly features eight doublets, as expected for the eight

diastereotopic methylene groups in a C_2-symmetric *HH*-[HgCuZn($\mathbf{L^3}$)$_2$]$^{5+}$ helicate.

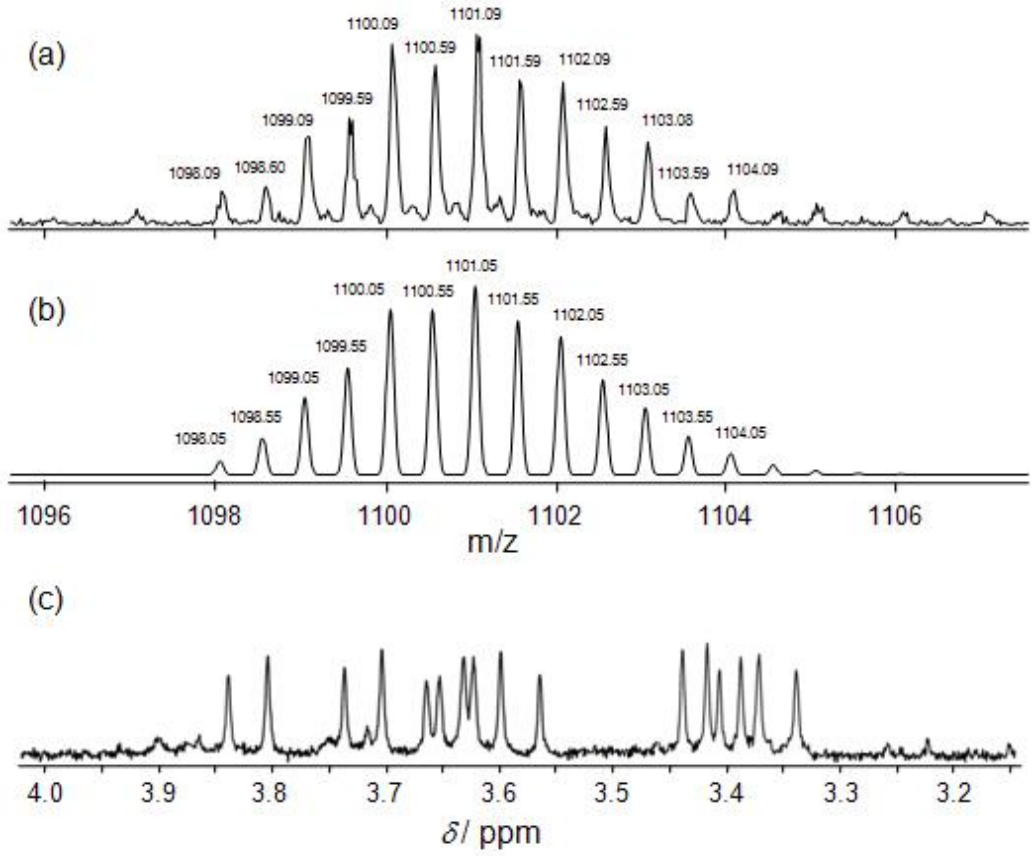

Figure 2.12. (a) Observed and (b) calculated isotropic distribution patterns for molecular ion [HgCuZn($\mathbf{L^3}$)$_2$(PF_6)$_3$]$^{2+}$, and (c) methylene region in the ^{1}H NMR spectrum (CD_3CN) of *HH*-[HgCuZn($\mathbf{L^3}$)$_2$]$^{5+}$.

In an analogous fashion to $\mathbf{L^2}$ reaction of the tritopic ligand $\mathbf{L^3}$ with $Zn(ClO_4)_2{\cdot}6H_2O$ and $Hg(ClO_4)_4{\cdot}4H_2O$ will result in the smaller Zn^{2+} ion coordinated by the tz-py-py domain and the larger Hg^{2+} ion coordinated by the isomeric py-tz-py domain. The Cu^+ ion, will be coordinated by the bidentate central bipyridine unit so that assembly of a double helicate assembly will result in the metal adopting a 4-coordinate tetrahedral geometry. As a result of the information held within the ligand strand a heterometallic trinuclear double helicate *HH*-[HgCuZn($\mathbf{L^3}$)$_2$]$^{5+}$ is formed.

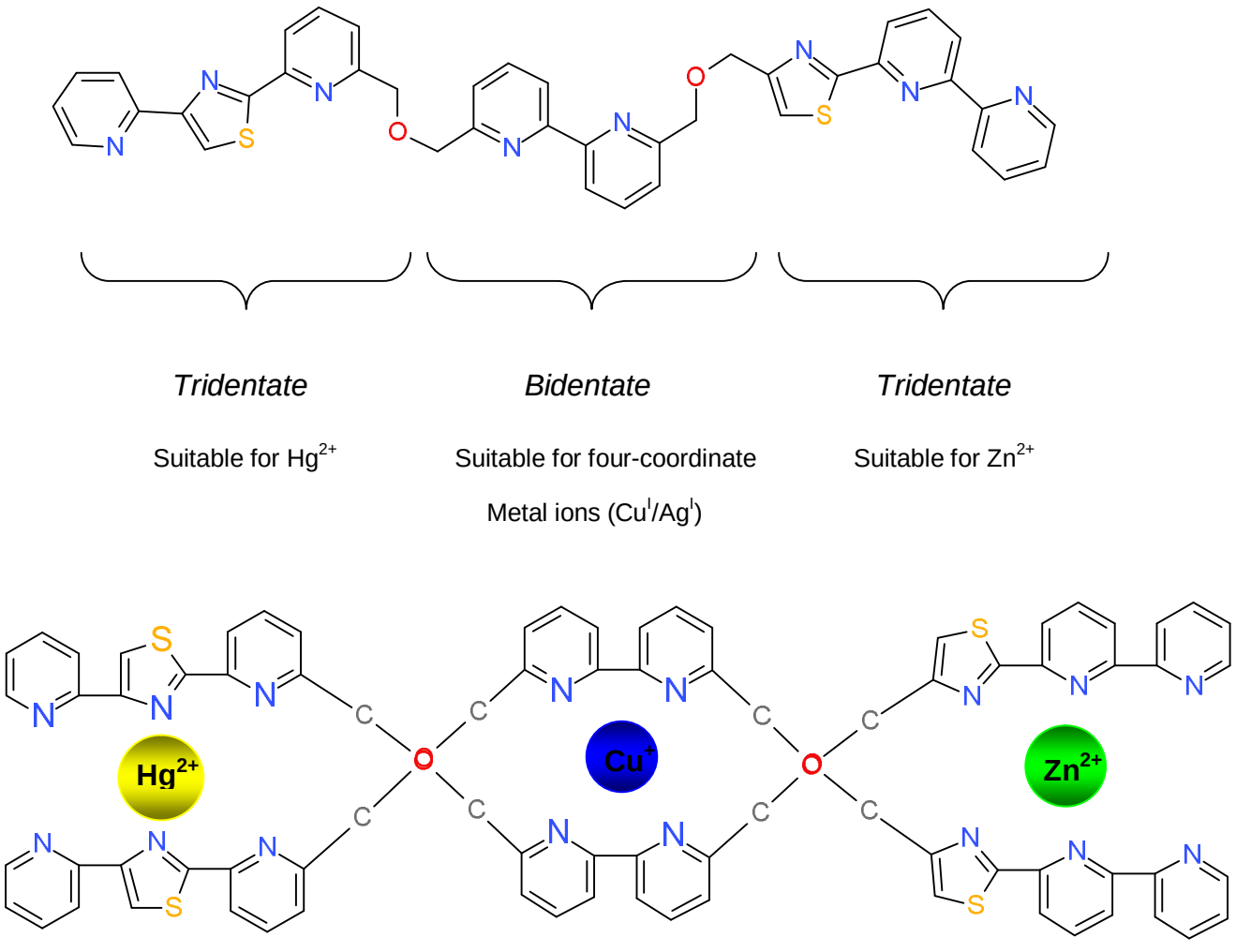

Figure 2.13. Illustration of binding domains of **L^3.**

In the absence of structural data we cannot be completely sure that a heterometallic trinuclear double helicate has formed or is the only product. However, the proposed structure is one of a very few that adequately accounts for the ESI and ^{1}H NMR data.

2.3 Conclusion

In conclusion, three novel ligands **L^1**, **L^2** and **L^3** were successfully synthesised and these ligands have shown how subtle geometric changes caused simply by varying the order of N-heterocyclic rings in a tridentate binding unit can lead to pronounced recognition effects. These changes dramatically modify the size of the binding unit and, consequently, allow for metal ion selectivity to be tuned. Combined with a classic bidentate chelate for selectively binding

tetrahedral cation, this approach has enabled the insertion of *three* different metals into a helical polynuclear array.

3. Control of Metallosupramolecular Assemblies by Metal Ionic Radii

Described in this chapter is the synthesis and coordination chemistry of a potentially hexadentate N-donor ligand, which forms either dinuclear double-stranded or pentanuclear circular helicates with different transition metal cations. This particular ligand **L**^{4}, contains two identical tridentate thiazole-pyridyl-pyridyl N_3 binding domains separated by a phenylene unit (Figure 3.1).

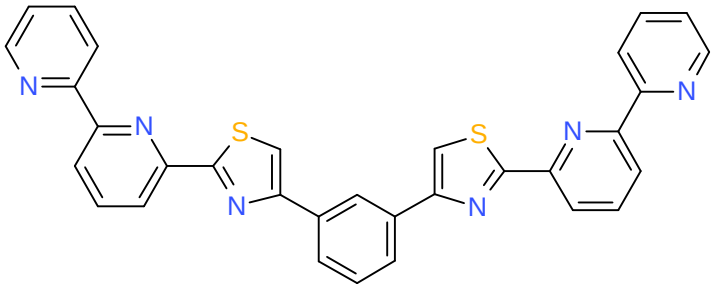

Figure 3.1. The potentially hexandentate ligand **L**^{4}.

3.1.1 Synthesis of L^{4}

The synthesis of **L**^{4} is outlined in scheme 3.1. The ligand was prepared by reaction of 2,2'-bipyridine-6-thioamide[88] with 1,3-di(α-bromoacetyl)benzene in EtOH and refluxed for 8 hours, during which time a white precipitate formed. Filtration followed by washing with EtOH and Et_2O afforded **L**^{4} as a white solid. Confirmation of the successful formation of **L**^{4} was obtained by ^{1}H NMR which showed a total of 11 aromatic signals including three signals arising from the phenyl spacer. Furthermore an ion in the ESI-MS was observed at *m/z* 552 corresponding to (**L**^{4} + H^{+}).

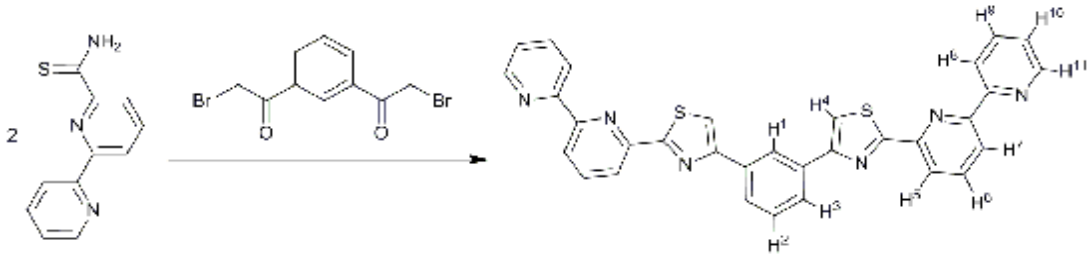

Scheme 3.1. Synthesis of **L**^{4}. Reagents and conditions: 1,3-di(α-bromoacetyl)benzene, EtOH, reflux.

3.2 Coordination Chemistry

3.2.1 Complexes of L^4 with Cadmium (II)

The reaction of **L^4** with an equimolar amount of $Cd(ClO_4)_2 \cdot 6H_2O$ in nitromethane results in a colourless solution. Analysis by ESI-MS gave ions at *m/z* 1076 and 1629 which correspond to $\{[Cd_2(\mathbf{L^4})](ClO_4)_3\}^+$ and $\{[Cd_2(\mathbf{L^4})_2](ClO_4)_3\}^+$ respectively, indicative of formation of a dinuclear double-stranded helicate complex $[Cd_2(\mathbf{L^4})_2]^{4+}$. The ^{1}H NMR studies are consistent with the formation of a helicate species with 11 signals, corresponding to the tridentate chelate and phenyl spacer units, present between 7.0 and 8.4 ppm. Slow diffusion of dichloromethane into the resulting solution afforded colourless crystals of X-ray quality. Single crystal X-ray diffraction studies confirmed the formation of the dinuclear double-stranded helicate $[Cd_2(\mathbf{L^4})_2]^{4+}$ (Figure 3.2).

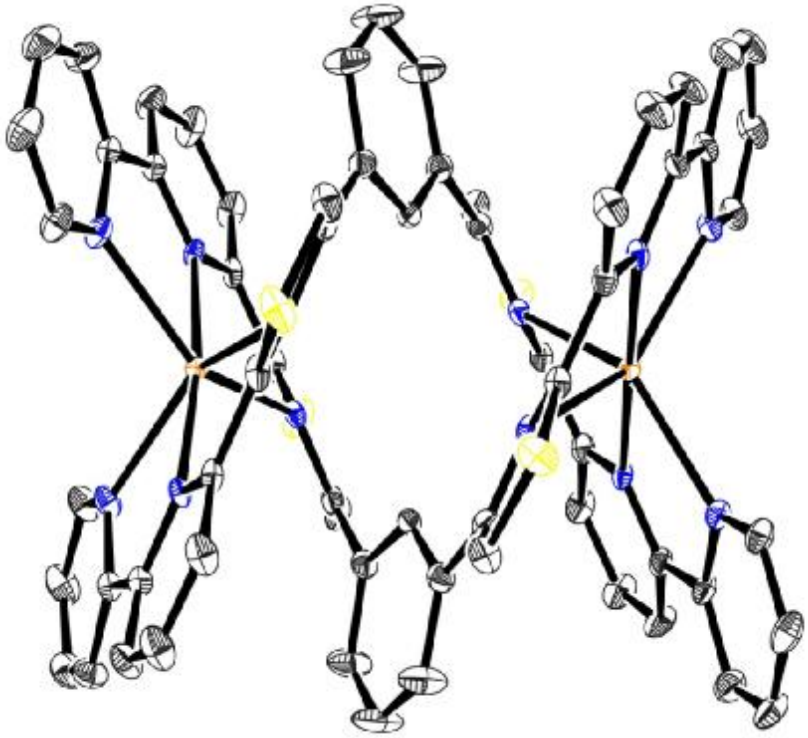

Figure 3.2. Solid state structure of complex cation $[Cd_2(\mathbf{L^4})_2]^{4+}$.

In the solid state the ligand partitions into two tridentate domains, each of which coordinates a different metal ion. The cadmium(II) centres have

distorted octahedral geometries, imparted by coordination of one tridentate thiazole-pyridyl-pyridyl domain from each ligand (Cd-N: 2.306(5)-2.464(5) Å).

Bond	Bond length (Å)
Cd(1)-N(11)	2.365(5)
Cd(1)-N(11')	2.365(5)
Cd(1)-N(21)	2.306(6)
Cd(1)-N(21')	2.306(6)
Cd(1)-N(31)	2.417(4)
Cd(1)-N(31')	2.417(4)
Cd(2)-N(51)	2.464(5)
Cd(2)-N(51')	2.464(5)
Cd(2)-N(61)	2.282(4)
Cd(2)-N(61')	2.282(4)
Cd(2)-N(71)	2.370(6)
Cd(2)-N(71')	2.370(6)

Table 5. Selected bond lengths (Å) for the complex cation $[Cd_2(\mathbf{L}^4)_2]^{4+}$.

Bond	Bond angle (º)	Bond	Bond angle (º)
N(11)-Cd(1)-N(21)	69.5(2)	N(51)-Cd(2)-N(61)	69.8(2)
N(11)-Cd(1)-N(33)	138.9(2)	N(51)-Cd(2)-N(71)	139.5(2)
N(11)-Cd(1)-N(11)	114.2(2)	N(51)-Cd(2)-N(51)	108.5(2)
N(11)-Cd(1)-N(21)	106.8(2)	N(51)-Cd(2)-N(61)	110.6(2)
N(11)-Cd(1)-N(31)	80.0(2)	N(51)-Cd(2)-N(71)	79.3(2)
N(21)-Cd(1)-N(31)	69.5(2)	N(61)-Cd(2)-N(71)	70.3(2)
N(21)-Cd(1)-N(11)	106.8(2)	N(61)-Cd(2)-N(51)	110.6(2)
N(21)-Cd(1)-N21)	173.5(2)	N(61)-Cd(2)-N(61)	179.3(2)
N(21)-Cd(1)-N(31)	114.3(2)	N(61)-Cd(2)-N71)	109.3(2)

N(31)-Cd(1)-N(11)	80.0(2)	N(71)-Cd(2)-N(51)	79.3(2)
N(31)-Cd(1)-N(21)	114.3(2)	N(71)-Cd(2)-N(61)	109.3(2)
N(31)-Cd(1)-N(31)	115.6(2)	N(71)-Cd(2)-N71)	121.1(2)
N(11)-Cd(1)-N(21)	69.5(2)	N(51)-Cd(2)-N(61)	69.8(2)
N(11)-Cd(1)-N(31)	138.9(2)	N(51)-Cd(2)-N(71)	139.5(2)
N(21)-Cd(1)-N(31)	69.5(2)	N(61)-Cd(2)-N(71)	70.3(2)

Table 6. Selected bond angles (°) for the complex cation $[Cd_2(\mathbf{L^4})_2]^{4+}$.

3.2.2 Complexes of L^4 with Zinc(II)

Reaction of $\mathbf{L^4}$ with one equivalent of $Zn(ClO_4)_2{\cdot}6H_2O$ in acetonitrile results in a colourless solution and ESI-MS studies show a number of low nuclearity fragments (*m/z*: 980, 1269 and 1532 corresponding to $\{[Zn_2(L^4)](ClO_4)_3\}^+$, $\{[Zn(L^4)_2](ClO_4)\}^+$ and $\{[Zn_2(L^4)_2](ClO_4)_3\}^+$ respectively), but also a peak at *m/z* 1942 corresponding to the pentanuclear species $\{[Zn_5(L^4)_5](ClO_4)_8\}^{2+}$. Crystals suitable for X-ray diffraction were grown by layering a solution of $Zn(CF_3SO_3)_2$ with $\mathbf{L^4}$ in acetonitrile with diethyl ether. Structural analysis by single crystal X-ray diffraction confirmed the formation of the pentanuclear cyclic helicate $[Zn_5(L^4)_5]^{10+}$ (Figure 3.3).

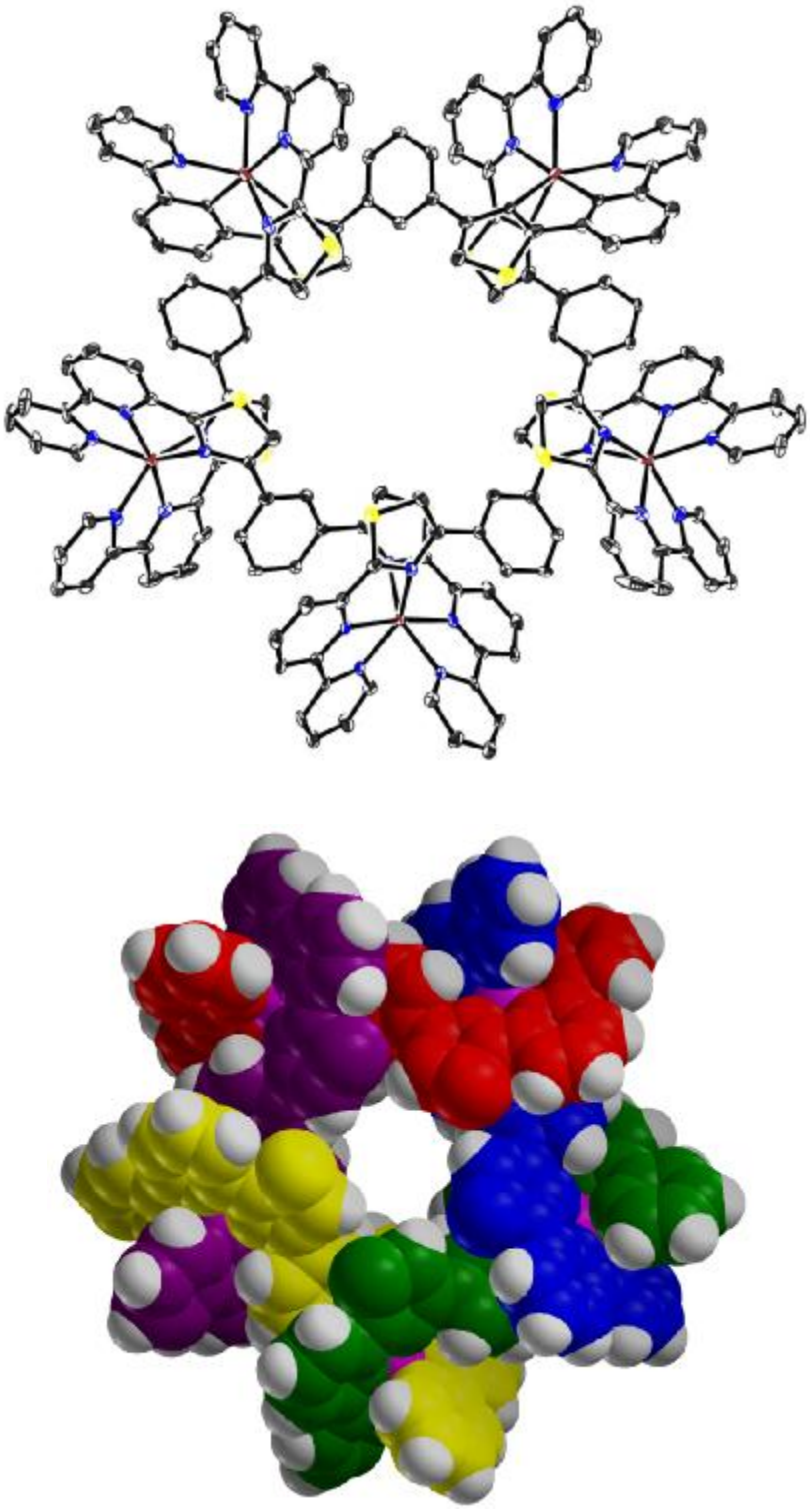

Figure 3.3. Two views of the complex cation $[Zn_5(\mathbf{L}^4)_5]^{10+}$: (i) Solid state structure and (ii) a space-filling picture showing all atoms and their van der Waals radii.

In the crystal, there are five zinc ions coordinated by five ligands and all five Zn^{2+} ions are six-coordinate, arising from the coordination of two tridentate thiazole-pyridyl-pyridyl domains from two different ligands (Zn-N: 2.072(8)-

2.327(8) Å). The 1,3-phenylene spacers bridge each of the tridentate domains in an 'over-and-under' conformation, giving rise to a helical cyclic oligomer as opposed to a face-to-face array associated with more grid-like architectures.

Bond	Bond length (Å)
Zn(1)-N(11)	2.181(7)
Zn(1)-N(11')	2.181(7)
Zn(1)-N(21)	2.091(7)
Zn(1)-N(21')	2.091(7)
Zn(1)-N(31)	2.238(7)
Zn(1)-N(31')	2.238(7)
Zn(2)-N(51)	2.225(7)
Zn(2)-N(61)	2.106(7)
Zn(2)-N(71)	2.182(9)
Zn(2)-N(81)	2.191(7)
Zn(2)-N(91)	2.096(7)
Zn(2)-N(101)	2.257(7)
Zn(3)-N(121)	2.262(9)
Zn(3)-N(131)	2.073(9)
Zn(3)-N(141)	2.237(8)
Zn(3)-N(151)	2.149(7)
Zn(3)-N(161)	2.082(7)
Zn(3)-N(171)	2.329(7)

Table 7. Selected bond lengths (Å) for the complex cation $[Zn_5(\mathbf{L}^4)_5]^{10+}$.

Bond	Bond angle (°)	Bond	Bond angle (°)
N(11)-Zn(1)-N(21)	75.7(3)	N(51)-Zn(2)-N(61)	75.0(3)
N(11)-Zn(1)N(31)	150.9(3)	N(51)-Zn(2)-N(71)	148.9(3)
N(11)-Zn(1)-N(11)	88.3(3)	N(51)-Zn(2)-N(81)	102.9(3)
N(11)-Zn(1)-N(21)	99.5(3)	N(51)-Zn(2)-N(91)	113.4(3)
N(11)-Zn(1)-N(31)	100.3(3)	N(51)-Zn(2)-N(101)	84.5(3)
N(21)-Zn(1)-N(31)	75.5(3)	N(61)-Zn(2)-N(71)	74.7(3)
N(21)-Zn(1)-N(11)	99.5(3)	N(61)-Zn(2)-N(81)	98.9(3)
N(21)-Zn(1)-N(21)	173.5(3)	N(61)-Zn(2)-N(91)	170.0(3)
N(21)-Zn(1)-N(31)	109.5(3)	N(61)-Zn(2)-N(101)	112.2(3)
N(31)-Zn(1)-N(11)	100.3(3)	N(71)-Zn(2)-N(81)	88.3(3)
N(31)-Zn(1)-N(21)	109.5(3)	N(71)-Zn(2)-N(91)	97.5(3)
N(31)-Zn(1)-N(31)	85.7(3)	N(71)-Zn(2)-N(101)	100.8(3)
N(11)-Zn(1)-N(21)	75.7(3)	N(81)-Zn(2)-N(91)	74.3(3)
N(11)-Zn(1)-N(31)	150.9(3)	N(81)-Zn(2)-N(101)	149.9(3)
N(21)-Zn(1)-N(31)	75.5(3)	N(91)-Zn(2)-N(101)	75.0(3)
N(121)-Zn(3)-N(131)	75.2(3)	N(131)-Zn(3)-N(171)	104.9(3)
N(121)-Zn(3)-N(141)	149.7(3)	N(141)-Zn(3)-N(151)	85.6(3)
N(121)-Zn(3)-N(151)	104.7(3)	N(141)-Zn(3)-N(161)	101.0(3)
N(121)-Zn(3)-N(161)	109.1(3)	N(141)-Zn(3)-N(171)	104.2(3)
N(121)-Zn(3)-N(171)	81.5(3)	N(151)-Zn(3)-N(161)	75.4(3)
N(131)-Zn(3)-N(141)	74.6(3)	N(151)-Zn(3)-N(171)	149.6(3)

N(131)-Zn(3)-N(151)	105.5(3)	N(161)-Zn(3)-N(171)	74.4(3)
N(131)-Zn(3)-N(161)	175.4(3)		

Table 8. Selected bond angles (°) for the complex cation $[Zn_5(\mathbf{L}^4)_5]^{10+}$.

3.3 Solution Studies

3.3.1 Solution state characterisation of $[Cd_2(L^4)_2]^{4+}$

Further evidence for the formation of $[Cd_2(\mathbf{L}^4)_2]^{4+}$ was gained through ^{1}H and two-dimensional spin-spin (^{1}H-^{1}H COSY) and dipole-dipole (^{1}H-^{1}H NOESY) NMR spectra of solutions of $[Cd_2(\mathbf{L}^4)_2]^{4+}$ in CD_3NO_2 (500 MHz, 298 K), shown in Figures 3.4, 3.5 and 3.6, respectively.

The one-dimensional spectrum of solution $[Cd_2(\mathbf{L}^4)_2](ClO_4)_4$ in CD_3NO_3 shows the expected 11 aromatic resonances for a complex with *D2* symmetry. Protons corresponding to the tridentate chelate units appear between 7.0 and 8.4 ppm consistent with the aromatic heterocycles on $\mathbf{L}^4$ being coordinated to two metal ions (Figure 3.4).

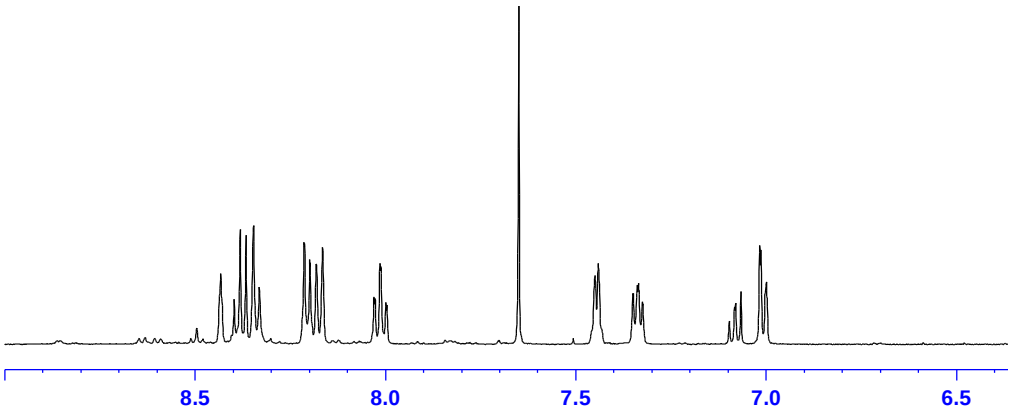

Figure 3.4. Aromatic regions in the ^{1}H NMR spectrum (CD_3NO_2) of $[Cd_2(\mathbf{L}^4)_2]^{4+}$.

The ^{1}H-^{1}H COSY NMR spectrum shows couplings between protons on the phenylene ring (red), the internal pyridine ring (blue) and the terminal pyridine ring (green). Analysis by ^{1}H-^{1}H COSY NMR allows assignment of some of the observed signals through a combination of coupling constants and COSY interactions. However, complete assignment is non-trivial but it is possible to ascertain which proton signal belongs to which aromatic unit (i.e. phenyl

spacer, terminal/internal pyridine). For example, the doublet of doublets at 7.0 ppm couples to a triplet at 7.10 ppm and a triplet at 8.45 ppm, the absence of any further coupling between these protons and their multiplicity is indicative of the central phenyl unit (H^1-H^3). Signals at 8.25 ppm (d), 8.35 (d) and 8.45 (dd) correspond to the internal pyridine ring (H^5-H^7) whereas signals at 7.35 ppm (dd), 7.45 (d), 8.0(dd) and 8.20 (dd) correspond to the terminal pyridine ring (H^8-H^{11}).

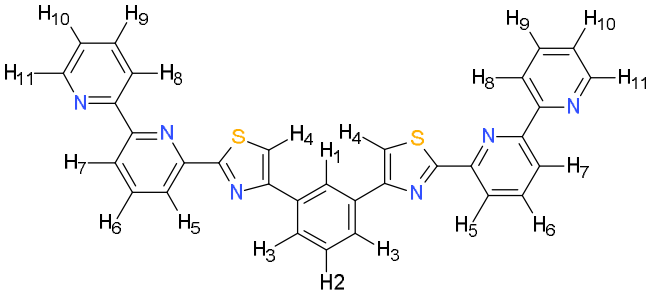

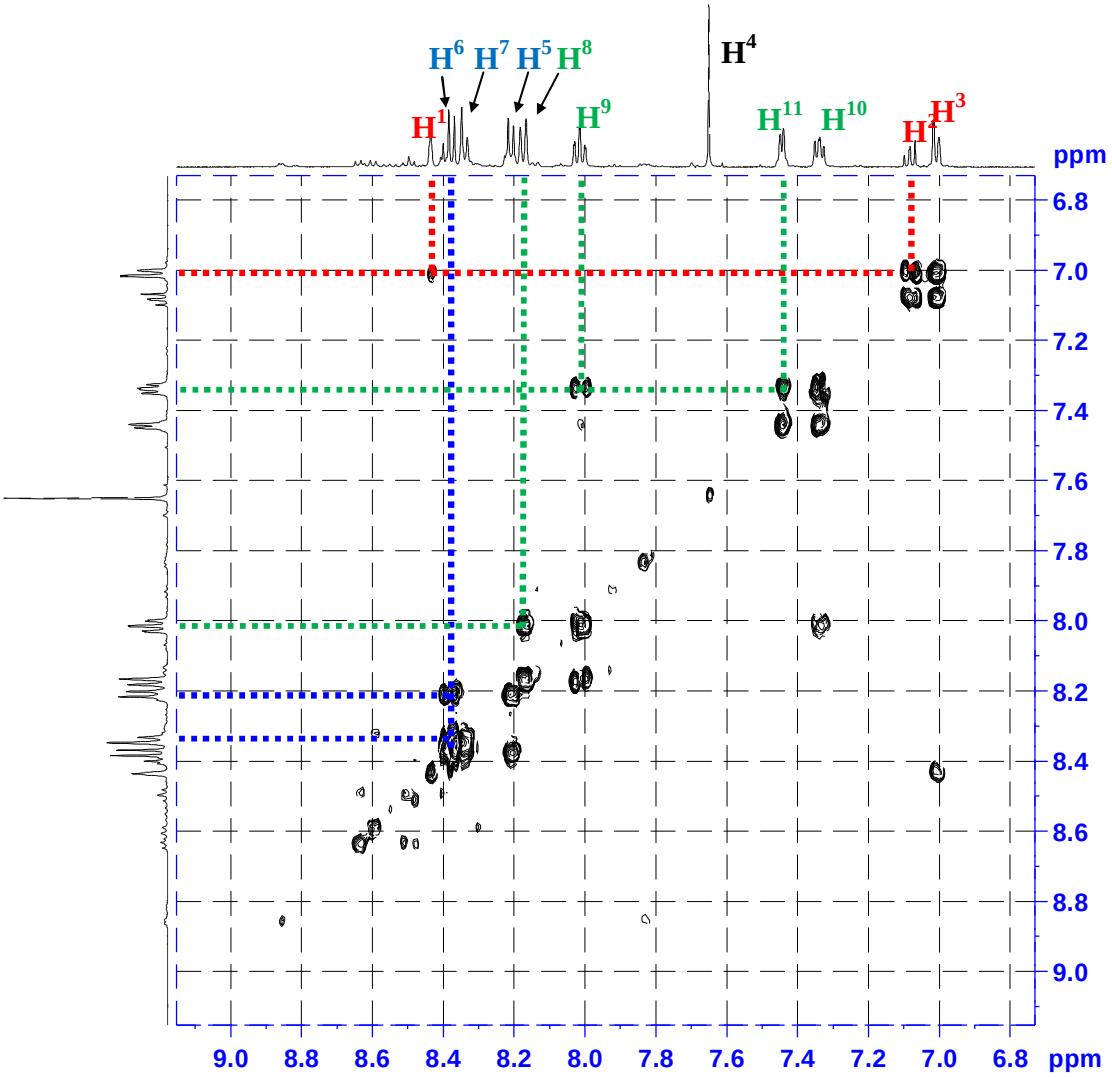

Figure 3.5. ^{1}H-^{1}H COSY spectrum (CD_3NO_2) of $[Cd_2(\mathbf{L}^4)_2]^{4+}$.

The ^{1}H-^{1}H NOESY shows selected intra- (red) and inter-ligand (blue) through-space interactions. The number of inter-ligand interactions is surprisingly small. However, interactions between the thiazole protons and both the pyridyl ring (H^5) and the phenyl ring (H^3) are observed as well as intra-pyridyl interactions (H^7 –H^8).

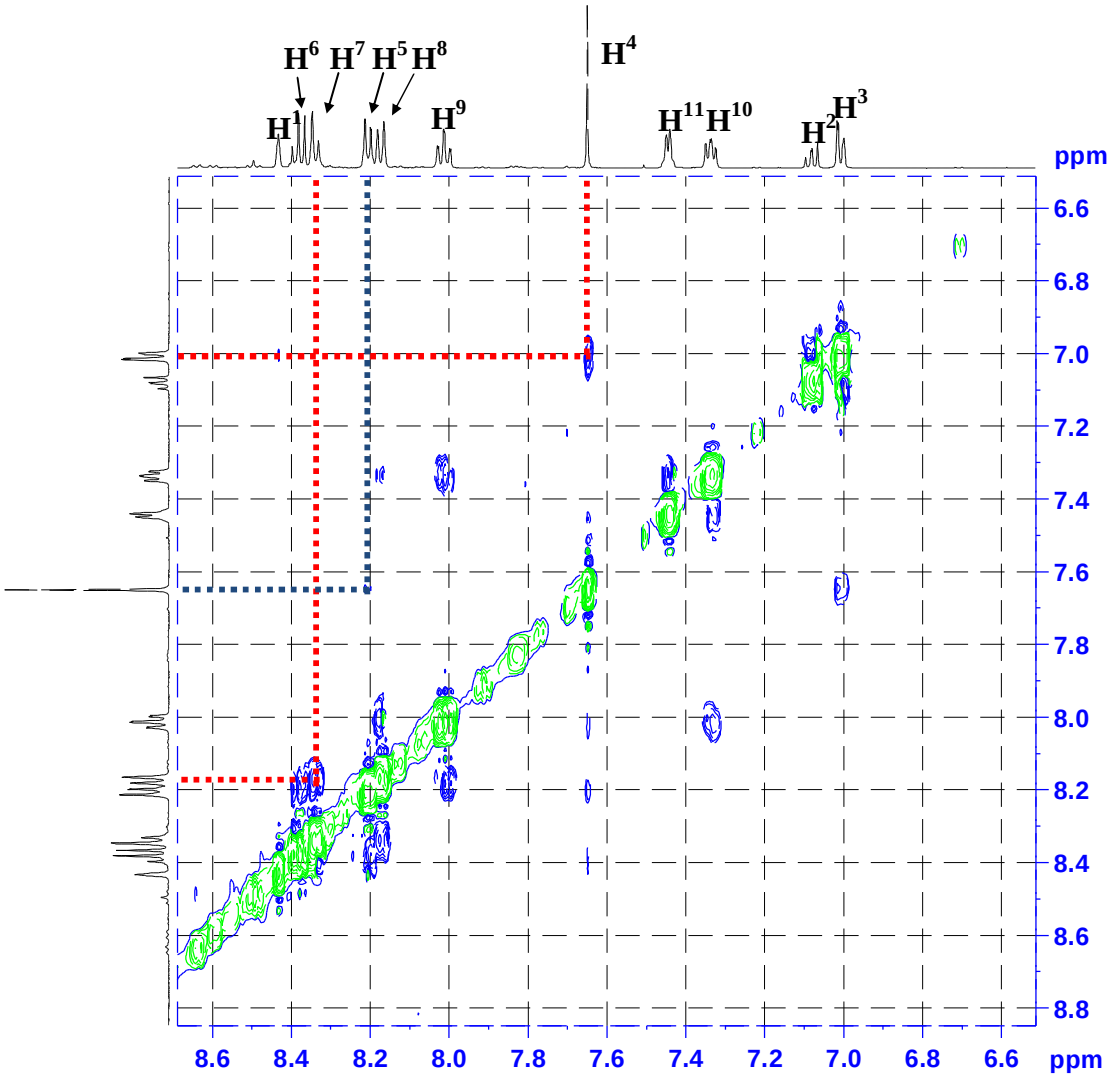

Figure 3.6. Aromatic region of the ^{1}H-^{1}H NOESY spectrum (CD_3NO_2) of $[Cd_2(\mathbf{L}^4)_2]^{4+}$.

3.3.2 Solution state characterisation of $[Zn_5(L^4)_5]^{10+}$

In a similar manner to $[Cd_2(\mathbf{L^4})_2]^{4+}$ further evidence for the formation of $[Zn_5(\mathbf{L^4})_5]^{10+}$ was gained through ^1H and two-dimensional spin-spin (^1H-^1H COSY) and dipole-dipole (^1H-^1H NOESY) NMR spectra of solutions of $[Zn_5(\mathbf{L^4})_5]^{10+}$ in CD_3NO_2 (500 MHz, 298 K), shown in Figures 3.7, 3.8 and 3.9, respectively.

The one-dimensional ^1H NMR spectrum of solution $[Zn_5(\mathbf{L^4})_5](CF_3SO_3)_{10}$ in CD_3NO_2 shows the expected 11 aromatic resonances for a complex with *D5* symmetry. Protons on the tridentate chelate units appear between 7.0. and 8.4 ppm consistent with the aromatic heterocycles on $\mathbf{L^4}$. However, for the pentanuclear species the three protons on the bridging phenylene unit resonate at a much lower frequency (5.9 – 7.1 ppm) which unusual for aromatic protons.

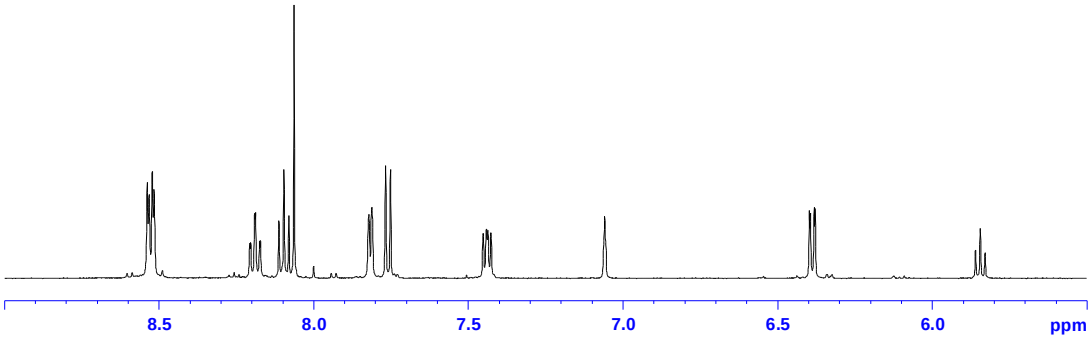

Figure 3.7. Aromatic region in the ^1H NMR spectrum (CD_3NO_2) of $[Zn_5(\mathbf{L^4})_5]^{10+}$.

The ^1H-^1H COSY NMR spectrum shows couplings between protons on the phenylene ring (red), the internal pyridine ring (blue) and the terminal pyridine ring (green). In a similar manner to $[Cd_2(\mathbf{L^4})_2]^{4+}$ via a mixture of coupling and COSY interactions protons belonging to each heterocycle can be assigned. For example, the triplet at 5.85 ppm couples to a doublet of doublets at 6.45 ppm which also couples to a triplet at 7.1 ppm (with a coupling constant consistent with the $^4J_{H1\text{-}H3}$ coupling). The absence of any further coupling between these and other protons and their multiplicity is indicative of the central phenyl unit (H^1-H^3). Signals at 7.8 ppm (d), 8.1 (dd) and 8.55 (d) correspond to the internal pyridine ring (H^5-H^7), whereas the signals at 7.45

(dd), 7.85 (d), 8.2 (dd) and 8.55 (d) correspond to the terminal pyridine ring (H^8-H^{11}). The signal at 8.55 ppm corresponds to two overlapping proton signals from the internal and terminal pyridine rings (Figure 3.8).

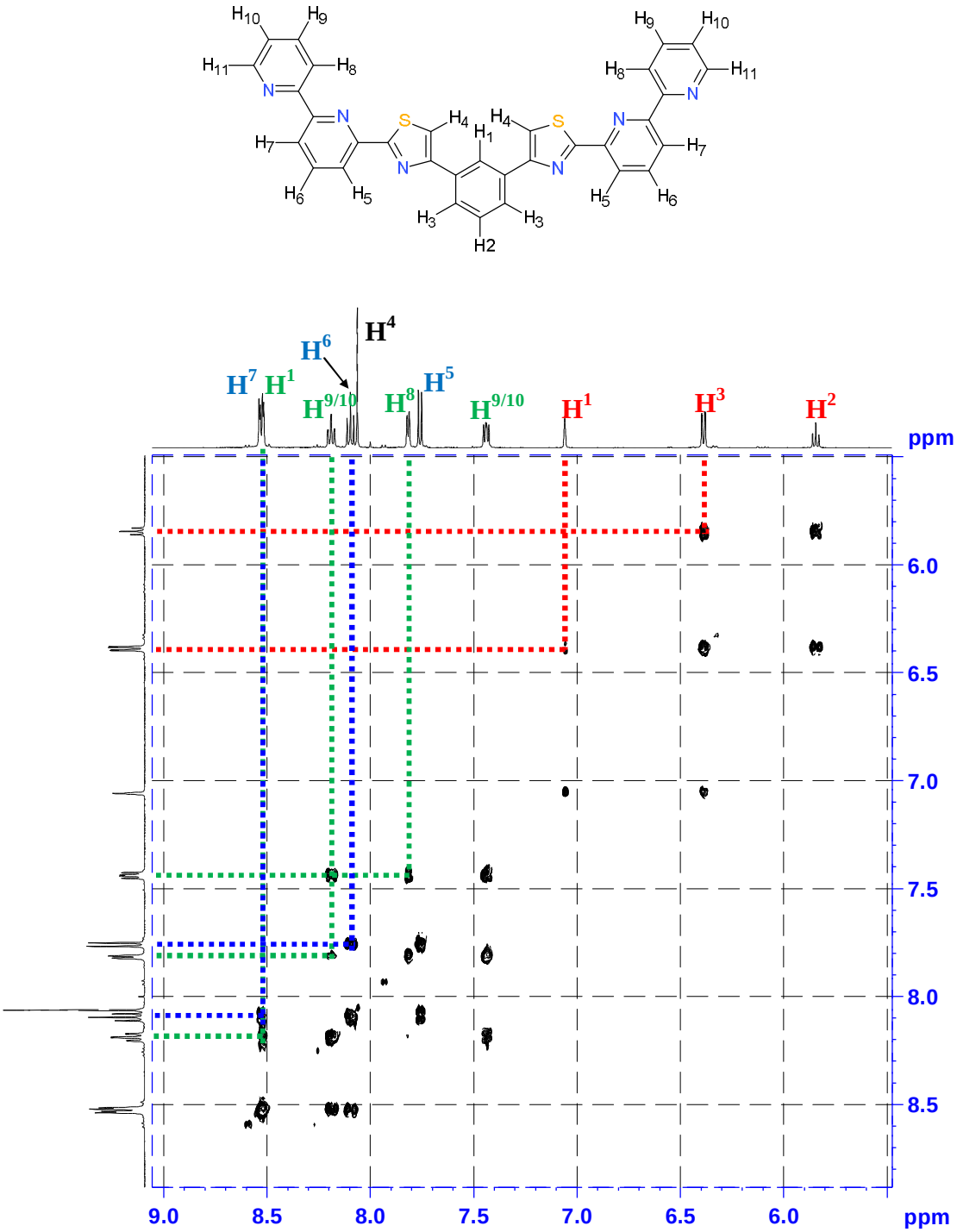

Figure 3.8. Aromatic region of the ^{1}H-^{1}H COSY spectrum (CD_3NO_2) of $[Zn_5(\mathbf{L}^4)_5]^{10+}$.

Additionally, evidence from the ^{1}H-^{1}H NOESY spectrum shows complex inter-ligand through-space interactions for $[Zn_5(\mathbf{L}^4)_5]^{10+}$ (red), where the cyclic

arrangement brings up to seven pairs of protons in sufficiently close proximity for dipole-dipole induced relaxation effects to be observed. A diagnostic intra-ligand NOE effect also occurs between phenylene proton H^1 and thiazole proton H^4 (blue) (Figure 3.9).

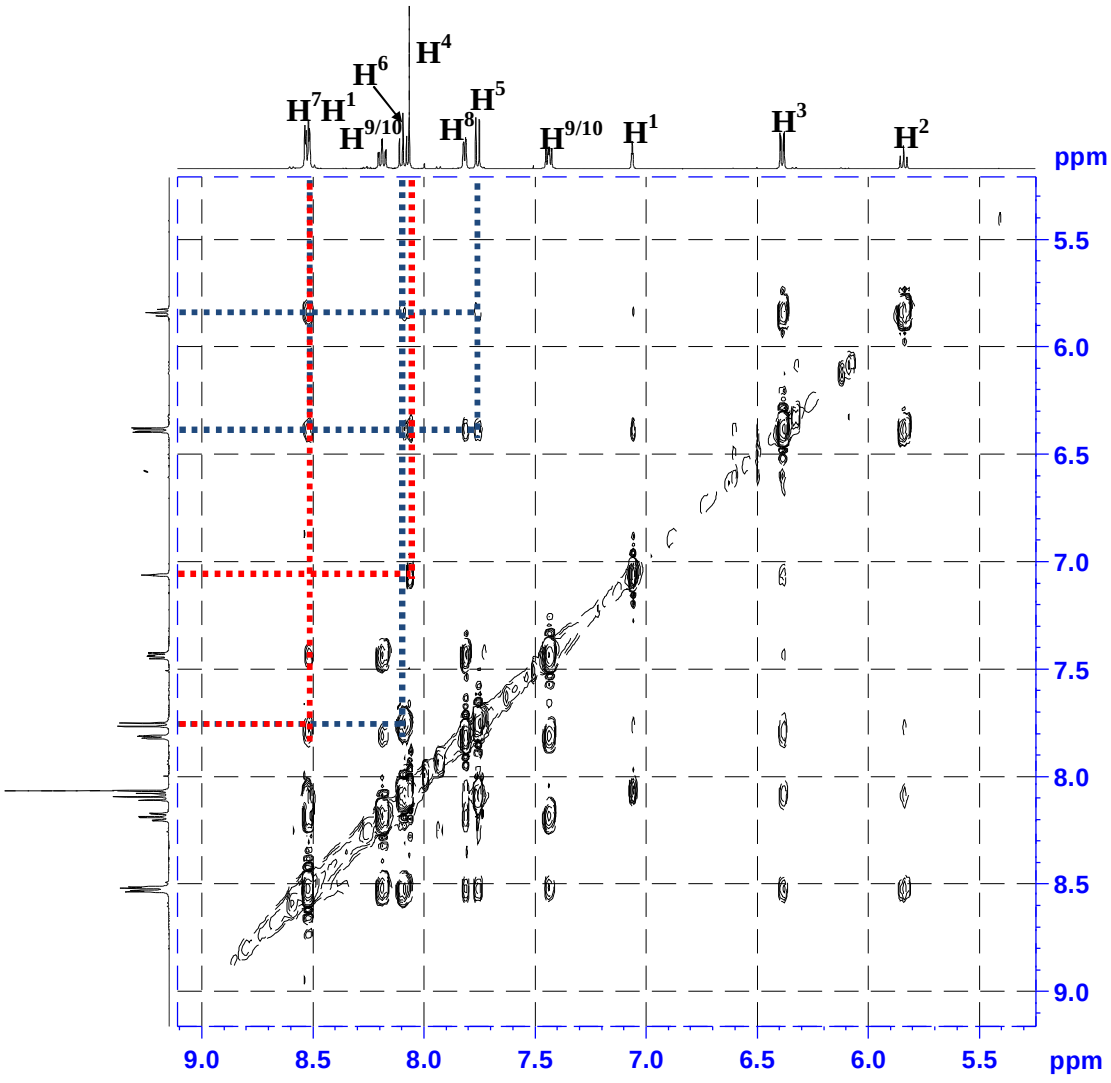

Figure 3.9. Aromatic region of ^{1}H-^{1}H NOESY spectrum (CD_3NO_2) of $[Zn_5(\mathbf{L^4})_5]^{10+}$.

Interestingly there are more inter-ligand NOE interactions than observed in the $[Cd_2(\mathbf{L^4})_2]^{4+}$ with, amongst others, cross peaks corresponding to H^3 – H^5, H^2 – H^5 and H^2 – H^6 dipole-dipole induced relaxation effects observed.

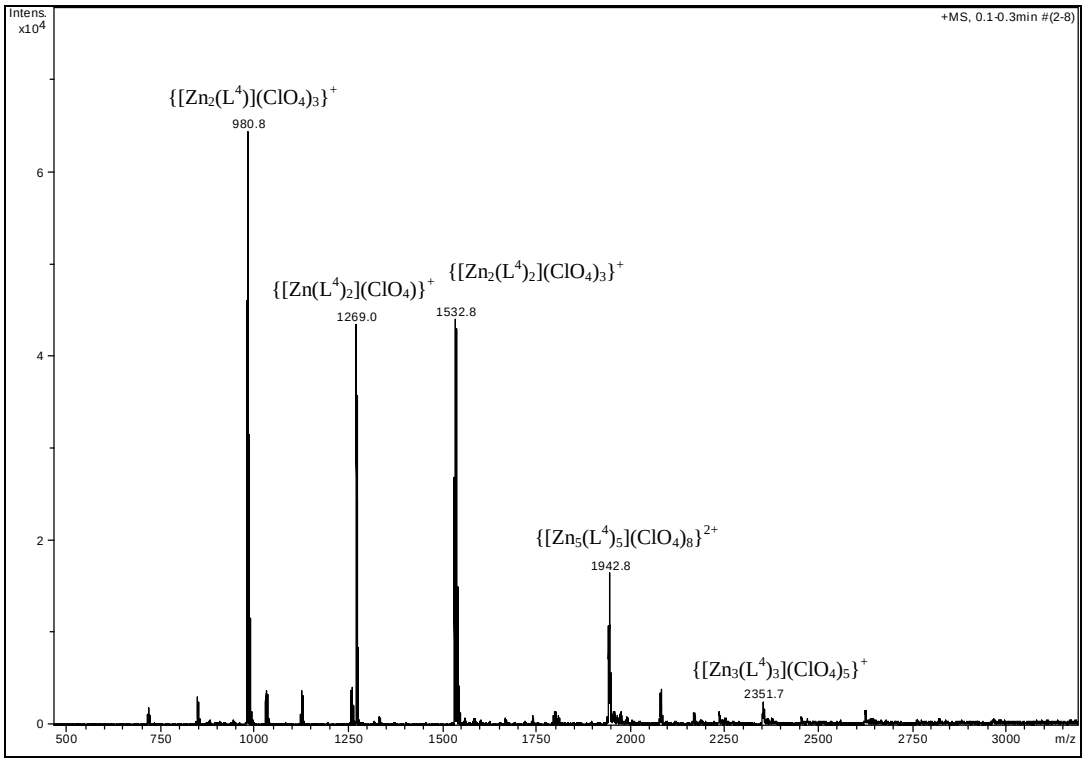

Figure 4.0. ESI-MS spectrum of $[Zn_5(\mathbf{L^4})_5](ClO_4)_{10}$.

The ESI-mass spectrum of $[Zn_5(\mathbf{L^4})_5]^{10+}$ is also consistent with the formation of the cyclic species in the solution/gas phase showing singly charged ions corresponding to $\{[Zn_2(\mathbf{L^4})](ClO_4)_3\}^+$, $\{[Zn(\mathbf{L^4})_2](ClO_4)\}^+$, $\{[Zn_2(\mathbf{L^4})_2](ClO_4)_3\}^+$ and $\{[Zn_3(\mathbf{L^4})_3](ClO_4)_5\}^+$ and a doubly charged ion corresponding to $\{[Zn_5(\mathbf{L^4})_5](ClO_4)_8\}^{2+}$.

3.4. Discussion

From the single-crystal X-ray crystallographic studies and the MS/NMR spectra it is clear that $[Cd_2(\mathbf{L^4})_2]^{4+}$ and $[Zn_5(\mathbf{L^4})_5]^{10+}$ are present both in the solid state and in solution. Comparison of the solid state structures with the data observed in solution is clearly consistent with the formation of di- and penta-nuclear species. For example, in the ^{1}H NMR of $[Zn_5(\mathbf{L^4})_5]^{10+}$ protons corresponding to the central phenyl ring have a considerably lower chemical shift than would be expected for aromatic protons (i.e. 5.9 – 7.1 ppm). This is attributed to the close distance between the phenyl ring and the tridentate py-py-tz domains (ave. centroid··· centroid distance 3.9(1) Å); the phenyl ring is shielded by the aromatic ring currents produced by the aromatic heterocycles on the two overlapping ligand strands and hence unusually low chemical

shifts are observed. The chemical shift of the phenyl spacer unit in the corresponding double helicate is more usual for an aromatic ring (8.4 – 7.0 ppm) as in the solid state the distance between this ring and the N-donor domain is longer (ave. centroid··· centroid distance 4.2 (1) Å) and as a result the chemical shift is not influenced by the ring currents of these adjacent heterocycles.

The more compact structure of $[Zn_5(\mathbf{L^4})_5]^{10+}$ is also supported by NOE interactions which provide evidence for a complex network of inter-ligand through-space interactions, where the cyclic arrangement brings up to seven pairs of protons into sufficiently close proximity for dipole-dipole induced relaxation effects to be observed. None of these interactions are observed for $[Cd_2(\mathbf{L^4})_2]^{4+}$ which has a less compact structure with the shortest corresponding non-bonded distances being up to *ca.* 2 Å longer (Table 9).

proton pair	H···H dist. (Å)	comment
Inter-strand		
$H^6\cdots H^2$	3.74 (5.20)	
$H^7\cdots H^2$	3.32 (4.23)	
$H^{11}\cdots H^3$	3.95 (5.37)	
$H^5\cdots H^2$	4.09 (6.11)	
$H^6\cdots H^3$	3.93 (4.46)	
$H^6\cdots H^8$	3.82 (5.19)	
$H^5\cdots H^3$	3.67 (4.72)	
$H^5\cdots H^4$	4.64 (3.19)	**only** obs. in $[Cd_2(L^4)_2]^{4+}$
Intra-strand		
$H^4\cdots H^1$	2.52 (4.32)	
$H^7\cdots H^8$	2.23 (2.21)	**also** obs. in $[Cd_2(L^4)_2]^{4+}$

Table 9. Selected proton pairs in $[Zn_5(\mathbf{L^4})_5]^{10+}$ for which through-space couplings are observed and their shortest corresponding non-bonded distances taken from the solid-state structure (analogous values for $[Cd_2(\mathbf{L^4})_2]^{4+}$ are given in parentheses for comparison).

Further evidence for the retention of the respective solid-state structures in solution was obtained by diffusion ordered NMR spectroscopy. Translational self-diffusion coefficients (in CD_3NO_2, 298 K) were determined to be 3.4(3) × 10^{-10} and 6.3(2) × 10^{-10} m^2s^{-1} for $[Zn_5(\mathbf{L^4})_5]^{10+}$ and $[Cd_2(\mathbf{L^4})_2]^{4+}$ respectively. Conversion of these values into meaningful hydrodynamic radii is not trivial since microfrictional and shape effects can profoundly influence the apparent relationship between diffusion constant and molecular size.[89] The significantly lower value obtained for $[Zn_5(L^4)_5]^{10+}$ is nonetheless consistent with it being the larger of the two diffusing species in solution.

On the basis of all the data obtained by these experiments it is quite clear that both structures have the same formulation (i.e. di- and pentanuclear) in the solution state to that observed in the solid state.

It is worth noting that the dicadmium(II) helicate was obtained as the perchlorate salt whereas single crystals of the pentanuclear structure were only successfully obtained in the presence of the triflate anion. Indeed, in the latter structure, a disordered triflate anion resides within the central cavity of the circular complex cation. To investigate the potential role of the counter anion in the two self-assembly reactions solutions (CD_3NO_2) containing the two respective assemblies were monitored by ^{1}H NMR as increasing amounts of the other anion were added (as the tetrabutylammonium salts). Even in the presence of 20 eq. of the corresponding anion no changes were observed in either case and so the anions influence in directing the assembly is clearly minimal. An alternative explanation for why $\mathbf{L^4}$ gives such different structures with the two spherical d^{10} cations requires consideration of the potential steric interactions that occur between the protons of the central phenylene units in the two respective structures. The phenylene spacers force the ligand to partition into two tridentate domains, thereby preventing formation of the mononuclear species. Formation of the double helicate structure brings them into relatively close proximity with one another (Figure 3.2), the inter-strand $C^1\cdots C^1$ distance between these two rings is *ca*. 4.2 Å in $[Cd_2(\mathbf{L^4})_2]^{4+}$. Six-coordinate zinc(II) is smaller than cadmium(II) (0.75 *Vs*. 0.95 Å respectively). As result of the shorter Zn-N bonds it is likely that any steric and/or electrostatic repulsion between the phenyl protons would be notably

emphasized in an isostructural dizinc(II) helicate. The formation of the alternative pentanuclear species, which does not require that the two phenylene rings reside in such close proximity, is presumably a result of destabilisation of the zinc-containing double helicate structure.

In conclusion, it has been demonstrated how subtle changes in the metal/ligand bond distance can influence inter-ligand steric interactions and have a pronounced effect on the outcome of a self-assembly reaction. Furthermore, the inclusion of a 1,3-phenylene spacer within a ligand strand sufficiently destabilises dinuclear double helicates (with 1^{st} row transitions metal ions) so that a cyclic helicate species results. It is shown in the following work that use of such a spacer unit can be employed to prepare cyclic helicates of higher complexity.

4. Head-to-tail and Heteroleptic Circular Helicates

In the previous chapter we demonstrated that we have developed a robust approach for generating circular helicates. As a result this allows us to investigate the formation of circular helicates with diverse structural complexity. Described in this chapter is the synthesis and coordination chemistry of a potentially pentadentate N-donor ligand and a potentially tetradentate N-donor ligand, **L**^{5} and **L**^{6} respectively. **L**^{5} contains two binding domains, which consist of a tridentate thiazole-pyridine-pyridine N_3 binding domain and a bidentate thiazole-pyridine N_2 binding domain separated by a phenylene unit. **L**^{6} contains two identical bidentate thiazole-pyridine N_2 binding domains again separated by a phenylene unit (Figure 4.1).

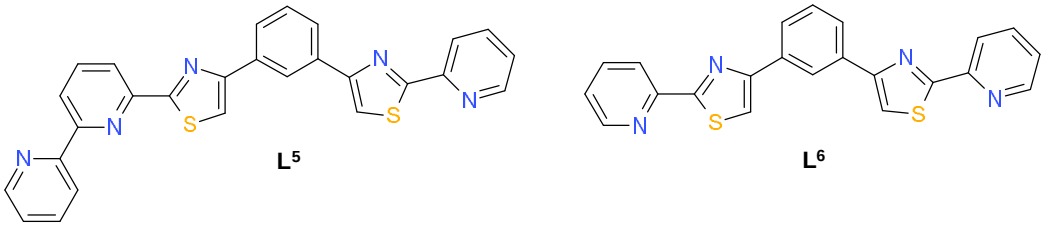

Figure 4.1. Multidentate ligands **L**^{5} and **L**^{6}.

4.1.1 Synthesis of L^{5}

The synthesis of **L**^{5} is outlined in scheme 4.1. To a solution of 1,3-di(α-bromoacetyl)benzene in DCM was added pyridine-2-thioamide and the reaction stirred at room temperature for 12 hours. The resulting precipitate was isolated by filtration and neutralized. Purification by column chromatography gave the mono-pyridylthiazole (**1**). Reaction of **1** with 2,2'-bipyridine-6-thioamide in EtOH at reflux for 8 hours resulted in a yellow precipitate which was isolated by filtration. Suspension in concentrated NH_3 followed by filtration and washing with H_2O, EtOH and Et_2O gave ligand **L**^{5} as a pale cream solid. Confirmation of the successful formation of **L**^{5} was obtained from the ^{1}H NMR spectrum which showed 15 different proton environments and contained, amongst others, signals corresponding to a 1,3-disubstituted phenyl ring and two different thiazole proton environments as would be expected for the unsymmetrical ligand.

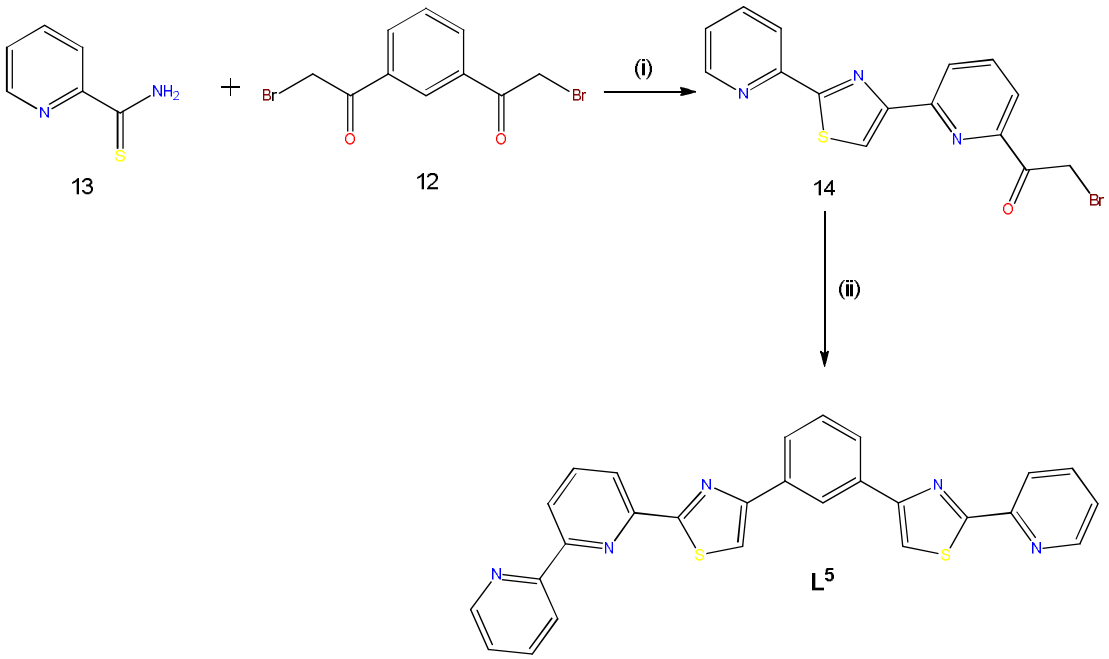

Scheme 4.1. Synthesis of **L^5.** Reagents and conditions: (i) 1,3-di(α-bromoacetyl)benzene, DCM, reflux (ii) 2,2'-bipyridine-6-thioamide, EtOH, reflux.

4.1.2 Synthesis of L^6

The synthesis of **L^6** is outlined in scheme 4.2. An excess of pyridine-2-thioamide was reacted, at reflux, with 1,3-di(α-bromoacetyl)benzene for 8 hours, during which time a precipitate formed. Filtration, washing and neutralisation gave ligand **L^6** as a cream solid. The ^{1}H NMR spectrum showed a total of 14 signals corresponding to the two pyridyl-thiazole units and the phenyl ring.

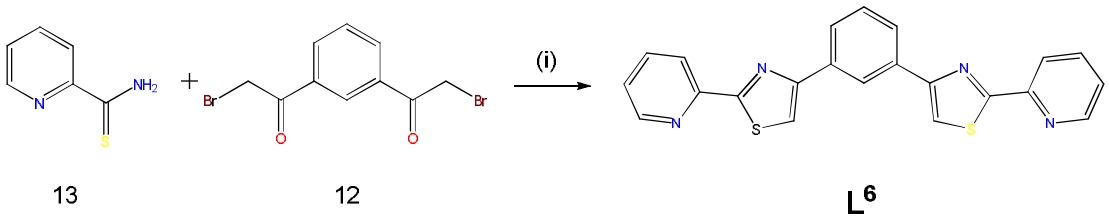

Scheme 4.2. Synthesis of **L^6**. Reagents and conditions: (i) 1,3-di(α-bromoacetyl)benzene, EtOH, reflux.

4.2 Coordination Chemistry

4.2.1 Complexes of L^5 with Copper (II).

The reaction of **L^5** with an equimolar amount of $Cu(ClO_4)_2 \cdot 6H_2O$ in acetonitrile gave a light green solution from which a crystalline solid was deposited in high

yield (*ca*. 80%) upon slow diffusion of chloroform. Analysis of this material by ESI-MS showed a number of low nuclearity fragments, e.g. $\{[Cu_2(\mathbf{L^5})](ClO_4)_3\}^+$ (*m/z* 901, 3%), $\{[Cu(\mathbf{L^5})_2](ClO_4)\}^+$ (*m/z* 1114, 50%), $\{[Cu_2(\mathbf{L^5})_2](ClO_4)_3\}^+$ (*m/z* 1367, 100%) and $\{[Cu_3(\mathbf{L^5})_3](ClO_4)_5\}^+$ (*m/z* 2114, 5%), but also a peak at *m/z* 1745 corresponding to $\{[Cu_5(\mathbf{L^5})_5](ClO_4)_8\}^{2+}$, with the correct isotope pattern for a dicationic species. Single crystal X-ray crystallographic analysis confirmed the formation of a pentanuclear circular helicate $[Cu_5(\mathbf{L^5})_5](ClO_4)_{10}$ (Figure 4.2).

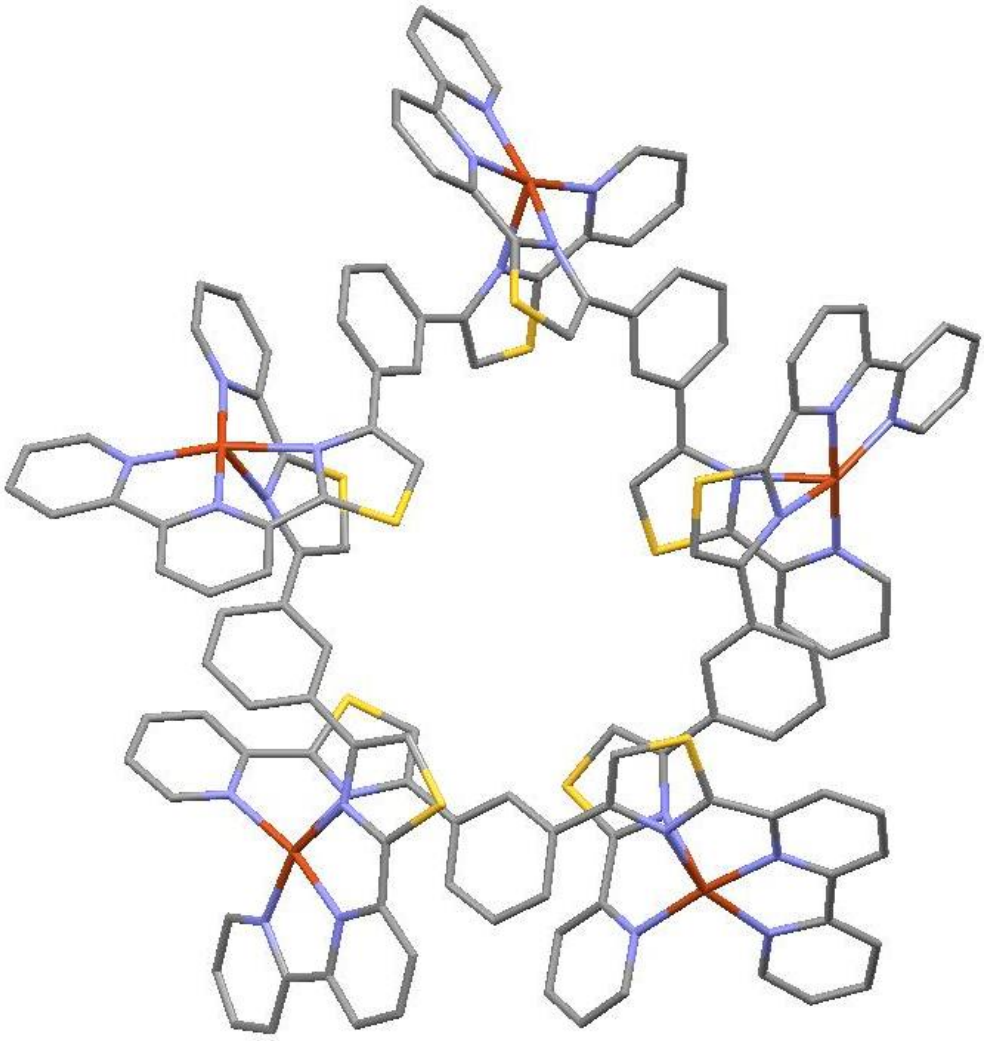

Figure 4.2. Solid state structure of the *HT*-$[Cu_5(\mathbf{L^5})_5]^{10+}$.

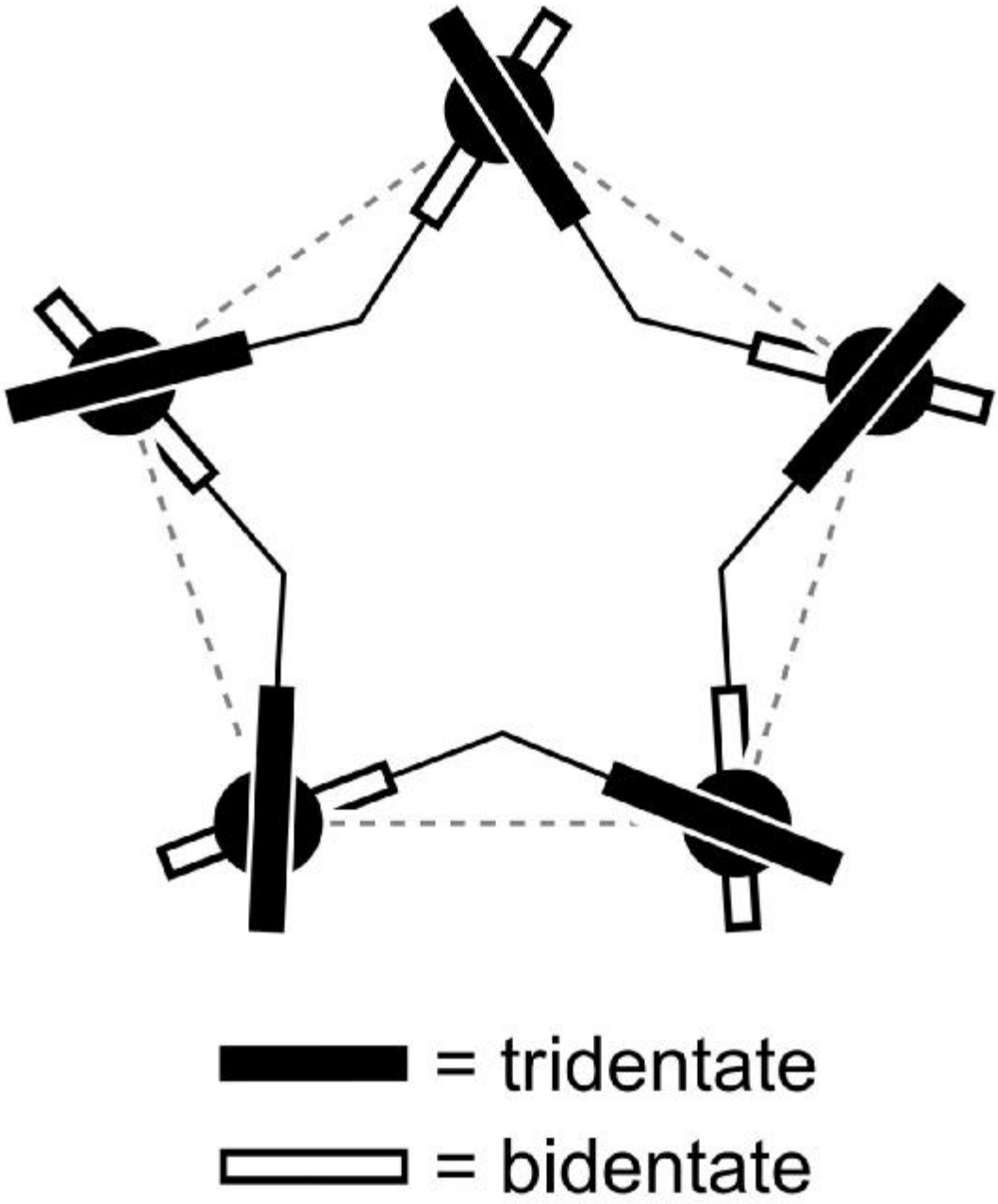

Figure 4.3. Schematic diagram of *HT-*[$Cu_5(\mathbf{L}^5)_5]^{10+}$ showing head-to-tail ligand arrangement (black circles represent 5 coordinate Cu^{II}).

In the crystal structure, there are five copper ions coordinated by five ligands in a head-to-tail (HT) arrangement. All five Cu^{2+} ions are five-coordinate, displaying distorted square-pyramidal geometries (Cu-N bond lengths: 1.936(9)-2.327(9) Å), arising as the ligands adopt the anticipated '3 + 2' binding mode, where the bidentate and tridentate N-donor domains span two different Cu^{II} metal centres. Furthermore, the ligands are arranged in such a manner that each metal is coordinated by the bidentate domain of one ligand

and a tridentate domain of different ligand. By analogy with the HT-linear helicate the complex cation $[Cu_5(\mathbf{L}^5)_5]^{10+}$ may be considered a HT-circular helicate.

Bond	Bond length (Å)	Bond	Bond length (Å)
Cu(1)-N(11)	2.05(1)	Cu(3)-N(141)	1.95(1)
Cu(1)-N(21)	1.956(8)	Cu(3)-N(151)	2.189(8)
Cu(1)-N(31)	2.20(1)	Cu(4)-N(171)	2.309(9)
Cu(1)-N(281)	2.26(1)	Cu(4)-N(181)	2.00(1)
Cu(1)-N(291)	2.03(1)	Cu(4)-N(191)	2.05(1)
Cu(2)-N(51)	2.237(8)	Cu(4)-N(201)	1.97(1)
Cu(2)-N(61)	2.006(8)	Cu(4)-N(211)	2.167(9)
Cu(2)-N(71)	2.033(8)	Cu(5)-N(221)	2.235(8)
Cu(2)-N(81)	1.952(8)	Cu(5)-N(231)	2.00(1)
Cu(2)-N(91)	2.164(8)	Cu(5)-N(241)	2.02(1)
Cu(3)-N(111)	2.328(8)	Cu(5)-N(251)	1.94(1)
Cu(3)-N(121)	1.984(8)	Cu(5)-N(261)	2.08(1)
Cu(3)-N(131)	2.057(9)		

Table 10. Selected bond lengths (Å) for the complex cation $[Cu_5(\mathbf{L}^5)_5]^{10+}$.

Bond	Bond angle (°)	Bond	Bond angle (°)
N(11)-Cu(1)-N(21)	79.4(4)	N(121)-Cu(3)-N(141)	179.4(4)
N(11)-Cu(1)-N(31)	156.5(4)	N(121)-Cu(3)-N(151)	101.7(3)
N(11)-Cu(1)-N(281)	111.4(4)	N(131)-Cu(3)-N(141)	80.6(4)
N(11)-Cu(1)-(291)	99.2(4)	N(131)-Cu(3)-N(151)	158.3(4)
N(21)-Cu(1)-N(31)	77.8(4)	N(141)-Cu(3)-N(151)	78.2(4)
N(21)-Cu(1)-N(281)	104.4(4)	N(171)-Cu(4)-N(181)	77.5(4)
N(21)-Cu(1)-N(291)	177.4(4)	N(171)-Cu(4)-N(191)	105.3(4)
N(31)-Cu(1)-N(281)	79.9(3)	N(171)-Cu(4)-N(201)	106.7(3)
N(31)-Cu(1)-N(291)	103.4(4)	N(171)-Cu(4)-N(211)	81.5(3)
N(281)-Cu(1)-N(291)	78.5(4)	N(181)-Cu(4)-N(191)	93.3(4)
N(51)-Cu(2)-N(61)	78.5(3)	N(181)-Cu(4)-N(201)	173.0(4)
N(51)-Cu(2)-N(71)	109.8(3)	N(181)-Cu(4)-N(211)	108.1(4)
N(51)-Cu(2)-N(81)	113.0(3)	N(191)-Cu(4)-N(201)	80.4(4)
N(51)-Cu(2)-N(91)	82.0(3)	N(191)-Cu(4)-N(211)	158.6(4)
N(61)-Cu(2)-N(71)	95.0(3)	N(201)-Cu(4)-N(211)	78.2(4)
N(61)-Cu(2)-N(81)	168.4(3)	N(221)-Cu(5)-N(231)	79.1(4)
N(61)-Cu(2)-N(91)	106.0(3)	N(221)-Cu(5)-N(241)	103.0(4)
N(71)-Cu(2)-N(81)	79.4(3)	N(221)-Cu(5)-N(251)	113.1(4)
N(71)-Cu(2)-N(91)	157.8(3)	N(221)-Cu(5)-N(261)	84.9(4)
N(81)-Cu(2)-N(91)	78.7(3)	N(231)-Cu(5)-N(241)	93.5(4)
N(111)-Cu(3)-N(121)	78.2(3)	N(231)-Cu(5)-N(251)	166.9(4)

N(111)-Cu(3)-N(131)	109.8(3)	N(231)-Cu(5)-N(261)	107.5(4)
N(111)-Cu(3)-N(141)	101.2(3)	N(241)-Cu(5)-N(251)	79.6(4)
N(111)-Cu(3)-N(151)	79.0(3)	N(241)-Cu(5)-N(261)	158.7(4)
N(121)-Cu(3)-N(131)	99.5(4)	N(251)-Cu(5)-N(261)	79.1(4)

Table 11. Selected bond angles (°) for the complex cation $[Cu_5(\mathbf{L^5})_5]^{10+}$.

4.2.2 Heteroleptic complexes of L^6 with L^4 and Copper (II).

The ability of Cu^{2+} to adopt a 5-coordinate geometry was exploited in the synthesis of a heteroleptic circular helicate. Reaction of $\mathbf{L^6}$ with the C_{2v}-symmetric bis-tridentate ligand, $\mathbf{L^4}$, (see previous chapter 3) and $Cu(CF_3SO_3)_2$ in acetonitrile in a 1:1:2 ratio, respectively, gave a clear green solution. Upon diffusion of ethyl acetate into the solution a homogeneous crystalline material was deposited in high yield (*ca*. 75%) after several days. Single crystal X-ray crystallographic analysis of the material confirmed the formation of the target heteroleptic circular helicate $[Cu_5(\mathbf{L^4})_3(\mathbf{L^6})_2]^{10+}$ (Figure 4.4).

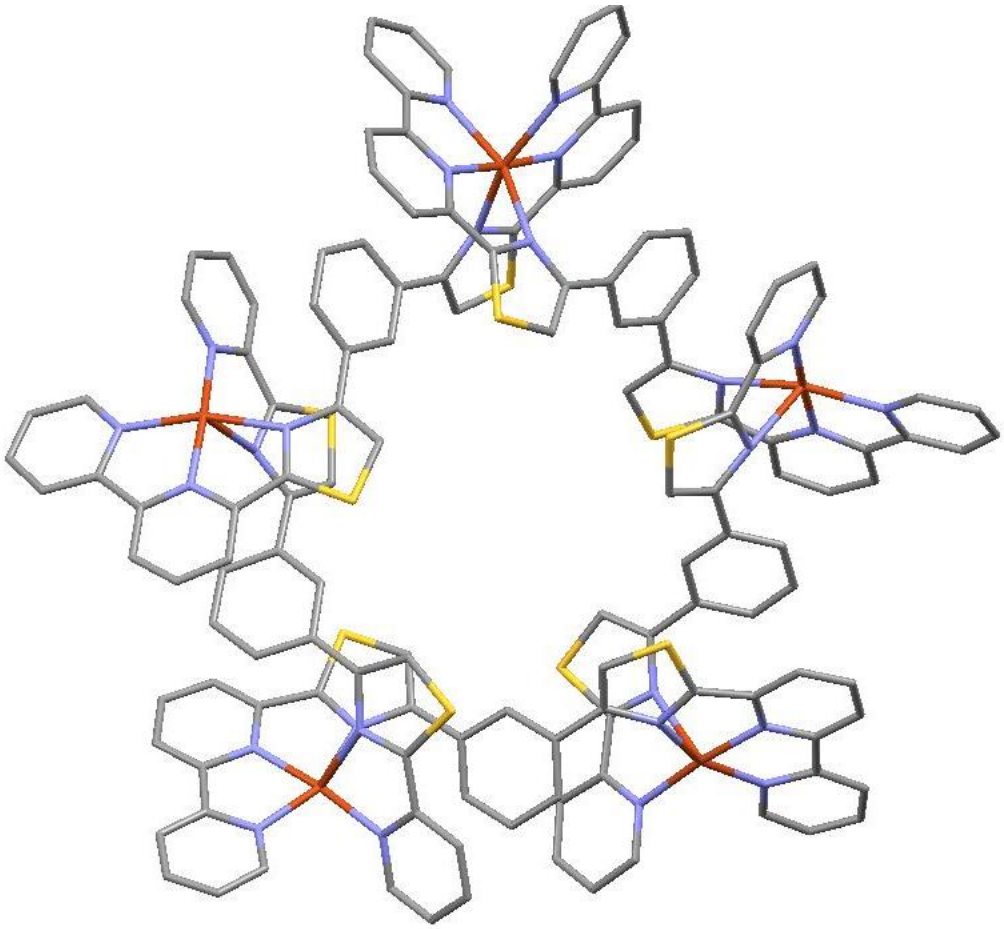

Figure 4.4. Solid state structure of the heteroleptic $[Cu_5(\mathbf{L}^4)_3(\mathbf{L}^6)_2]^{10+}$ circular helicate.

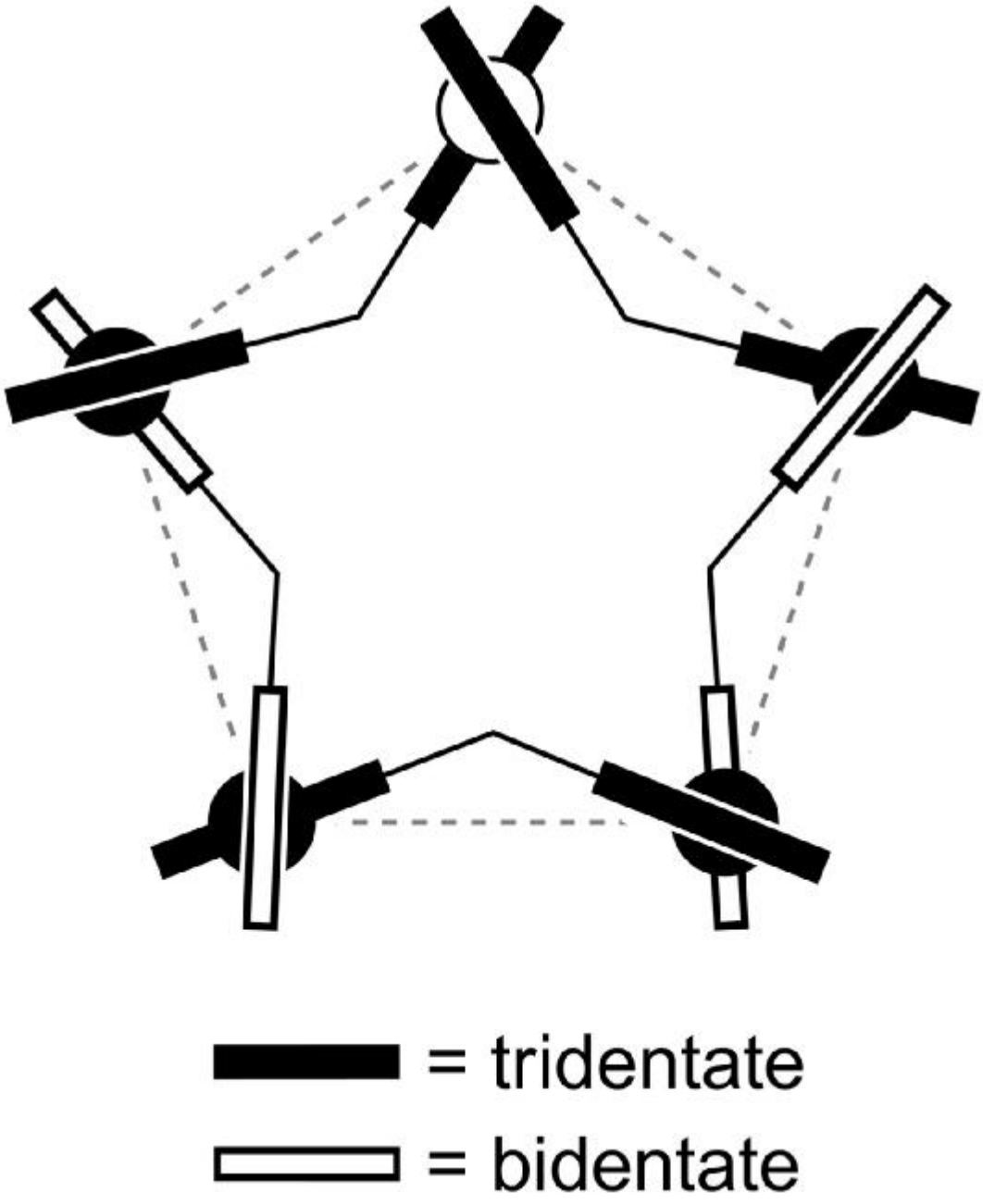

Figure 4.5. Schematic diagram of $[Cu_5(\mathbf{L}^4)_3(\mathbf{L}^6)_2]^{10+}$ (black and open circles represent 5- and 6-coordinate Cu^{II}, respectively.

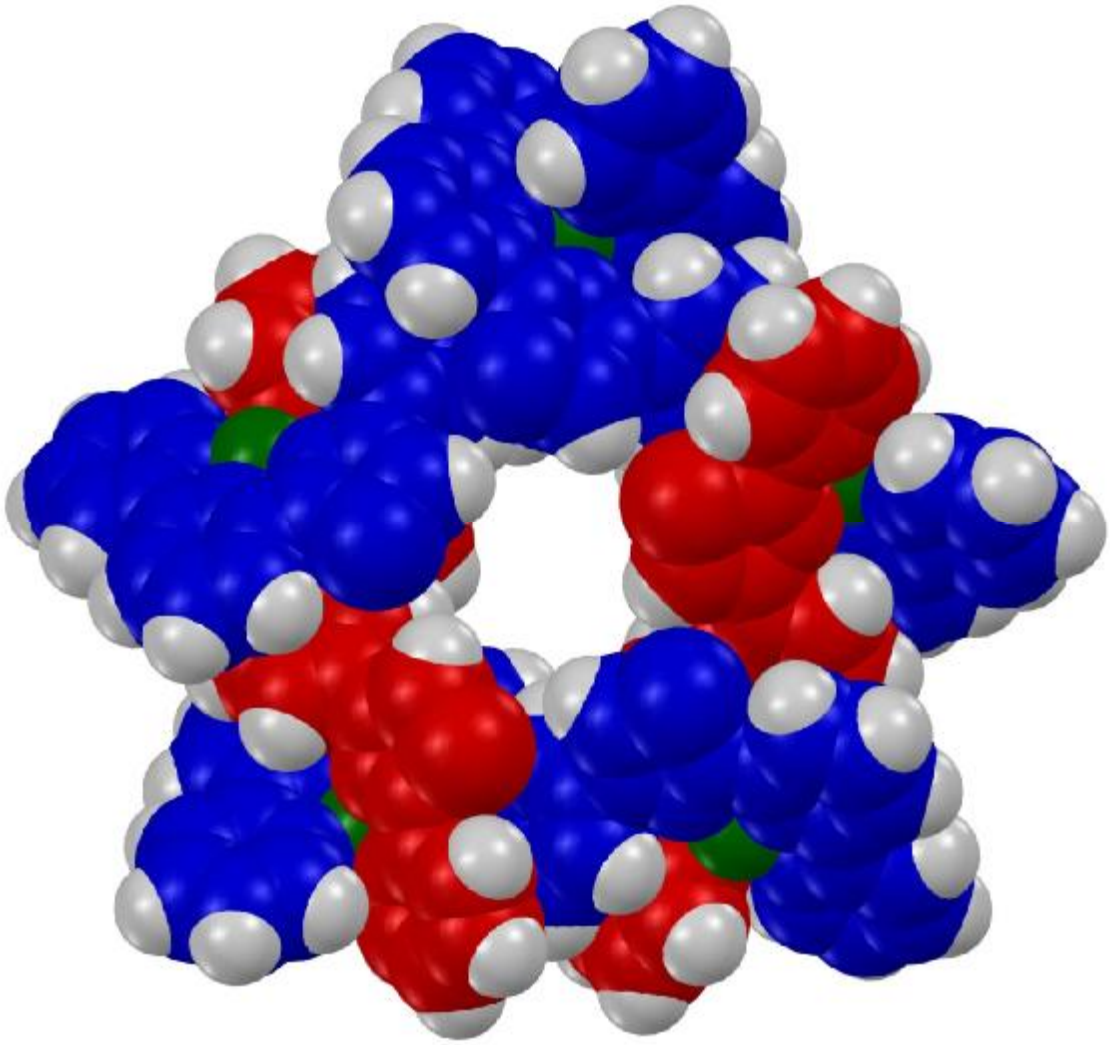

Figure 4.6. Space-filling view of the complex cation $[Cu_5(\mathbf{L^4})_3(\mathbf{L^6})_2]^{10+}$, blue = L^4, red = L^6, green = Cu^{2+}.

In the crystal structure, there is a cyclic array of five copper(II) ions, coordinated by three strands of $\mathbf{L^4}$ and two strands of $\mathbf{L^6}$. As the assembly has an odd number of ligands one of the Cu^{II} centres is 6-coordinate, formed by two tridentate thiazole-pyridyl-pyridyl domains from $\mathbf{L^4}$. The remaining four Cu^{II} centres are coordinated by a tridentate domain from $\mathbf{L^4}$ and a bidentate domain from $\mathbf{L^6}$, resulting in 5-coordinate donor sets. The ligands bridge adjacent metal ions in an "over and under" conformation giving the complex a circular helicate topology with approximate C_2-symmetry.

Bond	Bond length (Å)	Bond	Bond length (Å)
Cu(1)-N(11)	2.18(1)	Cu(3)-N(131)	2.06(1)
Cu(1)-N(21)	1.97(1)	Cu(3)-N(141)	1.949(9)
Cu(1)-N(31)	2.263(7)	Cu(3)-N(151)	2.16(1)
Cu(1)-N(291)	2.231(9)	Cu(4)-N(171)	2.171(8)
Cu(1)-N(301)	1.94(1)	Cu(4)-N(181)	1.955(9)
Cu(1)-N(311)	2.11(1)	Cu(4)-N(191)	2.04(1)
Cu(2)-N(51)	2.19(1)	Cu(4)-N(201)	2.02(1)
Cu(2)-N(61)	1.98(1)	Cu(4)-N(211)	2.29(1)
Cu(2)-N(71)	2.06(1)	Cu(5)-N(231)	2.37(1)
Cu(2)-N(81)	2.010(9)	Cu(5)-N(241)	2.034(9)
Cu(2)-N(91)	2.359(8)	Cu(5)-N(251)	2.06(1)
Cu(3)-N(111)	2.287(8)	Cu(5)-N(261)	1.921(7)
Cu(3)-N(121)	1.99(1)	Cu(5)-N(271)	2.16(1)

Table 12. Selected bond lengths (Å) for the complex cation $[Cu_5(\mathbf{L}^{4})_3(\mathbf{L}^{6})_2]^{10+}$.

Bond	Bond angle (°)	Bond	Bond angle (°)
N(11)-Cu(1)-N(21)	79.3(4)	N(61)-Cu(2)-N(81)	175.1(4)
N(11)-Cu(1)-N(31)	155.9(4)	N(61)-Cu(2)-N(91)	101.5(4)
N(11)-Cu(1)-N(291)	101.4(4)	N(71)-Cu(2)-N(81)	95.9(5)
N(11)-Cu(1)-N(301)	97.9(4)	N(71)-Cu(2)-N(91)	106.9(4)
N(11)-Cu(1)-N(311)	87.8(5)	N(81)-Cu(2)-N(91)	76.8(3)
N(21)-Cu(1)-N(31)	76.8(3)	N(111)-Cu(3)-N(121)	78.0(4)
N(21)-Cu(1)-N(291)	106.4(4)	N(111)-Cu(3)-N(131)	103.9(3)
N(21)-Cu(1)-N(301)	175.6(4)	N(111)-Cu(3)-N(141)	106.8(3)
N(21)-Cu(1)-N(311)	97.5(4)	N(111)-Cu(3)-N(151)	82.8(3)
N(31)-Cu(1)-N(291)	82.7(3)	N(121)-Cu(3)-N(131)	95.2(4)
N(31)-Cu(1)-N(301)	106.1(3)	N(121)-Cu(3)-N(141)	173.4(4)
N(31)-Cu(1)-N(311)	98.1(4)	N(121)-Cu(3)-N(151)	106.6(4)
N(291)-Cu(1)-N(301)	77.4(4)	N(131)-Cu(3)-N(141)	79.4(4)
N(291)-Cu(1)-N(311)	155.5(4)	N(131)-Cu(3)-N(151)	158.1(3)
N(301)-Cu(1)-N(311)	78.9(4)	N(141)-Cu(3)-N(151)	78.7(3)
N(51)-Cu(2)-N(61)	79.2(4)	N(171)-Cu(4)-N(181)	79.2(4)
N(51)-Cu(2)-N(71)	159.2(4)	N(171)-Cu(4)-N(191)	158.5(4)
N(51)-Cu(2)-N(81)	104.9(4)	N(171)-Cu(4)-N(201)	104.7(4)
N(51)-Cu(2)-N(91)	79.2(3)	N(171)-Cu(4)-N(211)	82.9(3)
N(61)-Cu(2)-N(71)	80.1(5)	N(181)-Cu(4)-N(191)	79.3(4)
N(181)-Cu(4)-N(201)	174.2(4)	N(231)-Cu(5)-N(271)	79.5(3)

N(181)-Cu(4)-N(211)	108.0(4)	N(241)-Cu(5)-N(251)	97.7(4)
N(191)-Cu(4)-N(201)	96.8(4)	N(241)-Cu(5)-N(261)	176.3(4)
N(191)-Cu(4)-N(211)	104.2(4)	N(241)-Cu(5)-N(271)	104.7(4)
N(201)-Cu(4)-N(211)	77.0(4)	N(251)-Cu(5)-N(261)	78.8(4)
N(231)-Cu(5)-N(241)	76.6(3)	N(251)-Cu(5)-N(271)	157.6(4)
N(231)-Cu(5)-N(251)	105.7(4)	N(261)-Cu(5)-N(271)	78.8(4)
N(231)-Cu(5)-N(261)	103.4(3)		

Table 13. Selected bond angles (°) for the complex cation $[Cu_5(\mathbf{L^4})_3(\mathbf{L^6})_2]^{10+}$.

4.3 Solution Studies

4.3.1 Solution state characterization of $[Cu_5(L^5)_5]^{10+}$

Although there was an ion in the ESI-mass spectrum at *m/z* 1745 corresponding to the dication $\{[Cu_5(\mathbf{L^5})_5](ClO_4)_8\}^{2+}$ (Figure 4.7), evidence for the selective formation of $[Cu_5(\mathbf{L^5})_5]^{10+}$ in solution was gained via tandem MS ascertaining whether the low nuclearity species observed in the ESI-mass spectrum of $[Cu_5(\mathbf{L^5})_5](ClO_4)_{10}$ are present in solution or merely products of gas-phase fragmentation in the ion source (Figure 4.9). The results demonstrated that selective collision-induced fragmentation of the ion at *m/z* 1745 gave rise to peaks at *m/z* 901, 1376 and 2114, indicating clear correlation between the pentanuclear parent ion and $\{[Cu_2(\mathbf{L^5})](ClO_4)_3\}^+$, $\{[Cu_2(\mathbf{L^5})_2](ClO_4)_3\}^+$ and $\{[Cu_3(\mathbf{L^5})_3](ClO_4)_5\}^+$, respectively (Figure 4.8). However, due to the paramagnetic nature of the d^9 metal ion analysis by ^1H NMR spectrometry is precluded. However, the distribution of species in the ESI-MS of $[Cu_5(\mathbf{L^5})_5](ClO_4)_{10}$ is strikingly similar to that observed for the previously reported zinc-based circular helicate $[Zn_5(\mathbf{L^4})_5](CF_3SO_3)_{10}$, whose solid-state structure was shown to be quantitatively retained in solution.

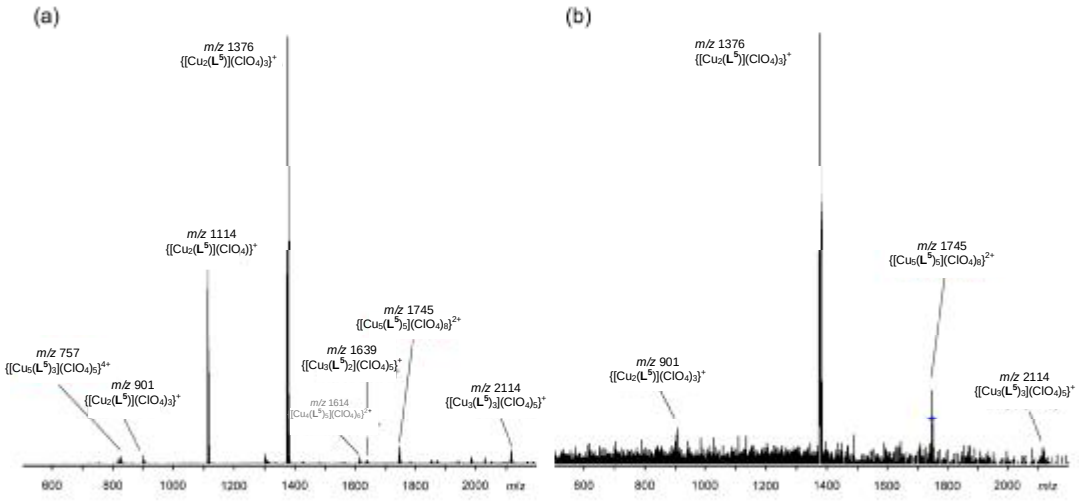

Figure 4.7. (a) Selected assignments in the ESI-mass spectrum of $[Cu_5(\mathbf{L^5})_5](ClO_4)_{10}$ and (b) tandem-MS experiment showing selective collision-induced fragmentation of the ion at *m/z* 1745 corresponding to the dication $\{[Cu_5(\mathbf{L^5})_5](ClO_4)_8\}^{2+}$. $[\mathbf{L}]_{tot} = 10^{-4}$ M. The ion at *m/z* 2114 ($\{[Cu_3(\mathbf{L^5})_3](ClO_4)_5\}^{+}$), although small, persisted under a variety of collision conditions indicating that this is not an artefact but a true product ion of $\{[Cu_5(\mathbf{L^5})_5](ClO_4)_8\}^{2+}$.

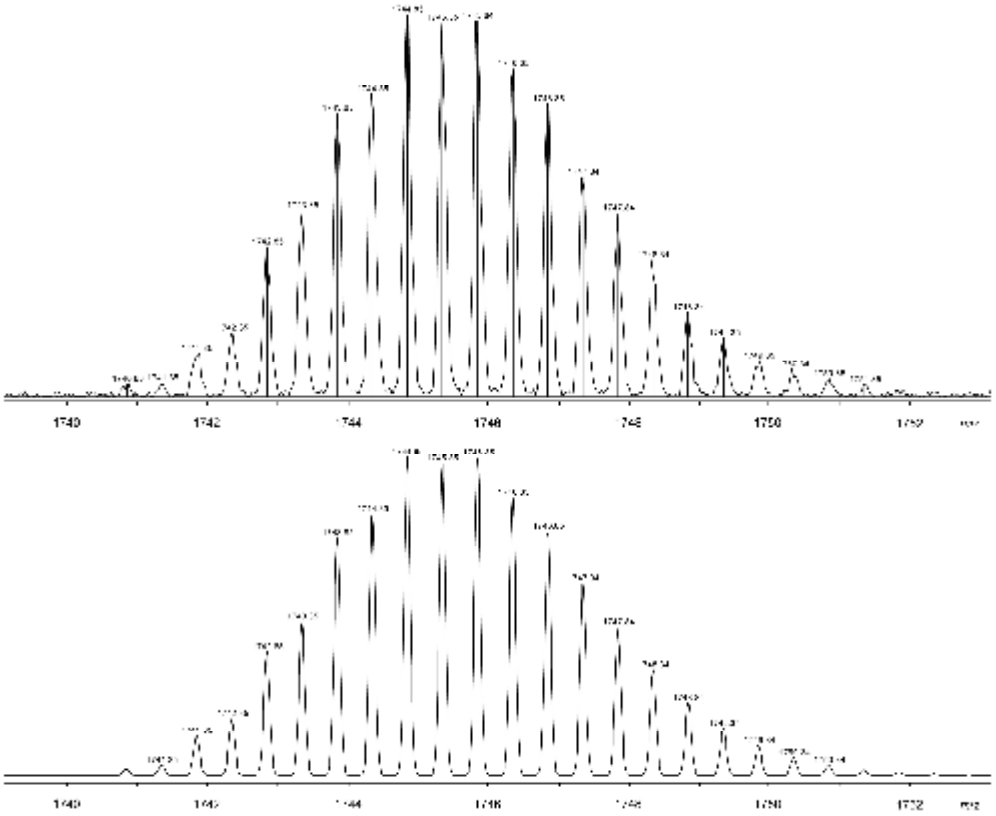

Figure 4.8. Observered (top) and calculated (bottom) isotope distribution patterns for the ion at *m/z* 1745 corresponding to the dication $\{[Cu_5(\mathbf{L^5})_5](ClO_4)_8\}^{2+}$.

4.3.2 Solution state characterization of $[Cu_5(L^4)_3(L^6)_2]^{10+}$

Although an ion in the ESI-mass spectrum corresponding to $\{[Cu_5(\mathbf{L^4})_3(\mathbf{L^6})_2](ClO_4)_8\}^{2+}$ is clearly present, studies indicate that reaction of Cu^{2+} with $\mathbf{L^4}$ and $\mathbf{L^6}$ in the ideal ratio (i.e. 5:3:2 respectively) not only forms the desired pentanuclear heteroleptic circular helicate complex $\{[Cu_5(\mathbf{L^4})_3(\mathbf{L^6})_2](ClO_4)_8\}^{2+}$, but other $\mathbf{L^4}$-rich species such as $\{[Cu_5(\mathbf{L^4})_5](ClO_4)_8\}^{2+}$, $\{[Cu_5(\mathbf{L^4})_4(\mathbf{L^6})](ClO_4)_8\}^{2+}$; related fragments are also present (Figure 4.9).

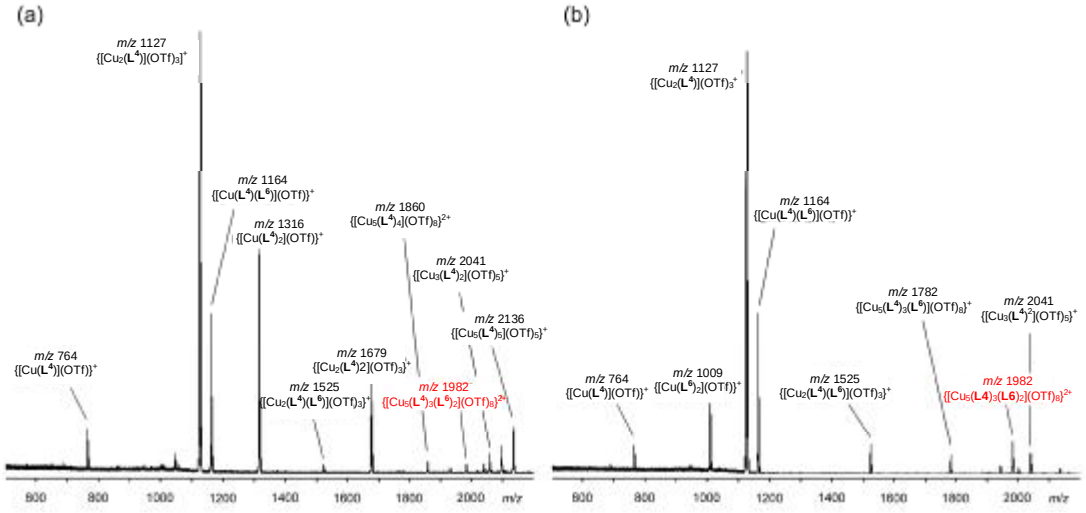

Figure 4.9. Selected assignments in the ESI-mass spectra of solutions containing $Cu(OTf)_2$, $\mathbf{L^4}$ and $\mathbf{L^6}$ in (a) a 5:3:2 ratio and (b) a 2:1:1 ratio. $[\mathbf{L}]_{tot} = 10^{-4}$ M.

However, combining Cu^{II}, $\mathbf{L^4}$ and $\mathbf{L^6}$ in 2:1:1 ratio, respectively, in acetonitrile, gave a solution for which ESI-MS showed virtually no traces of $\{[Cu_5(\mathbf{L^4})_5](ClO_4)_8\}^{2+}$ and $\{[Cu_5(\mathbf{L^4})_4(\mathbf{L^6})](ClO_4)_8\}^{2+}$. Since the components were combined in non-stoichiometric quantities, the solution clearly contains a mixture of inter-converting species. Lacking ESI-MS response factors for the ions observed in the gas-phase, we are not able to estimate the extent to which the target heteroleptic pentanuclear complex dominates in solution. However, it is clear that the heteroleptic complex is present in solution and not an artifact of crystallization. Furthermore, the formation of this species is highly repeatable as $[Cu_5(\mathbf{L^4})_3(\mathbf{L^6})_2](CF_3SO_3)_{10}$ can be obtained in good yield (~75 %) from either $MeNO_2$ or MeCN by diffusion of a variety of non-polar solvents. Several batches of crystals were produced from both solvents and

either a full data set or unit cell collected, each time giving the same cell parameters as those observed for the structure reported.

4.4 Conclusion

We have demonstrated the first reported examples of head-to-tail and heteroleptic cyclic helicates. Both solid state and solution studies indicate that the pentanuclear circular helicates *HT*-$[Cu_5(\mathbf{L^5})_5]^{10+}$ and $[Cu_5(\mathbf{L^4})_3(\mathbf{L^6})_2]^{10+}$ are formed. The structures of both *HT*-$[Cu_5(\mathbf{L^5})_5]^{10+}$ and $[Cu_5(\mathbf{L^4})_3(\mathbf{L^6})_2]^{10+}$ are analogous to their linear counterparts by virtue of both their specific structural features and the design principles employed in their synthesis. The formation of these head-to-tail (for $\mathbf{L^5}$) and heteroleptic (for $\mathbf{L^4}$ and $\mathbf{L^6}$) helicates is a result of two key factors. Firstly, the phenylene spacer units which connect various N-donor units and prevent the ligand from forming linear double-stranded assemblies (with small cations such as Zn^{II}). Secondly, the stereoelectronic preference of Cu^{II}, demonstrating versatility enabling both (1) all 5- or all 6-coordinate sites, or (2) a mixture of 5- and 6-coordinate sites to occur in the same polynuclear array. In summary, we have established that some of the basic algorithms for programming structural complexity in linear helicates can also be applied to related cyclic complexes.

5. Formation of a Pyrene-Containing Tetranuclear Circular Helicate.

Described in this chapter is the synthesis and coordination chemistry of a potentially hexadentate N-donor ligand **L**[7]. This ligand contains two identical tridentate thiazole-pyridine-pyridine N_3 binding domains separated by a pyrene unit (Figure 5.1).

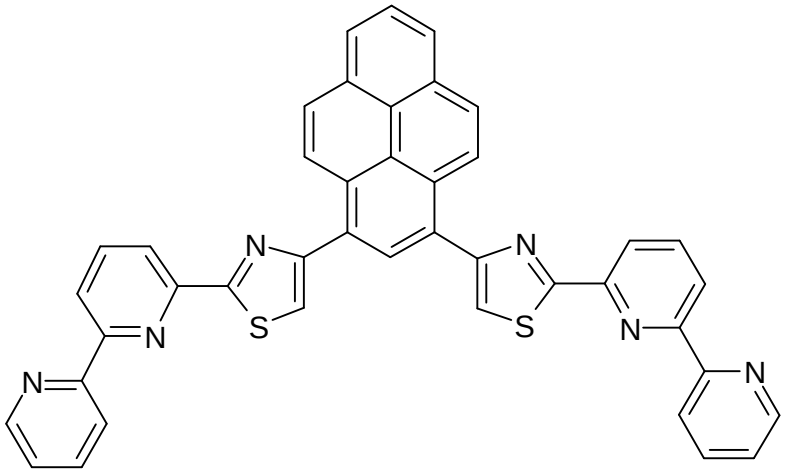

Figure 5.1. The potentially hexandentate ligand **L**[7].

5.1.1 Synthesis of L[7]

The synthesis of **L**[7] is outlined in scheme 5.1. Synthesis of 1,3-diacetyl pyrene was achieved by Freidel-Craft acylation of pyrene with excess acetyl chloride and aluminum chloride resulting in the desired isomer 1,3-diactylpyrene (**2**), as well as two other unwanted isomers, 1,6- and 1,8-diactylpyrene, respectively. Although the 1,3- isomer was the minor product (> 3%) it can be isolated in usable quantities through a combination of crystallization and extensive column chromatography.[90,91] Reaction of the diketone (**2**) with bromine in chloroform gave variable yields of the corresponding 1,3-dibromoacetylpyrene (**3**). However, reaction of (**2**) with bromine in acetic acid gave the dibrominated species more reliably and in greater yields. Reaction of the dibromo-ketone (**3**) and 2,2'-bipyridine-6-thioamide in EtOH at reflux afforded **L**[7] as a pale yellow solid. Confirmation of the successful formation of **L**[7] was obtained by ^{1}H NMR which showed 13 aromatic signals including 5

arising from the pyrene spacer. Furthermore an ion in the ESI-MS was observer at m/z 677 corresponding to ($\mathbf{L^7}$ + H^+).

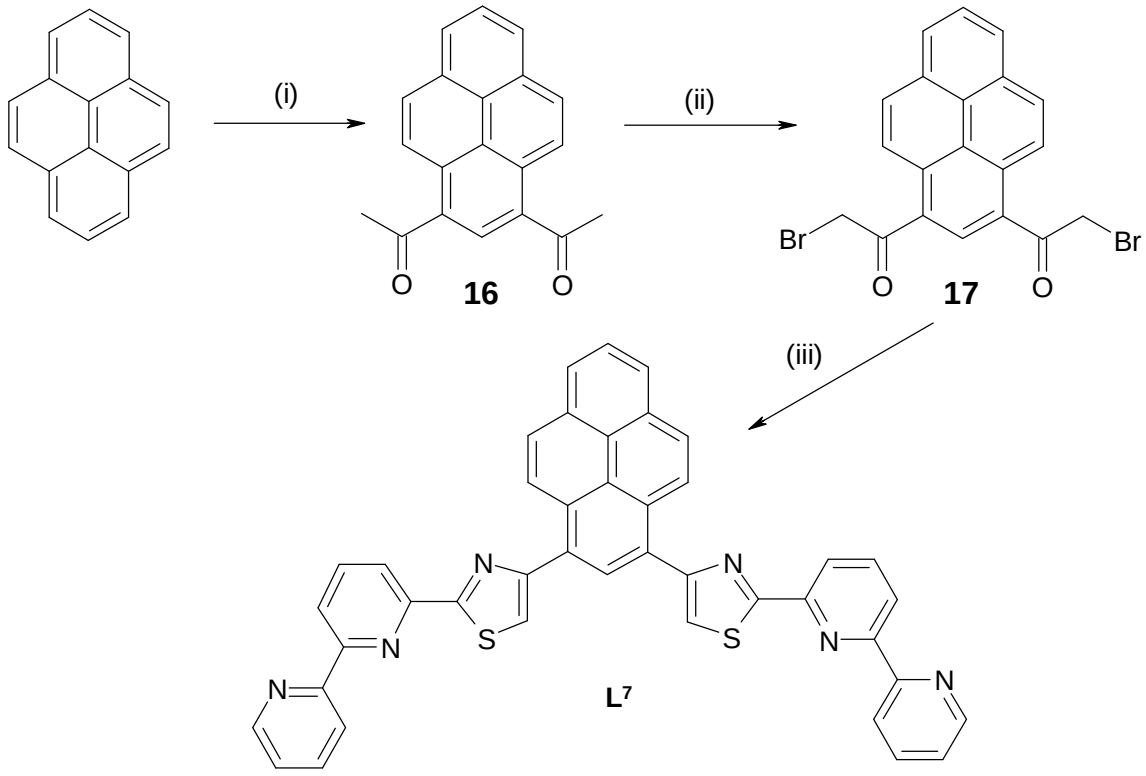

Scheme 5.1. Synthesis of $\mathbf{L^7}$. Reagents and conditions; (i) $AlCl_3$, CH_3COCl, CS_2, 60°C (ii) Br_2, CH_3COOH , 80°C (iii) 2,2'-bipyridine-6-thioamide, EtOH, reflux.

5.2 Coordination Chemistry

5.2.1 Coordination Chemistry of L^7 with Zinc(II)

The reaction of $\mathbf{L^7}$ with an equimolar amount of $Zn(CF_3SO_3)_2$ in acetonitrile results in a pale yellow solution. Analysis by ESI-MS studies show a number of low nuclearity fragments (m/z: 891, 1254 and 1567, corresponding to {[M($\mathbf{L^7}$)] (CF_3SO_3)}+, {[M_2($\mathbf{L^7}$)$(CF_3SO_3)_3$]}+ and {[M($\mathbf{L^7}$)$_2$](CF_3SO_3)}+ respectively), but also a peak at *m/z* 1931 which corresponds to the tetranuclear species {[Zn_4($\mathbf{L^7}$)$_4(CF_3SO_3)_6$}$^{2+}$ but despite exhaustive attempts suitable crystals for X-ray diffraction could not be grown. However, heating a

solution of $\mathbf{L^7}$ and $Zn(CF_3SO_3)_2$ in MeCN at 60˚C overnight followed by slow diffusion of ethyl acetate resulted in large yellow crystals. Structural analysis by single crystal X-ray diffraction confirmed the formation of the tetranuclear cyclic helicate $[Zn_4(\mathbf{L^7})_4]^{8+}$ (Figure 5.2).

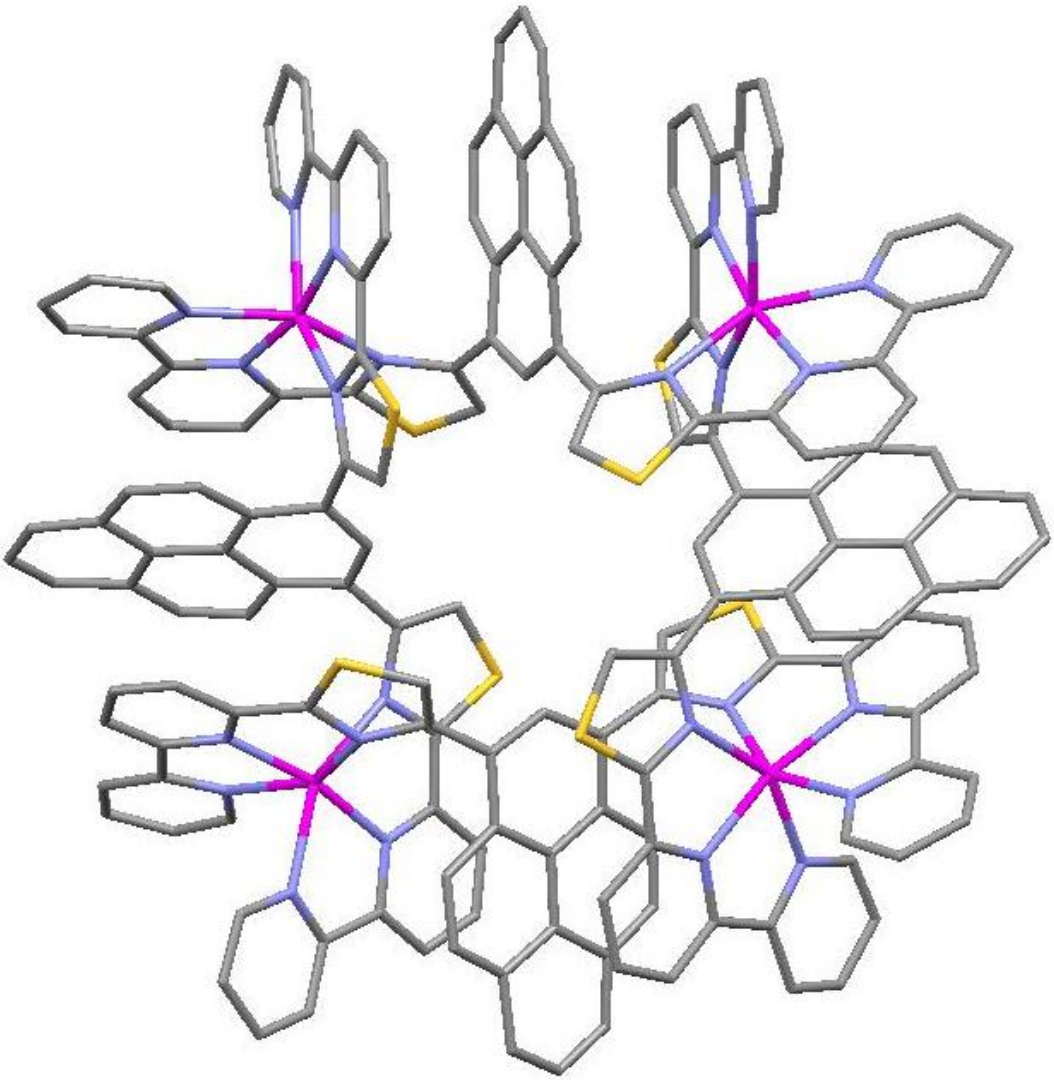

Figure 5.2. Solid state structure of the cyclic helicate $[Zn_4(\mathbf{L^7})_4]^{8+}$.

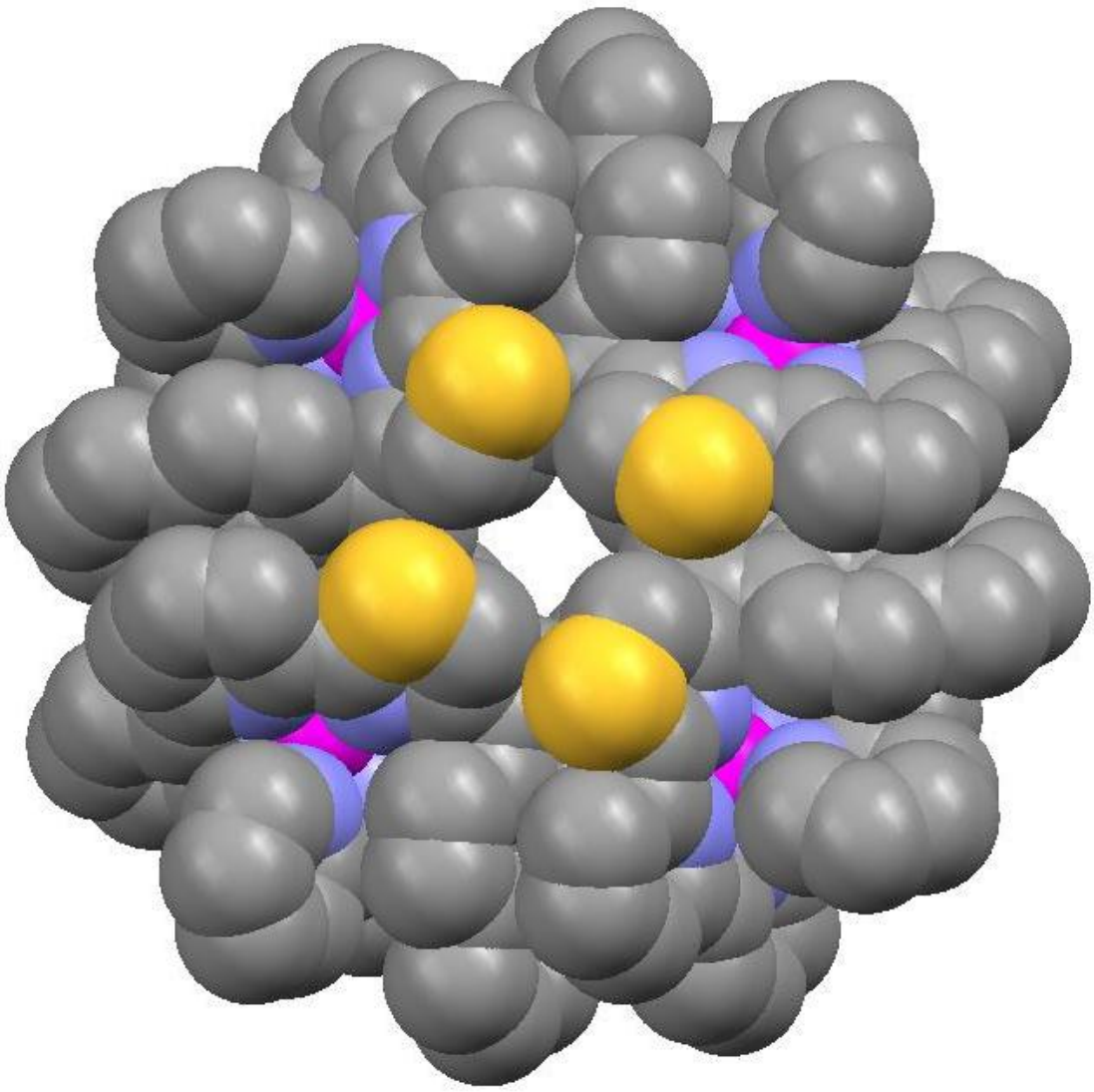

Figure 5.3. Space-filling picture showing atoms with their van der Waals radii of the cyclic helicate $[Zn_4(\mathbf{L}^7)_4]^{8+}$.

In the solid state there are four zinc metal ions coordinated by four ligands with all Zn^{2+} ions adopting a six-coordinate distorted octahedral coordination geometry, arising from the coordination of two tridentate thiazole-pyridyl-pyridyl domains from two different ligands (Zn-N: 2.074(1)-2.250(1) Å). The 1,3-pyrene spacers bridge each of the tridentate domains in an 'over and under' conformation.

Bond	Bond length (Å)	Bond	Bond length (Å)
Zn(1)-N(11)	2.079(4)	Zn(2)-N(51)	2.201(4)
Zn(1)-N(11')	2.079(4)	Zn(2)-N(51')	2.201(4)
Zn(1)-N(21)	2.232(4)	Zn(2)-N(61)	2.101(4)
Zn(1)-N(21')	2.232(4)	Zn(2)-N(61')	2.101(4)
Zn(1)-N(81)	2.191(4)	Zn(2)-N(71)	2.194(4)
Zn(1)-N(81')	2.191(4)	Zn(2)-N(71')	2.194(4)

Table 14. Selected bond lengths (Å) for the complex cation $[Zn_4(\mathbf{L}^7)_4]^{8+}$.

Bond	Bond angles (°)	Bond	Bond angles (°)
N(11)-Zn(1)-N(21)	76.6(2)	N(51)-Zn(2)-N(61)	75.4(2)
N(11)-Zn(1)-N(81)	75.7(2)	N(51)-Zn(2)-N(71)	149.1(2)
N(11)-Zn(1)-N(11)	168.3(2)	N(51)-Zn(2)-N(51)	85.8(1)
N(11)-Zn(1)-N(21)	113.6(2)	N(51)-Zn(2)-N(61)	113.9(2)
N(11)-Zn(1)-N(81)	95.6(2)	N(51)-Zn(2)-N(71)	99.3(2)
N(21)-Zn(1)-N(81)	150.7(2)	N(61)-Zn(2)-N(71)	74.7(2)
N(21)-Zn(1)-N(11)	113.6(2)	N(61)-Zn(2)-N(61)	168.1(2)
N(21)-Zn(1)-N(21)	83.2(1)	N(61)-Zn(2)-N(71)	96.8(2)
N(21)-Zn(1)-N(81)	103.1(2)	N(71)-Zn(2)-N(71)	91.8(2)
N(81)-Zn(1)-N(81)	85.4(2)		

Table 15. Selected bond angles (°) for the complex cation $[Zn_4(\mathbf{L}^7)_4]^{8+}$.

5.3 Solution Studies

5.3.1 Solution state characterization of $[Zn_4(L^7)_4]^{8+}$.

Reaction of **L^7** with an equimolar amount of $Zn(CF_3SO_3)_2$ in CD_3CN and directly obtaining a ^1H NMR gave a complex spectrum with some very broad peaks as well as a small amount of sharp signals (Figure 5.4 (a)). After heating for 1hr at 60˚C the broad peaks disappeared and only the sharp signals remain (Figure 5.4 (b)). Analysis by ^1H / ^1H COSY NMR indicates that there are two species present with one set of signals corresponding to ~90% of the products. Further heating results in an increase in the ratio of the minor species (Figure 5.4 (c)) and after heating for 36 hrs the species which was originally the minor product in now the sole species.

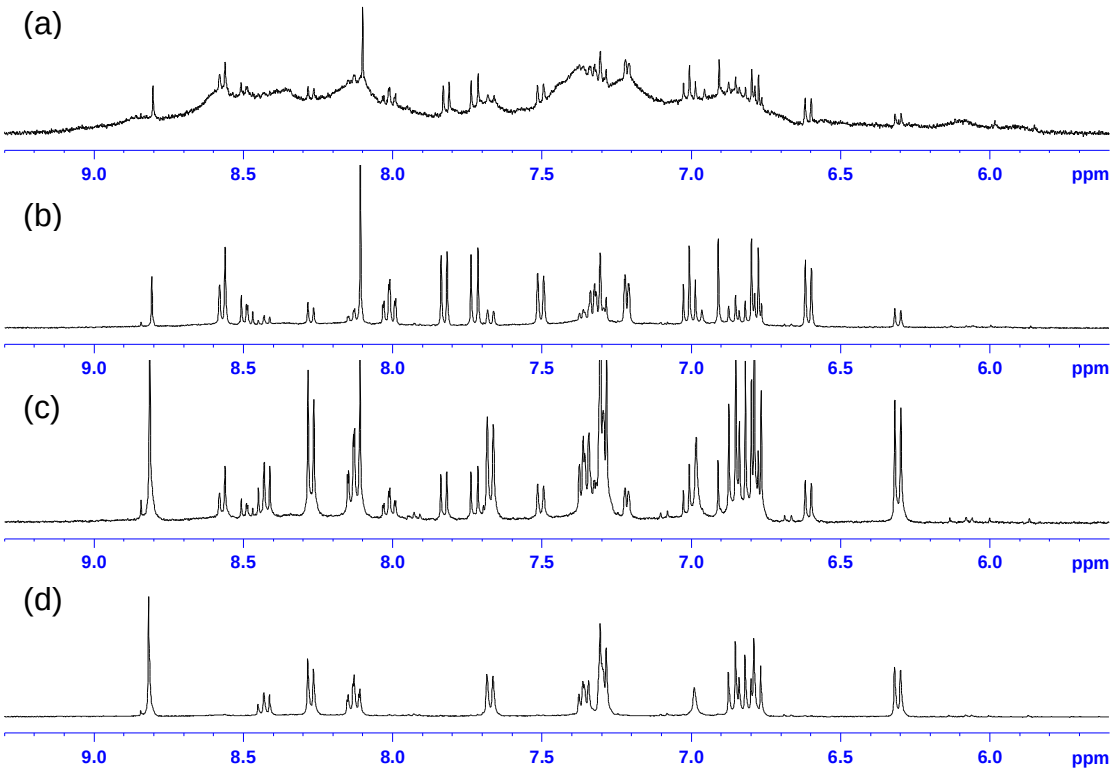

Figure 5.4. Aromatic regions in the ^1H NMR spectra of the reaction of **L^7** and $Zn(CF_3SO_3)_2$ (CD_3CN) (a) T_0 (b) T = 1 hour at 60°C (c) T = 16 hours at 60°C and (d) T = 36 hours at 60°C.

A change in the ESI-MS upon heating is also observed. After mixing the ligand and zinc triflate the sample was analyzed by mass spectrometry and a number of ions were observed (m/z: 891, 1254 and 1567, corresponding to

{[M($\mathbf{L^7}$)] (CF_3SO_3)}+, {[M_2($\mathbf{L^7}$)(CF_3SO_3)$_3$]}+ and {[M($\mathbf{L^7}$)$_2$](CF_3SO_3)}+ respectively and an ion at *m/z* 1931 corresponding to {[Zn_4($\mathbf{L^7}$)$_4$(CF_3SO_3)$_6$}$^{2+}$. After heating the sample the lower molecular weight ions significantly reduced in intensity and correspondingly the ion at *m/z* 1931 was the most predominant species.

5.4 Discussion

It is clear that reaction of $\mathbf{L^7}$ with an equimolar amount of $Zn(CF_3SO_3)_2$ in CD_3CN gives, after heating for 36 hrs, gives the tetranuclear cyclic helicate [Zn_4($\mathbf{L^7}$)$_4$]$^{8+}$ as the sole product. In an analogous fashion to the cyclic helicates discussed previously, the formation of the cyclic species is controlled by the spacer unit as this prevents formation of the "simple" dinuclear species due to intra-ligand steric repulsion. However, unlike the 1,3-phenylene analogues which result in the pentanuclear species [M_5**(L)**$_5$]$^{10+}$, the 1,3-pyrene spacer forms a tetranuclear species. As both pyrene and phenyl have the same substitution pattern (i.e. 1,3-) the formation of the lower nuclearity species must be a consequence of the ability of the pyrene to undergo π-stacking (an effect that is observed quite often with pyrene). In the pentanuclear species [Zn_5($\mathbf{L^4}$)$_5$]$^{10+}$ the angle between the planes formed by the two py-py-tz domains is 16.66˚, but in the tetranuclear species this angle is reduced to 9.71˚ as a result of the π-stacking interaction between the pyrene unit and the py-py-tz domain. This reduction in angle results in the formation of a tetranuclear species as the two domains are close to parallel (a requirement for the formation of a four-sided species) (figure 5.5).

As a result of the steric requirements the distance between the two py-py-tz binding domains increases but the distance between the spacer unit (e,g, Ph or pyrene) decreases (Table 16).

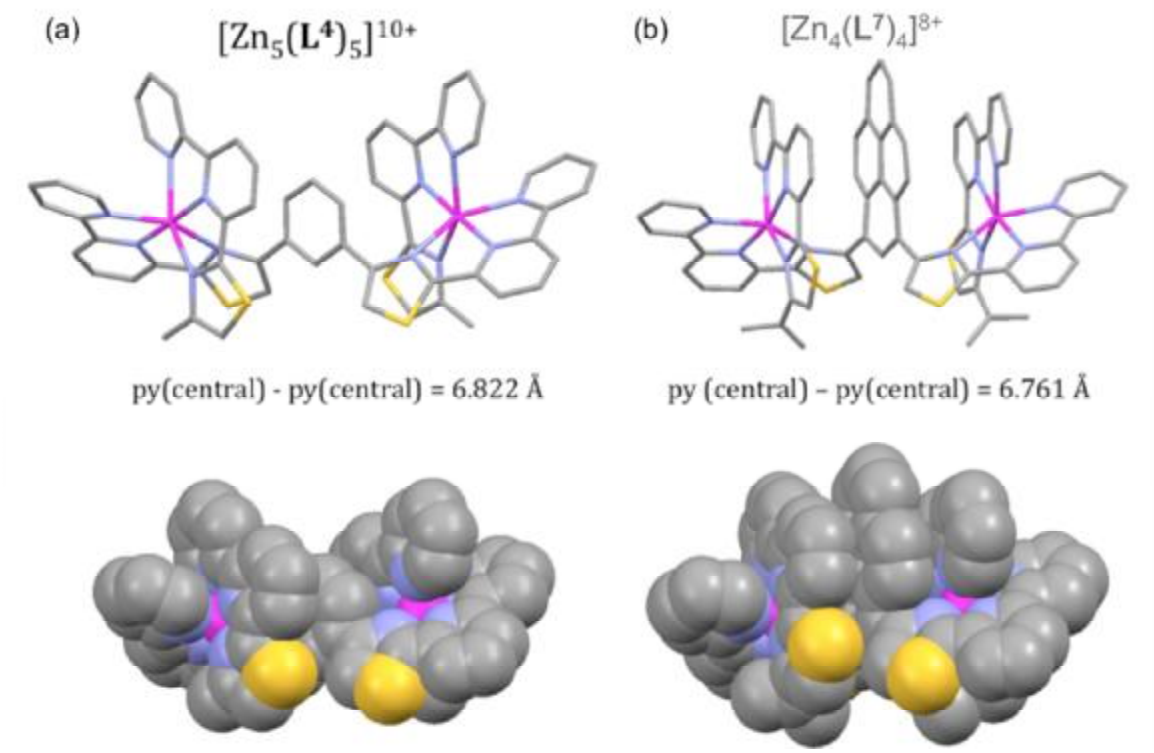

Figure 5.5. Two views of (a) $[Zn_5(\mathbf{L^4})_5]^{10+}$ and (b) $[Zn_4(\mathbf{L^7})_4]^{8+}$ taken from a section of the molecular structure obtained by crystallography.

	$[Zn_5(\mathbf{L^4})_5]^{10+}$	Vs	$[Zn_4(\mathbf{L^7})_4]^{8+}$
py - ph	3.936 – 4.106 Av. = 4.021	>	3.710 – 4.042 Av. = 3.899
py - py	6.761 Av. = 6.761	<	6.595 – 7.055 Av. = 6.822

Table 16. Selected distances for the complex cations $[Zn_5(\mathbf{L^4})_5]^{10+}$ and $[Zn_4(\mathbf{L^7})_4]^{8+}$, respectively.

The ability of the pyrene unit to undergo *π*-stacking also explains why the reaction need to be heated for 36 hrs to go to completion. Upon mixing $\mathbf{L^7}$ and

Zn^{2+} the ^{1}H NMR indicates that, although some discrete complexes are formed, the broad signals present are indicative of oligomers/polymers. The polymeric species are quickly converted into distinct complexes by heating for 1 hr. From chemical shift values it is clear that the minor species is the tetranuclear cyclic helicate. Diffusion ordered NMR spectroscopy (DOSY) analysis of the mixed species shows that the signal at 6.26 ppm ($[Zn_4(\mathbf{L^7})_4]^{8+}$) has at diffusion coefficient = 6.889 (± 0.156) 10^{-10} m^2s^{-1}, whereas an analogous signals for the major product (after 1hr at 60 ˚C) has a diffusion coefficient 6.55 ppm = 7.725 (± 0.212) 10^{-10} m^2s^{-1}. The same difference in magnitude is observed with other analogous signals e.g. 7.59 ppm = 6.553 (± 0.133) 10^{-10} m^2s^{-1} ($[Zn_4(\mathbf{L^7})_4]^{8+}$) and 7.66 ppm = 7.967 (± 0.220) 10^{-10} m^2s^{-1} (initial species). The DOSY analysis shows that the initial species has a higher diffusion coefficient than the tetranuclear species and therefore this implies that this unknown species is smaller. Furthermore, the dinuclear species can be discounted, due to the unfavourable steric interaction between the two pyrene rings which prevents formation of the $[Zn_2(\mathbf{L^7})_2]^{4+}$. Therefore, in the absence of structural data it would seem likely that the initial species is the trinuclear cyclic helicate $[Zn_3(\mathbf{L^7})_3]^{6+}$ and this is slowly converted to the larger tetranuclear species $[Zn_4(\mathbf{L^7})_4]^{8+}$.

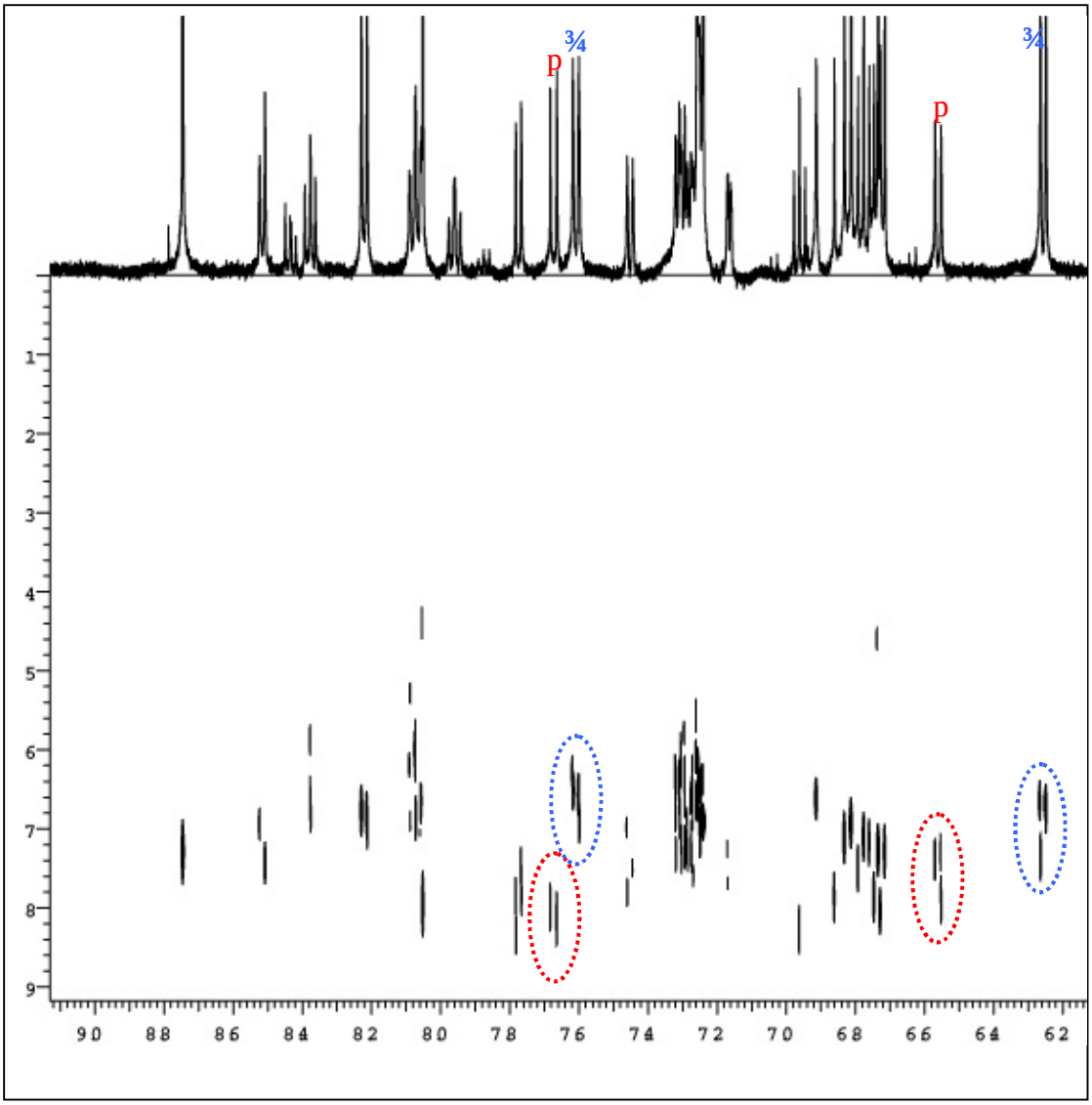

Figure 5.6. Diffusion Ordered NMR Spectroscopy of the reaction of $\mathbf{L^7}$ with $Zn(CF_3SO_3)_2$ after heating for 10 hrs (p = $[Zn_3(\mathbf{L^7})_3]^{6+}$, ¾ = $[Zn_4(\mathbf{L^7})_4]^{8+}$)

Conversion of the trinuclear species into $[Zn_4(\mathbf{L^7})_4]^{8+}$ requires heating for ~ 30 hrs at 60˚C as this conversion requires disassembly of the trimetallic helicate which is disfavoured due to the π-stacking between the pyrene and py/tz binding domain. As a result for full conversion to occur the reaction needs to be heated for prolonged periods of time.

As a result we have shown that inclusion of pyrene unit within a ligand chain not only programmes a ligand to adopt a cyclic species but also, through π-stacking effects, can control the nuclearity of the resultant species.

6. Conclusion

In conclusion seven novel multidentate N-donor ligands **L**^{1} - **L**^{7}, have been successfully synthesised and the coordination chemistry of all these ligands investigated.

The potentially hexadentate ligand **L**^{2} contains two isomeric pyridyl-thiazole containing tridentate domains. Reaction of **L**^{2} with either Zn^{II} or Hg^{II} results in the formation of the **L**^{2}-containing dinuclear double helicates $[Zn_2(\mathbf{L}^{2})_2]^{4+}$ and $[Hg_2(\mathbf{L}^{2})_2]^{4+}$. However, reaction with both Zn^{II} or Hg^{II} results in the sole formation of the heterodimetallic helicate $[HgZn(\mathbf{L}^{2})_2]^{+}$. The selectivity of these two isomeric domains is attributed to the divergent nature of the 5-membered thiazole ring and demonstrates how subtle changes within a ligand strand can have a pronounced effect on the metal selectivity. Furthermore, the preference of this units for metal of different cationic size allows the construction of the heterotrimetallic polynuclear array [*HH*-$[HgCuZn(\mathbf{L}^{3})_2]^{5+}$.

The potentially hexadentate ligand **L**^{4} contains two tridentate py-py-tz domains separated by a 1,3-phenylene spacer unit. Reaction of this ligand with Cd^{II} results in the formation of a dinuclear double helicate $[Cd_2(\mathbf{L}^{4})_2]^{4+}$. In this structure the ligand partitions into two tridentate tz-py-py domains each of which coordinate a different metal ion. However, reaction of **L**^{4} with Zn^{II} results in the formation of a pentanuclear circular helicate $[Zn_5(\mathbf{L}^{4})_5]^{10+}$, with all the five zinc ions adopting a octahedral coordination geometry arising from the coordination of the two tridentate tz-py-py domains from two different ligand strands. This difference in structure is attributed to unfavourable steric interactions which prevent the formation of $[Zn_2(\mathbf{L}^{4})_2]^{4+}$ but these unfavourable interactions are not present with the larger Cd^{2+} ion.

The ability of a ligand strand that contains a 1,3-phenylene spacer unit to form cyclic helicates with 1st row transition metal ions allows the formation of polynuclear cyclic helicates of further complexity. For example, the ligand **L**^{5} contains both a bidentate and tridentate binding site separated by a phenylene spacer unit. Reaction of **L**^{5} with Cu^{II} results in the formation of a pentanuclear circular helicate $[Cu_5(\mathbf{L}^{5})_5]^{10+}$. Each of the Cu^{II} ions adopts a 5-

coordinate geometry formed by coordination of the bidentate domain of one ligand strand and the tridentate domain of a different ligand. As a result this gives a head-to-tail pentanuclear double helicate *HT*-$[Cu_5(\mathbf{L^5})_5]^{10+}$. A heteroleptic pentanuclear cyclic helicate can also be formed by reaction of the bis-tridentate ligand $\mathbf{L^6}$ and bis-bidentate ligand $\mathbf{L^4}$ with Cu^{II} giving the pentanuclear species $[Cu_5(\mathbf{L^4})_3(\mathbf{L^6})_2]^{10+}$. The cyclic array consists of five copper(II) ions, coordinated by three strands of $\mathbf{L^4}$ and two strands of $\mathbf{L^6}$. In this species four of the Cu^{II} adopt a 5-coordinate geometry arising from coordination of a tridentate domain from $\mathbf{L^4}$ and a bidentate domain from $\mathbf{L^6}$. The remaining copper ion is coordinated by two tridentate domains from $\mathbf{L^4}$ resulting in an octahedral coordination geometry.

Control over the nuclearity of these cyclic helicates can also be aceived. For example, the potentially hexadentate N-donor ligand $\mathbf{L^7}$ which comprises of two identical tridentate py-py-tz N_3 binding domains separated by a pyrene unit, forms upon reaction with Zn^{II} a tetranuclear circular helicate $[Zn_4(\mathbf{L^7})_4]^{8+}$. In this species all four zinc metal ions adopt a six-coordinate geometry arising from the coordination of two tridentate py-py-tz units from two different ligand strands. The formation of this lower nuclearity species (e.g. tetranuclear rather than pentanuclear) is attributed to the π-stacking between the pyrene unit and the py-py-tz domain.

Thus it has been shown that careful design of ligand strands can produce species that are selective to metal ions of different cationic sizes. Furthermore, the formation of polynuclear cyclic helicates can be controlled so that tetra- and pentadentate are formed as well as head-to-tail and heteroleptic cyclic arrays.

7. Experimental

7.1 Preparation of L^1, L^2 and L^3

7.1.1 Synthesis of bipyridine 1-N-oxide (2)

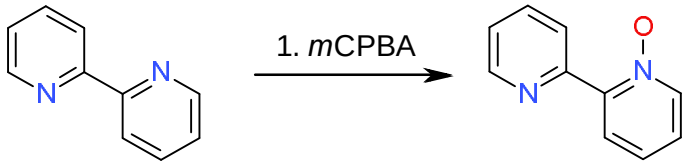

1 **2**

The synthesis of bipyridine 1-N-oxide, (**2**) was carried out in a similar manner to the procedure described previously by Rice and coworkers.[88] To a solution of 2,2'-bipridine (**1**) (1.0 g, 6.40 mmol) in DCM (40ml), *m*CPBA (77% 1.29 g, 5.76 mmol) was added slowly with stirring over 3 hours. The reaction was continually followed by TLC. Upon completion the solvent was reduced to half its volume by rotary evaporation, resulting in a viscose oil containing a mixture of both *mono* and *bis* N-oxidised derivatives and also un-reacted bipyridine. Purification of the crude product via column chromatography (1% MeOH in DCM, Al_2O_3) gave (**2**) as a white solid (0.89 g, 5.11 mmol, 80%).

^{1}H NMR [500 MHz, $CDCl_3$]: δ (ppm) 8.93 (d, *J* = 8.95, 1H), 8.75 (ddd, *J* = 4.8, 0.85, 1H), 8.35 (dd, *J* = 6.55, 1.1, 1H), 8.20 (dd, *J* = 8.0, 2.1, 1H), 7.86 (dt, *J* = 7.85, 1.8, 1H), (dt, *J* = 7.7, 1.2, 1H), 7.38 (dt, *J* = 7.55, 1.15 Hz, 1H), 7.30 (m, 1H).

7.1.2 Synthesis of 2,2'-bipyridine-6-carbonitrile, (3)

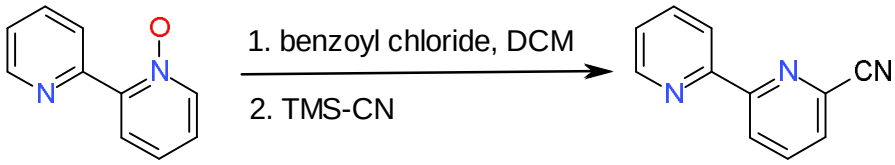

2 **3**

The synthesis of 2,2'-bipyridine 6-carbonitrile, (**3**) was carried out in a similar manner to the previous procedure described by Rice and coworkers.[88] A solution of 2,2'-bipyridine-1-oxide (**2**) (0.8 g, 4.65 mmol) and benzoyl chloride (0.71 g, 5.11 mmol) in DCM (50 ml) was refluxed, and trimethylsilyl cyanide (0.51 g, 5.11 mmol) was added slowly over a period of 30 minutes, followed by TLC and upon completion the solution was cooled and washed with $NaHCO_{3\ (aq)}$ (20 ml). Removal of the solvent by rotary evaporation gave the crude product as a brown oil, purification via column chromatography (1% MeOH in DCM, Al_2O_3) afforded 2'-bipyridine-6-carbonitrile (**3**) as a white solid (0.52 g, 62% yield).

^{1}H NMR [500 MHz, $CDCl_3$]: δ (ppm) 8.72 (m, 2H), 8.50 (d, *J* = 9.9, 1H), 7.97 (t, *J* = 9.8, 1H), 7.88 (dt, *J* = 9.7, 2.2, 1H), 7.72 (dd, *J* = 9.5, 1.2, 1H), 7.40 (ddd, *J* = 9.4, 5.9, 1.4 Hz, 1H).

ESI-MS *m/z* 181 (M^+).

7.1.3 Synthesis of 2,2'-bipyridine thioamide, (4)

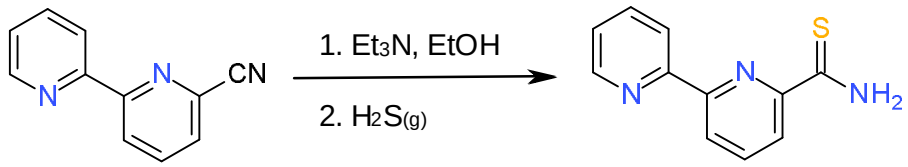

3 **4**

The synthesis of 2,2'-bipyridine 6-thioamide, (**4**) was carried out in a similar manner to the previous procedure described by Rice and coworkers.[88] To a solution of 2,2'-bipyridine-6-carbonitrile (**3**) (0.7 g, 3.84 mmol) in ethanol (20 ml), triethylamine (1.0 g, 9.9 mmol) was added and H_2S was slowly bubbled through the solution for 15 minutes, during which time the solution turned yellow. The yellow solution was allowed to stand for 48 hours during which time a yellow solid slowly precipitated. Collection via filtration gave pure 2,2'-bipyridine-6-thioamide (**4**) as a yellow solid (0.7 g, 85% yield).

^{1}H NMR [500 MHz, $CDCl_3$]: δ (ppm) 9.61 (broad s, 1H), 8.78 (d, *J* = 7.8, 1H), 8.73 (d, *J* = 4.7, 1H), 8.64 (d, *J* = 7.9, 1H), 8.38 (d, *J* = 7.95, 1H), 8.01 (t, *J* = 7.8, 1H), 7.88 (dt, *J* = 7.8, 1.5, 1H), 7.73 (br s, 1H), 7.39 (dd, *J* = 7.4, 4.8 Hz, 1H).

ESI-MS *m/z* 215 (M^+).

7.1.4 Synthesis of py-py-tz tridentate ester, (5)

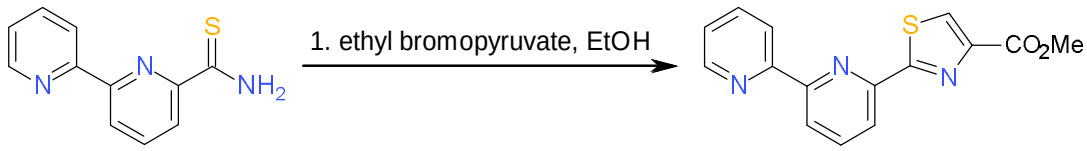

4 **5**

A solution of 2,2'-bipyridine-6-thioamide (**4**) (0.6 g, 2.79 mmol) and ethyl 3-bromopyruvate (0.60 g, 3.07 mmol) in ethanol (50 ml) was refluxed for 6 hours. On cooling large brown crystals of **5** slowly formed which were filtered and washed with ethanol (2 × 2 ml) and diethyl ether (2 × 2 ml) (0.5 g, 58% yield).

^{1}H NMR [500 MHz, $CDCl_3$]: δ (ppm) 9.19 (d, *J* = 5.5 Hz, 1H), 9.12 (d, *J* = 8.0 Hz, 1H), 8.85 (d, *J* = 8.0 Hz, 1H), 8.56 (d, *J* = 8.0 Hz, 1H), 8.54 (m, 1H), 8.33 (s, 1H), 8.18 (t, *J* = 8.0 Hz, 1H), 7.98 (t, *J* = 6.5 Hz, 1H), 4.45 (q, *J* = 7.0 Hz, 2H), 1.44 (t, *J* = 7.0 Hz, 3H).

ESI-MS *m/z* 312 ($M + H^+$).

7.1.5 Synthesis of py-py-tz tridentate alcohol, (6)

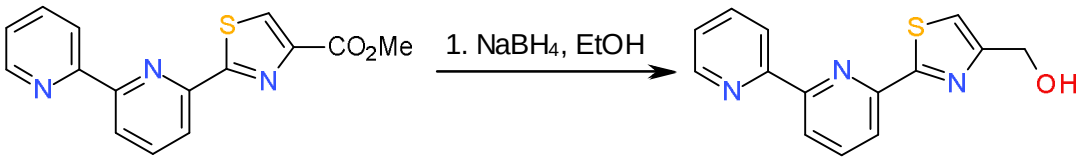

5 **6**

The tridentate ester (**5**) (0.2 g, 0.64 mmol) was added to a dry 100 ml two necked round bottom flask, under an atmosphere of nitrogen. Anhydrous THF (30 ml) was added to the flask and the resulting solution stirred in an ice bath at 0˚C for 15 minutes. To this lithium aluminium hydride, (1.0 M solution in diethyl ether, 1.28 ml, 1.28 mmol) was slowly added over the course of 20 minutes. Stirring was continued for 2 hours at 0˚C before removing the ice bath and allowing the reaction to gradually warm up to room temperature. Any remaining lithium aluminium hydride was quenched by slow addition of THF (2 ml), methanol (2 ml) and finally water (2 ml). The solvents were removed by rotary evaporation to leave a viscous yellow emulsion to which distilled water (20 ml) was added and extracted into DCM (4 × 50 ml). Evaporation of the organic solvent gave a yellow solid that was purified via column chromatography (1% MeOH in DCM, Al_2O_3) giving the tridentate alcohol (**6**) as a pale yellow solid (0.1 g, 58% yield).

^{1}H NMR [500 MHz, $CDCl_3$]: δ (ppm) 8.71 (d, *J* = 5.0 Hz, 1H), 8.57 (d, *J* = 8.0 Hz, 1H), 8.48 (d, *J* = 8.0 Hz, 1H), 8.19 (d, *J* = 7.0 Hz, 1H), 7.95 (t, *J* = 8.0 Hz, 1H), 7.9 (dt, *J* = 7.5, 1.5 Hz, 1H), 7.37 (ddd, *J* = 7.5, 5.0, 1.0 Hz, 1H), 7.34 (s, 1H), 4.89 (s, 2H), 2.45 (br s, 1H, -OH).

ESI-MS *m/z* 292 ($M+Na^+$).

7.1.6 Synthesis of py-tz-py tridentate ester, (8)

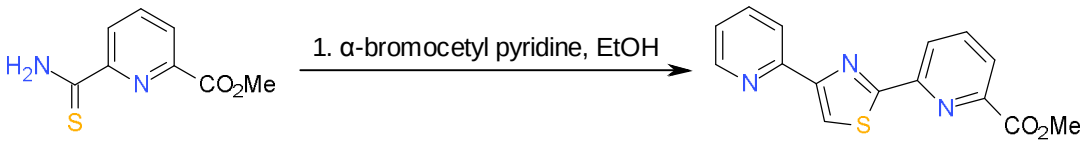

7 **8**

To a solution of methylpicolinate-6-thioamide (1.0 g, 5.1 mmol) in EtOH (25 ml) was added the hydrobromide salt of α-bromoacetyl pyridine (2.87 g, 10 mmol) and the solution refluxed for 6 hrs. The solution was then left to stand overnight during which time a precipitate formed, which was isolated by filtration giving the tridentate ester (**8**) as a tan solid (1.10 g, 73 % yield).

^{1}H NMR (400MHz, $CDCl_3$) δ 9.62 (s, 1H, tz), 8.96 (d, *J* = 5.6, 1H, py), 8.68 (d, *J* = 5.6, 1H, py), 8.61 (d, *J* = 7.8, 1H, py), 8.48 (dt, *J* = 7.8, 1.4, 1H, py), 8.20 (d, *J* = 6.8, 1H, py), 8.04 (t, *J* = 7.8, 1H, py), 7.84 (t, *J* = 7.2 Hz, 1H, py), 4.05 (s, 3H, -CH_3).

7.1.7 Synthesis of the py-tz-py tridentate alcohol, (9)

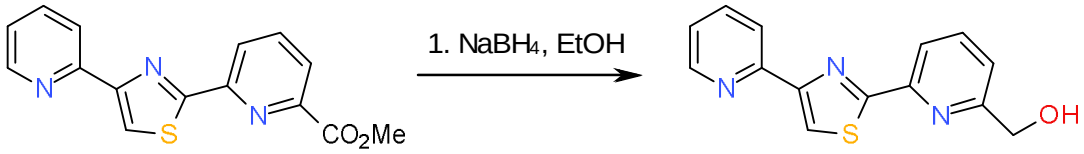

8 **9**

To a solution of the ester (**8**) (1.0 g, 3.4 mmol) in EtOH (25 ml) was added $NaBH_4$ (0.38 g, 10.2 mmol) and the solution refluxed for 6 hrs. The reaction was monitored by TLC (Al_2O_3 1% MeOH in DCM) for consumption of the starting material and periodically more $NaBH_4$ was added if required. Upon completion the solvent was removed and the product partitioned between $NaHCO_{3(aq)}$ and DCM, separation of the organic layer, drying and evaporation gave the alcohol (**9**) in sufficient purity to proceed to the next step (0.5 g, 55 % yield).

^{1}H NMR (400MHz, $CDCl_3$) δ 8.59 (m, 1H, py), 8.18 (m, 2H, overlapping, py), 8.14 (s, 1H, tz), 7.77 (t, *J* = 7.8, 1H, py), 7.75 (dt, *J* = 7.8, 1.8, 1H, py), 7.21 (m, 2H, overlapping, py), 4.77 (d, *J* = 5.0, 2H, -CH_2-), 3.67 (t, *J* = 5.1 Hz 1H, -CH_2O*H*).

7.1.8 Synthesis of the py-tz-py tridentate chloromethyl, (10)

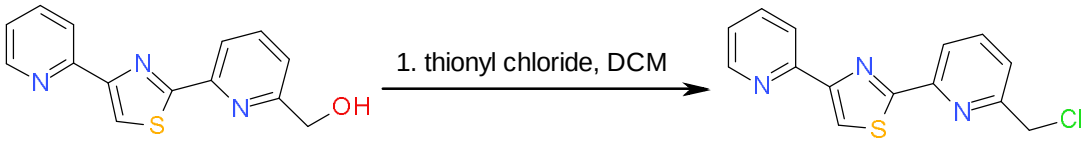

9 10

To a solution of the alcohol (**9**) (0.25 g, 0.9 mmol) in DCM (25 ml) was added Na_2CO_3 (1g) and thionyl chloride (0.6 g, 5 mmol) and the solution refluxed for 6 hrs. After this time the cooled reaction was carefully poured onto $NaHCO_{3(aq)}$ and the organic layer separated, dried and evaporated. Purification by column chromatography (Al_2O_3 1% MeOH in DCM) giving the chloro derivative (**10**) as a colorless solid (0.19 g, 74 yield %).

^{1}H NMR (400MHz, $CDCl_3$) δ 8.58 (ddd, J = 4.8, 1.7, 0.9, 1H, py), 8.19 (t, J = 7.6, 1H, py), 8.13 (s, 1H, tz), 7.80 (t, J = 7.8, 1H, py), 7.74 (dt, J = 7.7, 1.8, 1H, py), 7.48 (d, J = 7.8, 1H, py), 7.19 (m, 1H, overlapping with $CHCl_3$) 4.68 (s, 2H, -CH_2Cl).

7.1.9 Synthesis of, (L^1)

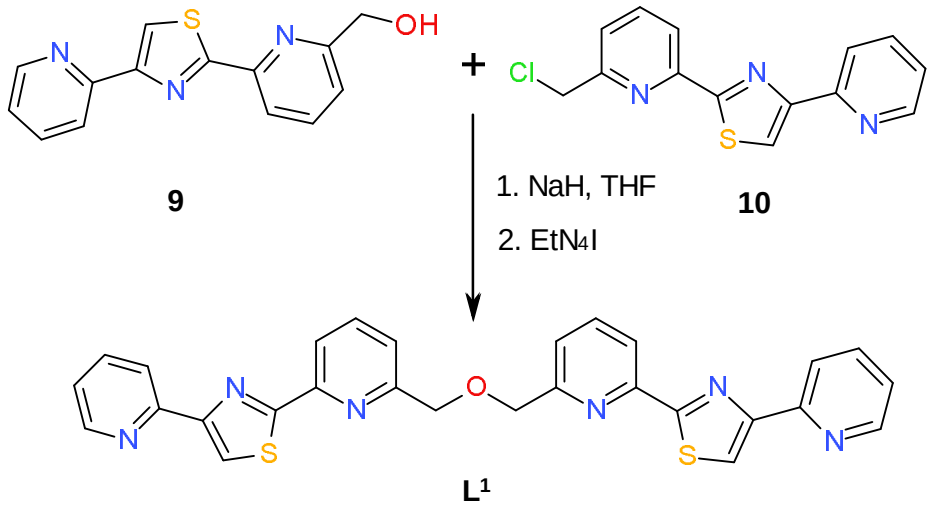

Both ligands were prepared in an analogous manner. In a typical procedure a solution of the alcohol (**9**) and tetraethylammonium iodide (0.005 g, cat) in anhydrous THF, under dinitrogen, was added an excess of NaH (typically 2 equivalents) and the reaction heated to 50 ˚C for 1 hr. To this was added a solution of one equivalent of the chloro derivative (**10**) in THF and the reaction refluxed. The reaction was monitored by TLC (Al_2O_3 5% MeOH in DCM) until the choloro derivative had disappeared. The reaction was then cooled, methanol added (to react with any remaining NaH) and evaporated. Purification by column chromatography (Al_2O_3 5% MeOH in DCM) gave ligand **L^1**. 61% yield.

^{1}H NMR (400MHz, $CDCl_3$) δ 8.65 (d, *J* = 4.8, 2H, py), 8.26 (d, *J* = 5.3, 2H, py), 8.24 (d, *J* = 5.0, 2H, py), 8.18 (s, 2H, tz), 7.88 (t, *J* = 7.7, 2H, py), 7.81 (dt, *J* = 7.7, 1.7, 2H, py), 7.64 (d, *J* = 7.6 Hz, 2H, py), 7.19 (m, 2H, overlap with $CHCl_3$, py), 4.85 (s, 4H, -CH_2-). ^{13}C (125 MHz, $CDCl_3$) 169.2, 158.5, 152.6, 150.7, 149.4, 137.6, 137.0, 122.8, 122.2, 121.1, 119.6, 118.5, 116.1, 73.6 (-CH_2O-). ESI-MS *m/z* 521 (M + H^+).

7.1.10 Synthesis of, (L^2)

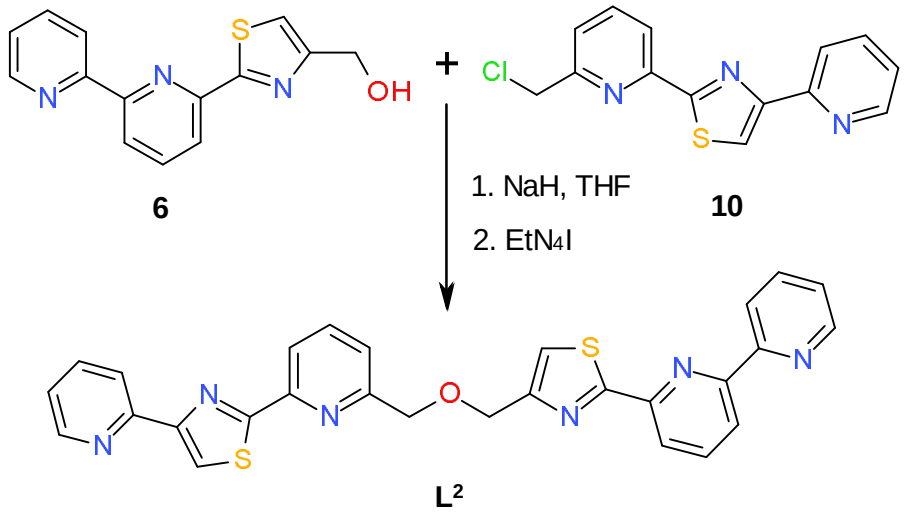

Both ligands were prepared in an analogous manner. In a typical procedure a solution of the alcohol (**6**) and tetraethylammonium iodide (0.005 g, cat) in anhydrous THF, under dinitrogen, was added an excess of NaH (typically 2 equivalents) and the reaction heated to 50 ˚C for 1 hr. To this was added a solution of one equivalent of the chloro derivative (**10**) in THF and the reaction refluxed. The reaction was monitored by TLC (Al_2O_3 5% MeOH in DCM) until the choloro derivative had disappeared. The reaction was then cooled, methanol added (to react with any remaining NaH) and evaporated. Purification by column chromatography (Al_2O_3 5% MeOH in DCM) gave ligand **L^2**. 55% yield.

^{1}H NMR (400MHz, $CDCl_3$) δ 8.70 (ddd, J = 4.8, 1.8, 0.9, 1H, py), 8.65 (ddd, *J* = 4.8, 1.8, 1.0, 1H, py), 8.57 (dt, *J* = 8.0, 1.0, 1H, py), 8.47 (dd, *J* = 7.9, 1.0, 1H, py), 8.24 (m, 3H, overlap, py), 8.18 (s, 1H, tz), 7.93 (t, *J* = 7.8, 1H, py), 7.87 (m, 2H, overlap, py), 7.81 (dt, *J* = 7.7, 1.8, 1H, py), 7.61 (d, *J* = 7.3, 1H, py), 7.48 (s, 1H, tz), 7.35 (ddd, *J* = 7.5, 4.8, 1.2 Hz, 1H, py), 7.26 (m, 1H, overlap with $CHCl_3$, py), 4.85 (s, 2H, -CH_2-) 4.82 (s, 2H, -CH_2-). ^{13}C (125 MHz, $CDCl_3$) 169.8, 169.1, 158.6, 156.5, 155.8, 155.4, 155.0, 150.7, 150.6, 149.5, 149.1, 145.4, 143.3, 137.9, 137.6, 136.9, 124.0, 122.8, 122.5, 121.7, 121.3, 121.1, 119.6, 119.4, 118.7, 118.4, 73.3 (-CH_2O-), 69.0 (-CH_2O-). ESI-MS *m/z* 521 (M + H^+).

7.1.11 Synthesis of (11)

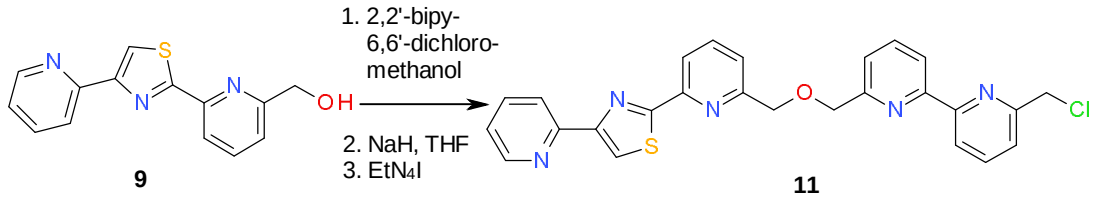

To a solution of py-tz-py tridentate alcohol (**9**) (0.05 g, 0.18 mmol) and tetraethylammonium iodide (0.005 g) in anhydrous THF (25 ml), under dinitrogen was added NaH (0.007 g, 0.29 mmol) and the reaction stirred at 50˚C for 1 hr. To this was then added a solution of 2,2'-bipyridine-6,6'-dichloromethyl^{X} (0.037 g, 0.16 mmol) in THF and the reaction was refluxed. The reaction was monitored by TLC (Al_2O_3 1 % MeOH in DCM) and once all the dichloro derivative had been consumed the reaction was cooled, evaporated and purified by column chromatography (Al_2O_3 1% MeOH in DCM) giving (**9**) as a colourless solid (0.06 g, 73 % yield).[86]

^{1}H NMR (400MHz, $CDCl_3$) δ 8.30 (dd, J = 7.6, 2.0, 1H, py), 8.58 (m, 2H overlapping, py), 8.17 (t, J = 9.0, 2H), 8.11 (s, 1H, tz), 7.80 (dd, J = 7.7, 3.4, 1H, py), 7.76 (m, 3H, overlapping, py), 7.54 (t, J = 6.7, 2H, py), 7.43 (d, J = 5.3 Hz, 1H, py), 7.19 (m, overlapping with $CHCl_3$, 1H), 4.85 (s, 2H, -CH_2-), 4.83 (s, 2H, -CH_2-), 4.69 (s, 2H, -CH_2-).

ESI-MS *m/z* 486 (M + H^+).

7.1.12 Synthesis of, (L^3)

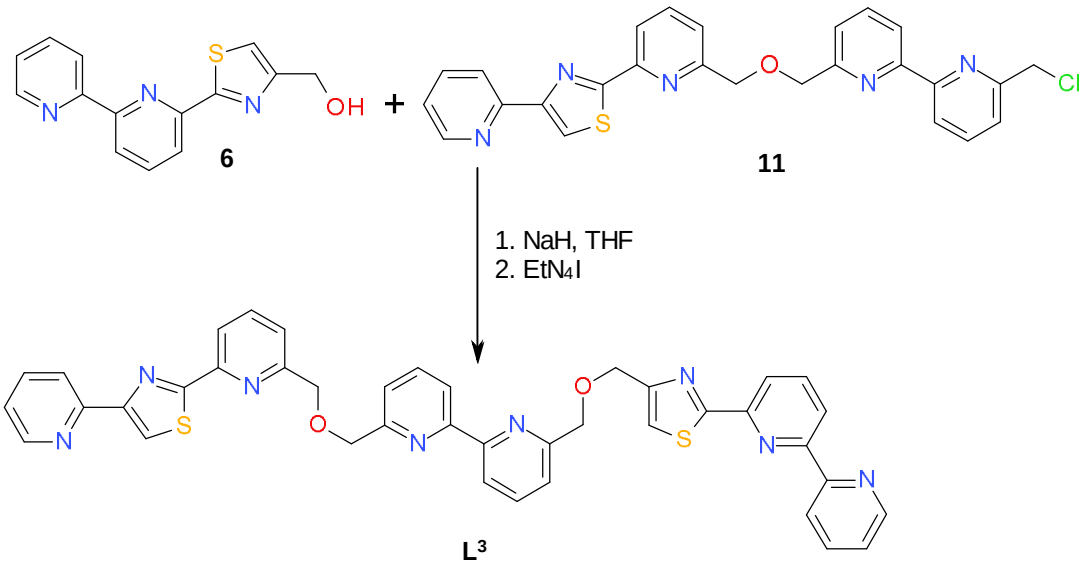

Both ligands were prepared in an analogous manner. In a typical procedure a solution of the alcohol (**6**) and tetraethylammonium iodide (0.005 g, cat) in anhydrous THF, under dinitrogen, was added an excess of NaH (typically 2 equivalents) and the reaction heated to 50 ˚C for 1 hr. To this was added a solution of one equivalent of the chloro derivative (**11**) in THF and the reaction refluxed. The reaction was monitored by TLC (Al_2O_3 5% MeOH in DCM) until the choloro derivative had disappeared. The reaction was then cooled, methanol added (to react with any remaining NaH) and evaporated. Purification by column chromatography (Al_2O_3 5% MeOH in DCM) gave ligand **L^3**. 65% yield.

^{1}H NMR (400MHz, $CDCl_3$) δ 8.70 (ddd, *J* = 4.8, 1.7, 0.9, 1H, py), 8.65 (ddd, *J* = 4.8, 1.7, 0.9, 1H, py), 8.57 (dt, *J* = 7.8, 1.1, 1H, py), 8.46 (dd, *J* = 7.8, 1.0, 1H, py), 8.33 (t, *J* = 7.2, 2H, py), 8.25 (dt, *J* = 8.1, 0.8, 2H, py), 8.21 (dd, *J* = 7.8, 0.9, 1H, py), 8.18 (s, 1H, tz), 7.93 (t, *J* = 7.8, 1H, py), 7.86 (m, 5H overlap, py), 7.60 (m, 3H, overlap, py), 7.46 (s, 1H, tz), 7.35 (ddd, *J* = 7.5, 4.8, 1.2 Hz, 1H, py) 7.26 (m, 1H, py), 4.92 (s, 2H, -CH_2-), 4.91 (s, 2H, -CH_2-), 4.90 (s, 4H, -CH_2-). ^{13}C (125 MHz, $CDCl_3$) 169.8, 169.2, 158.5, 157.7, 157.6,

155.9, 155.6, 155.5, 155.4, 155.3, 155.2, 154.9, 152.4, 150.5, 150.4, 149.1, 149.0, 138.0, 137.6, 137.5, 137.4, 137.2, 137.1, 124.0, 122.9, 122.2, 121.7, 121.5, 121.4, 121.3, 121.1, 121.0, 119.6, 119.5, 118.7, 118.4, 73.9 (-CH_2O-), 73.6 (-CH_2O-), 73.3 (-CH_2O-), 68.7 (-CH_2O-).

ESI-MS *m/z* 718 ($M + H^+$).

7.2 Preparation of L^4

7.2.1 Synthesis of, (L^4)

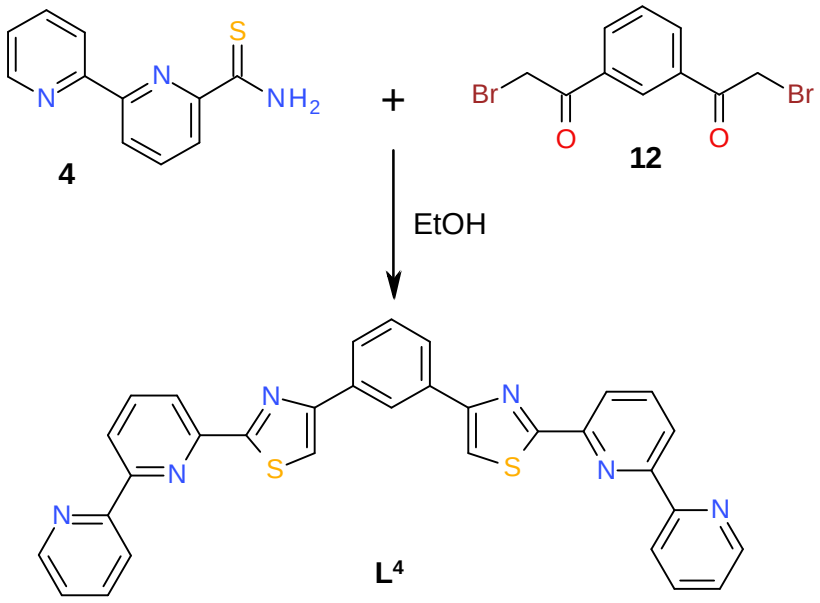

To a round bottomed flask charged with 2,2'-bipyridine-6-thioamine (0.10 g, 0.46 mmol) and 1,3-di(α-bromoacetyl)benzene[92] (0.067 g, 0.21 mmol) was added EtOH (50 ml) and the reaction refluxed for 8 hrs, after which time a white precipitated formed. Filtration followed by washing with EtOH (2 x 10 ml) and Et_2O (2 x 10 ml) gave the ligand L^1 as a white solid (0.075 g, 65 % yield).

^{1}H NMR (500MHz, $CDCl_3$) δ 8.68 (d, 2H, J = 4.3, H^{11}), 8.63 (s, 1H, H^1), 8.61 (d, 2H, *J* = 7.8, H^6), 8.46 (d, 2H, *J* = 7.6, H^7), 8.38 (d, 2H, *J* = 7.6, H^5), 8.02 (d, 2H, *J* = 7.7, H^3), 7.98 (t, 2H, *J* = 7.8, H^6), 7.89 (t, 2H, *J* = 7.7, H^9), 7.76 (t, 1H, *J* = 6.5, H^2), 7.36 (t, 2H, *J* = 6.7 Hz, H^{10}).

7.3 Preparation of L^5 and L^6

7.3.1 Synthesis of py-tz-ph bidentate bromoacetyl, (14)

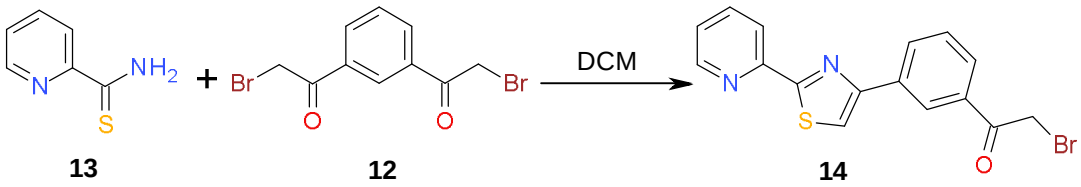

13 **12** **14**

To a solution of 1,3-di(α-bromoacetyl)benzene[92] (**12**) (0.20 g, 0.62 mmol) in dichloromethane (25 ml) was added pyridine-2-thioamide (**13**) (0.078 g, 0.56 mmol) and the reaction briefly heated to reflux and then allowed to stir at room temperature for 12 hrs. The resulting precipitate was isolated by filtration and suspended in $NaHCO_{3(aq)}$ (10 ml) and extracted into dichloromethane (3 x 25 ml). Purification by column chromatography (Al_2O_3 1% MeOH in DCM) gave (**14**) (0.12 g, 59 % yield).

^{1}H NMR (500 MHz, $CDCl_3$) δ 8.66 (d, 1H, *J* = 4.3, py), 8.65 (s, 1H, Ph), 8.37 (d, 1H, *J* = 7.8, py), 8.27 (d, 1H, *J* = 7.7, Ph), 8.00 (d, 1H, *J* = 7.9, Ph), 7.88 (t, 1H, *J* = 7.9, py), 7.74 (1H, s, tz), 7.62 (t, 1H, *J* = 7.7 Hz, Ph), 7.39 (dd, 1H, *J* = 7.2, 5.5 Hz, py), 4.58 (s, 2H, -CH_2Br).

7.3.2 Synthesis of, (L^5)

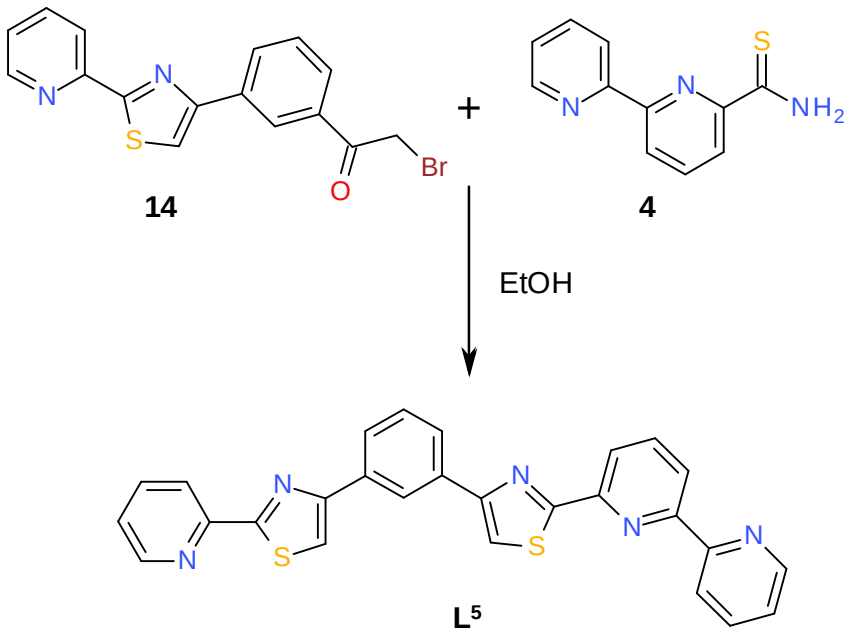

Reaction of (**14)** (0.10 g, 0.28 mmol) with 2,2'-bipridine-6-thioamide (**4**) (0.072 g, 0.33 mmol) in EtOH (25 ml) at reflux for 8 hrs results in a yellow precipitate which was isolated by filtration. Suspension in concentrated NH_3 (10 ml) followed by filtration and washing with H_2O (2 x 2ml), EtOH (2 x 2ml) and Et_2O (2 x 2 ml) gave the ligand L^2 as a pale cream solid (0.09 g, 68 % yield).

^{1}H NMR (500 MHz, $CDCl_3$) δ 8.74 (m, 1H, py), 8.68 (m, 1H, py), 8.66 (t, 1H, *J* = 1.5, Ph), 8.64 (d, 1H, *J* = 7.9, py), 8.53 (dd, 1H, *J* = 7.8, 0.9, py), 8.05 (m, 2H overlap, Ph), 8.01 (t, 1H, *J* = 7.8, py), 8.42 (dd, 1H, *J* = 7.8, 1.0, py), 8.43 (d, 1H, *J* = 7.8, py), 7.92 (dt, 1H, *J* = 7.7, 1.7 py), 7.88 (dt, 1H, *J* = 7.7, 1.7, py), 7.78 (s, 1H, tz), 7.77 (1H, s, tz), 7.59 (t, 1H, *J* = 7.8 Hz, Ph), 7.39 (m, 2H overlap, py). ^{13}C (125 MHz, $CDCl_3$) 169.36 (tz), 168.98 (tz), 156.60 (tz x2 coincident), 155.83 (py-cen), 155.50 (py-ter), 151.60 (py-ter), 150.82 (py-cen), 149.51 (py-ter), 149.18 (py-ter), 138.0 (py-cen), 136.99 (py-ter), 136.97 (py-ter), 135.18 (Ph), 135.14 (Ph), 129.26 (Ph), 126.30 (Ph x2 coincident),

124.52 (py-ter), 124.39 (Ph), 124.01 (py-ter), 121.80 (py-ter), 121.32 (py-cen), 119.98 (py-ter), 119.77 (py-ter), 115.73 (tz), 115.70 (tz).

ESI-MS *m/z* 476 ($M + H^+$), HRMS $C_{27}H_{18}N_5S_2$ requires 476.0998 found 476.0996.

7.3.3 Synthesis of, (L^6)

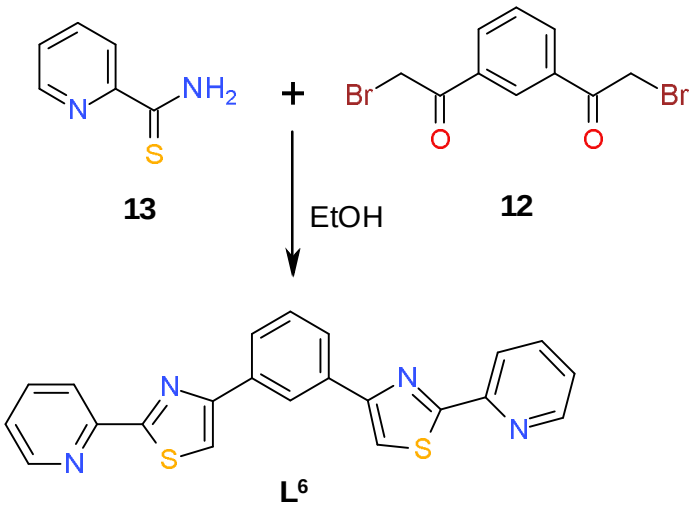

To a round bottom flask charged with pyridine-2-thioamide (**13**) (0.20 g, 1.45 mmol) and 1,3-di(α-bromoacetyl)benzene[92] (**12**) (0.21 g, 0.66 mmol) was added EtOH (25 ml) and the reaction refluxed for 8 hrs, during which time a precipitate formed. This was filtered and washed with EtOH (2 x 2ml) and Et_2O (2 x 2 ml) and suspended in aqueous ammonia (10 mls) for 12hrs. Filtration followed by washing with H_2O (2 x 2 ml) EtOH (2 x 2ml) and Et_2O (2 x 2 ml) gave the ligand **L^6** as a cream solid (0.18 g, 68 % yield).

^{1}H NMR (500 MHz, $CDCl_3$) δ 8.67 (ddd, 2H, *J* = 4.9, 1.7, 1.0, py), 8.63 (t, 1H, *J* = 1.7, Ph), 8.41 (dt, 2H, *J* = 7.9, 0.9, py), 8.04 (dd, 2H, *J* = 7.7, 1.7, Ph), 7.88 (dt, 2H, *J* = 7.7, 1.7, py), 7.75 (s, 2H, tz), 7.59 (t, 1H, *J* = 7.7, Ph), 7.39 (ddd, 2H, *J* = 7.6, 4.9, 1.1 Hz, py). ^{13}C (125 MHz, $CDCl_3$) 168.90 (tz), 156.52 (tz), 151.48 (py), 149.47 (py), 137.05 (py), 135.06 (Ph), 129.26 (Ph), 126.28 (Ph), 124.55 (py), 124.34 (Ph), 119.97 (py), 115.75 (tz).

ESI-MS *m/z* 399 (M + H^+), HRMS $C_{22}H_{15}N_4S_2$ requires 399.0733 found 399.0726.

7.4 Preparation of L[7]

7.4.1 Synthesis of 1,3-diacetyl pyrene, (16)

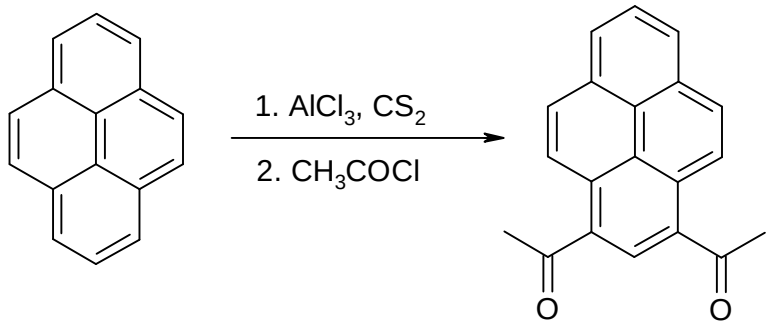

15 **16**

The synthesis of 1,3-diacetylpyrene (**16**) was carried out in a similar manner to the procedure described by Harvey and coworkers.[91]

To a solution of pyrene (2.5g, 12.37 mmol) in CS_2 (75 ml) at 0°C, $AlCl_3$ (10.01g, 74.98 mmol) was added to the mixture whilst stirring after addition the solution was allow to stir for a further 10 minutes. To this was then added CH_3COCl (4.28g, 54.52 mmol) was added dropwise to this aqueous solution at 0°C after which time the solution was heated to 60°C for 2 hours. After cooling ice (10 g) and HCl (12M 10 ml) was added and the solution stirred for 1 hr. The resultant yellow precipitate was then filtered and washed with water (30 ml) and CS_2 (30 ml). The dry solid was then dissolved in DCM (30 ml) and the solution cooled at -40˚C during which time a precipitate formed. The solid was then removed by filtration and the solution was concentrated to approximately 5 ml and purified by column chromatography (DCM, SiO_2) affording (**16**) as a yellow solid (0.08g, 0.29 mmol), 2.3% yield).

^{1}H NMR (500 MHz, $CDCl_3$) δ 8.94 (d, *J* = 9.4, 2H), 8.65 (s, 1H), 8.28 (d, *J* = 9.40, 2H), 8.26 (d, *J* = 7.60, 2H), 8.07 (t, *J* = 7.64 Hz, 1H), 2.86 (s, 6H).

7.4.2 Synthesis of 1,3-dibromo-diacetyl pyrene, (17)

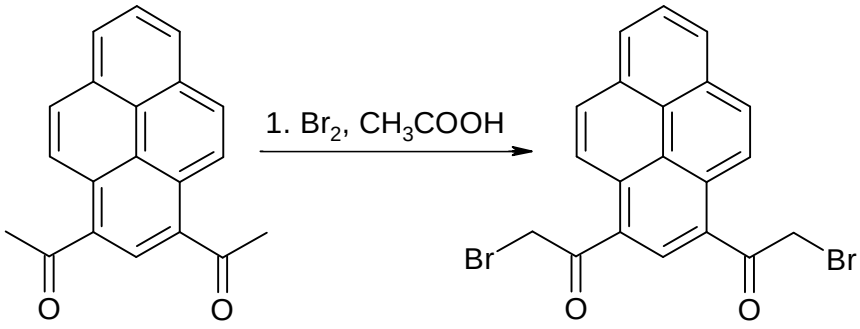

16 **17**

To a solution of 1,3-diacetylpyrene (**16**) (0.06 g, 0.22 mmol) in acetic acid (20 ml) at 80°C, Br_2 (0.067 g, 0.021 ml, 0.42 mmol) in 1 ml acetic acid was added dropwise, continuously and consistently. Once all Br_2 solution was added, the reaction was left a further 20 minutes, then cooled to room temperature. Water was then added drop wise (~ 5 ml) until a yellow solid was precipitated. The solid was then filtered and re-dissolved in DCM, dried with $MgSO_4$ and evaporated to dryness. The solid is crystallized from $CHCl_3$ giving the di-brominated species (**17**) as a light brown solid (0.05 g, 0.11 mmol, 53 % yield).

^{1}H NMR (500 MHz, $CDCl_3$) δ 8.90 (d, *J* = 9.5, 2H), 8.71 (s, 1H), 8.31 (d, *J* = 7.6, 2H), 8.30 (d, *J* = 9.5, 2H), 8.09 (t, *J* = 7.60 Hz, 1H), 4.65 (s, 4H).

7.4.3 Synthesis of, (L^7)

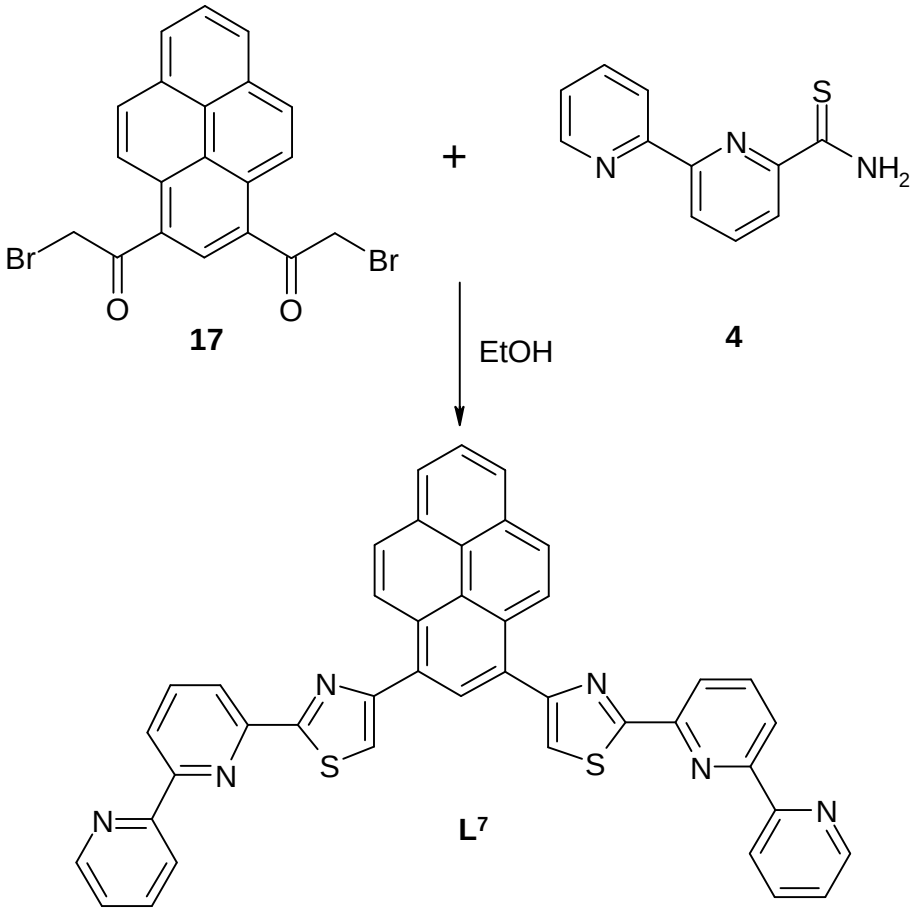

Reaction of (**17)** (0.025 g, 0.056 mmol) with 2,2'-bipridine-6-thioamide (**4**) (0.024 g, 0.11 mmol) in EtOH (25 ml) at reflux for 8 hrs results in a yellow precipitate. Filtration followed by washing with EtOH (2 x 2ml) and Et_2O (2 x 2 ml) gave the ligand L^7 as a pale yellow solid (0.017 g, 64 % yield).

^{1}H NMR (400 MHz, DMSO) δ 8.82 (d, *J* = 8, 2H), 8.78 (m, 2H), 8.71 (s, 1H), 8.58 (d, *J* = 8, 2H), 8.54 (d, *J* = 8, 2H), 8.49 (s, 2H), 8.42 (d, *J* = 8, 2H) 8.38 (d, *J* = 6, 2H), 8.36 (d, *J* = 6, 2H), 8.20 (m, 3H), 8.11 (dt, *J* = 6, 2 Hz, 2H).

7.5 Synthesis of complexes

7.5.1 Synthesis of the complex $[Zn_2(L^1)_2](ClO_4)_4$

Reaction of **L^1** (5 mg, 9.6 mmol) with $Zn(H_2O)_6(ClO_4)_2$ (3.5 mg, 9.4 mmol) in acetonitrile (2 ml) afforded a colorless solution. The solution was filtered then layered with diethyl ether (10 ml), gave small colourless crystals of $[Zn_2(\mathbf{L^1})_2](ClO_4)_4$. ESI-MS *m/z* 1469 $\{[Zn_2(\mathbf{L^1})_2](ClO_4)_2\}^{2+}$. For full spectroscopic details see text.

7.5.2 Synthesis of the complex $[Zn_2(L^2)_2](ClO_4)_4$

Reaction of **L^2** (5 mg, 9.6 mmol) with $Zn(H_2O)_6(ClO_4)_2$ (3.5 mg, 9.4 mmol) in acetonitrile (2 ml) afforded a colorless solution. The solution was filtered then layered with diethyl ether (10 ml), gave small colourless crystals of $[Zn_2(\mathbf{L^2})_2](ClO_4)_4$. ESI-MS *m/z* 1469 $\{[Zn_2(\mathbf{L^2})_2](ClO_4)_2\}^{2+}$. For full spectroscopic details see text.

7.5.3 Synthesis of the complex $[ZnHg(L^2)_2](ClO_4)_4$

Reaction of **L^2** (5 mg, 9.6 mmol) with with $Zn(H_2O)_6(ClO_4)_2$ (1.7 mg, 4.5 mmol) and $Hg(H_2O)_4(ClO_4)_2$ (2.2 mg, 4.7 mmol) in acetonitrile (2 ml) afforded a colourless solution. Filtration followed by the slow diffusion of diethyl ether vapour into the acetonitrile solution resulted in the formation colourless crystals of $[ZnHg(\mathbf{L^2})_2](ClO_4)_4$. ESI-MS *m/z* 1605. For full spectroscopic details see text.

7.5.4 Synthesis of the complex $[HgCuZn(L^3)_2](PF_6)_5$

Reaction of **L^3** (5 mg, 6.9 mmol) with with $Zn(H_2O)_6(ClO_4)_2$ (1.3 mg, 3.5 mmol) and $Hg(H_2O)_4(ClO_4)_2$ (1.6 mg, 3.4 mmol) and $Cu(MeCN)_4(PF)_6$ (1.3 mg, 3.5mmol)in acetonitrile (2 ml) afforded an orange solution. To this solution $Na(PF)_6$ was added affording a precipitate. ESI-MS *m/z* 2347. For full spectroscopic details see text.

7.5.5 Synthesis of the complex $[Cd_2(L^4)_2](ClO_4)_4$

Reaction of **L^4** (5 mg, 9.0 mmol) with $Cd(H_2O)_4(ClO)_6$ (2.8 mg, 9.0 mmol) in nitromethane (2 ml) afforded a colourless solution. Filtration followed by the slow diffusion of DCM vapour into the nitromethane solution resulted in the formation colourless crystals of $[Cd_2(\mathbf{L^4})_2](ClO_4)_4$. ESI-MS *m/z* 1629. For full spectroscopic details see text.

7.5.6 Synthesis of the complex $[Zn_5(L^4)_5](CF_3SO_3)_{10}$

Reaction of **L^4** (5 mg, 9.0 mmol) with $Zn(CF_3SO_3)_2$ (3.2mg, 8.8 mmol) in acetonitrile (2 ml) afforded a colourless solution. Filtration followed by layering with diethyl ether (10 ml), gave colourless crystals of $[Zn_5(\mathbf{L^4})_5](CF_3SO_3)_{10}$. ESI-MS *m/z* 1942. For full spectroscopic details see text.

7.5.7 Synthesis of the complex $[Cu_5(L^5)_5](ClO_4)_2$

Reaction of **L^5** (5 mg, 10.5 mmol) with $Cu(H_2O)_6(ClO_4)_2$ (3.9mg, 10.5 mmol) in acetonitrile (2 ml) afforded a light green solution. Filtration followed by the slow diffusion of chloroform vapour into the acetonitrile solution resulted in the formation light green crystals of $[Cu_5(\mathbf{L^5})_5](ClO_4)_2$. ESI-MS *m/z* 1745 $\{[Cu_5(\mathbf{L^5})_5](ClO_4)_8\}^{2+}$. For full spectroscopic details see text.

7.5.8 Synthesis of the complex $[Cu_5(L^4)_3(L^6)_2](CF_3SO_3)_{10}$

Reaction of **L^4** (3 mg, 5.4 mmol) with **L^6** (2 mg, 5.01 mmol) and $Cu(CF_3SO_3)_2$ (3.4 mg, 9.2 mmol) in acetonitrile (2 ml) afforded a clear green solution. Filtration followed by the slow diffusion of ethyl acetate vapour into the acetonitrile solution resulted in the formation clear green crystals of $[Cu_5(\mathbf{L^4})_3(\mathbf{L^6})_2](ClO_4)_{10}$. ESI-MS *m/z* 1982 $\{[Cu_5(\mathbf{L^4})_3(\mathbf{L^6})_2](ClO_4)_8\}^{2+}$. For full spectroscopic details see text.

7.5.9 Synthesis of the complex $[Zn_4(L^7)_4](CFSO_3)_2$

Reaction of **L^7** (5 mg, 7.3 mmol) with $Zn(CFSO_3)_2$ (2.7 mg, 7.4 mmol) in acetonitrile (2 ml) afforded a pale yellow solution. Filtration followed by the slow diffusion of ethyl acetate vapour into the acetonitrile solution resulted in the formation pale yellow crystals of $[Zn_4(\mathbf{L^7})_4](CFSO_3)_2$. ESI-MS *m/z* 1931. For full spectroscopic details see text.

References

1. J. W. Steed and J. L. Atwood, Supramolecular Chemistry, John Wiley & Sons, Chicester, 2000.
2. J-M. Lehn, Supramolecular Chemistry- Concepts and Prepectives, VCH, 1995.
3. P. D. Beer, P. A. Gale and D. K. Smith, Supramolecular Chemistry, Oxford University Press, 1999.
4. N. F. Curtis, *Journal of the Chemistry Society*, 1964, 2644-2650.
5. J. D. Curry and D. H. Busch, *J. Am. Chem. Soc.*, 1964, **86**, 592-594.
6. E. G. Jäger, *Zeitschrift für Chemie*, 1964, **4**, 437.
7. C. J. Pedersen, *J. Am. Chem. Soc.*, 1967, **89**, 2495.
8. C. J. Pedersen, *J. Am. Chem. Soc.*, 1967, **89**, 7017-7036.
9. D. J. Cram. *Angew. Chem.*, 1986, **98**, 1041-1060.
10. B. Dietrich, J-M. Lehn and J. P. Sauvage, *Tetrahedron Lett.*, 1969, **34**, 2889-2892.
11. J. W. Steed and J. L. Atwood, Supramolecular Chemistry, John Wiley & Sons, Chicester, 2000.
12. E. Fischer, *Berichte de Deutschen Chemischen Gasellschaft.*, 1894, **27**, 2985-2993.
13. J. M. Tinko, R. C. Helegson and D. J. Cram, *J. Am. Chem. Soc.*, 1978, 100(9), 2828-2834.
14. C. J. Pedersen, *J. Am. Chem. Soc.*, 1967, **89**, 7017.
15. T. Gunnlaugsson, B. Bichell and C. Nolan, *Tetrahedron*, 2004, **60**, 5799.
16. T. Gunnlaugsson, M. Nieuwenhuyzen, L. Richard and V. Thoss, *Tetrahedron Lett.*, 2001, **42**, 4725.
17. G. S. Hanan, D. Volkmer, U. S. Schubert, J-M. Lehn, G. Baum and D. Fenske, *Angew. Chem. Int. Ed.*, 1997, 37, No. **17**, 1842.
18. Z. R. Bell, L. P. Harding and M. D. Ward, *Chem. Commun.*, 2003, 2432-2433.

19. A. Credi, V. Balzani, S. Campagne and G. S. Hannan, *Chem. Phy. Lett.*, 1995, 243, 102.
20. B-Y. Lou, D-Q. Yuan, B-L. Wu, L. Han, F. L. Jaing and M-C. Hong, *Inorganic Chemistry Commun.*, 2005, **8**, 539- 542.
21. E. C. Constable and A. M. W. Cargill Thompson, *J. Chem. Soc. Dalton Trans*, 1994, 1409.
22. J-M. Lehn, *Chem. Soc. Rev.*, 2007, **36**, 151-160.
23. M. Ruben, J. Rojo, F. J. Romero-Salguero, L. H. Uppadine and J-M. Lehn, *Angew. Chem.*, **43**, (2004), 3644.
24. P. N. W. Baxter, J-M. Lehn, J. Fischer and M. T. Youino, *Angew. Chem. Int. Ed.*, 1994, **33**, 2284-2287.
25. G. S. Hanan, *Angew. Chem. Int. Ed.*, 1997, **36**,17.
26. S. Leniniger, B. Olenyuk and P. J. Stang, *Chem. Rev.*, 2000, 100, 853.
27. M. Fujita, S. Nagao and K. Ogura, *J. Am. Chem. Soc.*, 1995, 117, 1649.
28. D. W. Johnson and K. N. Raymond, *Supramol. Chem.*, 2001, **13**, 639.
29. K. Nakabayashi, M. Kawano, M. Yoshizawa, S. Ohkoshi and M. Fujita, *J. Am. Chem. Soc.*, 2004, **126**, 16694.
30. M. Yoshizawa, T. Kusukawa, M. Kawano, T. Ohhara, I. Tanaka, K. Kurihara, N. Niimura and M. Fujita., *J. Am. Chem. Soc.*, 2005, **127**, 2798.
31. G. S. Hanan, C. R. Arana, J-M. Lehn and D. Fenske., *Angew. Chem.*, 1995, **34**, 1122-1124.
32. K. N. Power, T. L. Heniger and M. J. Zaworoto, *New J. Chem.*, 1998, **22**, 177-181.
33. H. W. Roesky and M. Andruh, *Chem. Rev.*, 2003, 236, 91.
34. P. N. W. Baxter, G. S. Hanan and J-M. Lehn, *Chem. Commum.*, 1996, 2019.
35. J. D. Watson and F. H. C. Crick, *Nature*, 1953, **171**, 737.
36. J-M. Lehn, *Angew. Chem. Int. Ed.*, 1988, **27**, 89-112.
37. F. Vogtle, Supramolecular Chemistry, Wiley, Chicester, 1991.
38. J-M. Lehn, A. Riguault, J. Siegel, J. Harrowfield, B. Chevier and D. Moras*, Proc. Natl. Acad. Sci. Usa.*, 1987, **84**, 2565.

39. C. Piguet, G. Bernardeinelli, and G. Hopfgartner, *Chem. Rev.*, 1997, **97**, 2005-2062.
40. E. C. Constable, *Tetrahedron*, 1992, **48**, 2003.
41. C. Piguet, G. Bernardinelli, B. Bocquet, A. Quattropani and A. F. Williams, *J. Am. Chem. Soc.*, 1992, **114**, 7440.
42. C. J. Baylies, L. P. Harding, J. C. Jeffrey, R. Moon, C. R. Rice and T. Riis-Johannessen, *New J. Chem.*, 2007, **31**, 1525-1529.
43. V. C. M. Smith and J-M. Lehn, *Chem. Comm.*, 1996, 2733.
44. G. Baum, E. C. Constable, D. Fenske, C. E. Housecroft, T. Kulke, *Chem. Eur. J.*, 1999, **5**, 1862.
45. M. Greenwood, D. Wessley, E. Katz, I. Wilner and Y. Cohen, *J. Org. Chem.*, 2000, **65**, 1050.
46. M. Shaul and Y. Cohen, *J. Org. Chem.*, 1999, **64**, 9358.
47. K. T. Potts, M. Keshavarz, Fook S. Tham, H. D. Abruña and C. R. Arana, *Inorg. Chem.*, 1993, **32**, 4422-4453.
48. M. Barley, E. C. Constable, S. Corr, R. C. S. McQueen, J. C. Nutkins, M. D. Ward and M. G. B. Drew, *J. Chem. Soc. Dalton Trans.*, 1988, 2655.
49. E. C. Constable, F. Heirtzler, M. Neuburger, M. Zehnder, *J. Am. Chem. Soc.*, 1997, 119.
50. C. Piguet, E. Rivara-Minten, G. Hopfgartner and J-C. G. Buzli, *Helv. Chem. Acta.*, 1995, **78**, 154.
51. E. C. Constable, F. R. Heirtzler, M. Neuburger and M. Zhender, *Chem. Comm.*, 1996, 933.
52. E. C. Constable, A. J. Edwards, P. R. Raithby and J. V. Walker, Angew. Chem. Int. Ed., 1993, 32, 1465.
53. E. C. Constable, A. J. Edwards, P. R. Riathby, D. R. Smith, J. V. Walker and L. Whall, *Chem. Comm.*, 1996, 2551.
54. E. C. Constable and J. V. Walker, J. Chem. Soc, *Chem. Comm.*, 1992, 884.
55. H. L. Kwong, H-L. Yeung, W. S. Lee and W. T. Wong, *Chem. Comm,*. 1996, 2551.
56. E. C. Constable, T. Kulke, M. Neuburger, M. Zhender, *Chem. Comm.*, 1997, 489.

57. O. Mamual, A. Von Zelewsky, P. Brodard, C-W. Schläpfer, G. Bernardinelli and H. Stoeckli-Evans, *Chem. Eur. J.*, 2005, **11**, 3049-3057.
58. G. Baum, E. C. Constable, D. Fenske, T. Kulke,*Chem. Comm.*, 1997, 2043.
59. E. C. Constable, T. Kulke, G. Baum, D. Fenske, *Inorganic Chem. Comm.*, 1998, 80-82.
60. G. Baum, E. C. Constable, D. Fenske, C. E. Housecroft and T. Kulke, *Chem. Eur, J.*, 1999, 5 No. 6.
61. T. K. Ronson, H. Adams, T. Riis-Johannessen, J. C. Jeffrey and M. D. Ward, *New J. Chem.*, 2006, **30**, 26-28.
62. R. Krämer, J-M. Lehn and A. Marquis-Rigault, *Proc. Natl. Acad. Sci. USA.*, 1993, **99**, 5394-5398.
63. E. C. Constable and M. D. Ward, *J. Am. Chem. Soc.*, 1990, **112**, 1251-1258.
64. E. C. Constable, S. M. Eider and J. Healy, *J. Chem. Soc. Dalton Trans.*, 1990, 1669.
65. E. C. Constable, R. Chotalia, D. A. Tocher, *J. Am. Chem. Soc, Chem. Comm.*, 1992, 771.
66. R. Chotalia, E. C. Constable, M. Neuburger, D. R. Smith and M. Zhender, *J. Chem., Dalton Trans.*, 1996, 4207-4216.
67. C. R. Rice, S. Wörl, J. C. Jeffrey, P. L. Paul and M. D. Ward, *Chem. Comm.*, 2000, 1529-1530.
68. C. R. Rice, C. J. Baylies, L. P. Harding, J. C. Jeffrey, R. L. Paul and M. D. Ward, *J. Chem. Soc., Dalton Trans.*, 2001, 3039-3044.
69. C. R. Rice, C. J. Baylies, H. J. Clayton, J. C. Jeffrey, R. L. Paul and M. Ward, *Inorganic Chem. Acta.*, 351, 2003, 207-216.
70. C. R. Rice, S. Wörl, J. C. Jeffrey, R. L. Paul and M. D Ward, *J. Chem. Soc.*, Dalton Trans., 2001, 550-559.
71. P. N. W. Baxter, J. A. Connor, W. Bernd Schweizer and J. D. Wallis, *J. Chem. Soc.*, Dalton Trans., 1992, 3015.
72. J. Rebek and L. Marshall, *J. Am. Chem. Soc.*, 1983, **105**, 6668-6670.
73. J. Rebek, J. E. Trend, R. V. Wattley, S. Charkrovorti, *J. Am. Chem. Soc.*, 1979, **101**, 4333.

74. J. Rebek and R. V. Wattley, *J. Am. Chem. Soc.*, 1980, 102, 4853-4854.
75. C. J. Baylies, J. C. Jeffrey, T. A. Miller, R. Moon, C. R. Rice and T. Riis-Johannessen, *Chem. Comm.*, 2005, 4158-4160.
76. T. Riis-Johannessen, J. C. Jeffrey, A. P. H. Robson, C. R. Rice and L. P. Harding*, Inorg. Chemica Acta*, 358, 2005, 2781-2798.
77. C. J. Baylies, L. P. Harding, J. C. Jeffrey, T. Riis-Johannessen and C. R. Rice, *Angew. Chem. Int. Ed.*, 2004, **43**, 4515-4518.
78. G. Bokolinis, T. Riis-Johannessen, L. P. Harding, J. C. Jeffrey, N. McLay and C. R. Rice, *Chem. Comm.*, 2006, 1980-1982.
79. C. J. Baylies, T. Riis-Johannessen, L. P. Harding, J. C. Jeffrey, R. Moon, C. R. Rice and M. Whitehead, *Angew. Chem. Int. Ed.*, 2005, 44, 6909-6912.
80. E. C. Constable, G. Zhang, C. E. Housecroft and J. A. Zampese, *Cryst. Eng. Comm.*, 2010.
81. P. D. Beer and A. S. Rothin, *J. Chem. Soc., Chem. Comm.*, 1988, 52.
82. C. R. Rice, A. Guerroro, Z. R. Bell, R. L. Paul, G. R. Motson, J. C. Jeffrey and M. D. Ward, *New J. Chem.*, 2001, **25**, 185-187.
83. B. Hasenknopf, J-M. Lehn, N. Boumediene, A. Dupont-Gervais, A. Van Dorsselaer, B. Kneiser and D. Fenske, *J. Am. Chem. Soc.*, 1997, **119**, 10956-10962.
84. S. P. Argent, H. Adams, T. Riis-Johannessen, J. C. Jeffrey, L. P. Harding, O. Mamula and M. D. Ward, *Inorg. Chem.*, **45**, (10), 2006, 3905.
85. H. B. Tanh Jeazet, K. Gloe, T. Doert, O. N. Kataeva, A. Jäger, G. Geipel, G. Bernhard, B. Büchner and K. Gloe, *Chem. Comm.*, 2010.
86. G. R. Newkome, W. E. Puckett, G. E. Kiefer, V. K. Grupta, Y. Xia, M. Coreil and M.A. Hackney, *J. Org. Chem.*, 1982, **47**, 4116.
87. J-M. Senegas, S. Koeller and C. Piguet, *Chem. Comm.*, 2005, 2235-2237.
88. T. Riis-Johannessen, L. P. Harding, J. C. Jeffrey, R. Moon and C. R. Rice, *Dalton Trans.*, 2007, 1577-1587.
89. A. Macchioni, G. Ciancaleoni, C. Zuccaccia and D. Zuccaccia, *Chem. Soc. Rev.*, 2008, **37**, 479.
90. L. T. Scott and A. Neculia, *J. Org. Chem.*, 1996, **61**, 386-388.

91. R. G. Harvey, J. Pataki and H. Lee, *Org. Prep. Proced. Int.*, 1984, **16**, 144-8.
92. Hong-Bo Wang, J. A. Wisner and M. C. Jennings, *Beilstein J. Org. Chem.*, 2010, **6**, No 50.

Appendix 1: Crystal Data Tables

Table A1. Crystallographic data of L^1 complex $[Zn_2(L^1)_2]^{4+}$.[a]

Compound	$[Zn_2(\mathbf{L^1})_2]^{4+}$
Formula	$C_{66}H_{59}Cl_4N_{15}O_{19}S_4Zn_2$
M	1767.06
System, space group	Triclinic P $\bar{1}$
a / Å	12.4711(7)
b / Å	14.3884(9)
c / Å	22.274(1)
α / °	101.269(1)
β / °	97.531(1)
γ / °	99.022(1)
U / Å^3	3817.0(4)
Z	2
μ /mm^{-1}	1.537
Reflections collected:	67179
Total, independent, R_{int}	0.0745
Final R_1, wR_2 [b,c]	0.1445, 0.0561

[a] Bruker Apex Duo diffractometer equipped with graphite monochromated Mo(Kα) radiation source and a cold stream of N_2 gas; temperature of date collection 100K.

[b] Structure was refined on F_0^2 using all data; the value of R_1 is given for comparison with older refinements based on F_0 with typical threshold of $F \geq 4\sigma(F)$.

[c] $wR_2 = [\Sigma[w(F_0^2-F_c^2)^2]/\Sigma\, w(F_0^2)^2]^{1/2}$ where $w^{-1} = \sigma^2(F_0^2) + (aP)^2 + (bP)$ and $P = [\max(F_0^2, 0) + 2F_c^2]/3$.

Table A2. Crystallographic data of L^2 complex $[HgZn(L^2)_2]^+$.[a]

Compound	$[HgZn(\mathbf{L^2})_2]^+$
Formula	$C_{66}H_{64}Hg_1N_{13}O_{20}S_4Zn_1$
M	1951.57
System, space group	Monoclinic *C*2/*c*
a / Å	21.571(3)
b / Å	16.707(2)
c / Å	22.669(3)
α / °	90
β / °	113.375(3)
γ / °	90
U / Å^3	7499(2)
Z	4
μ /mm^{-1}	1.729
Reflections collected:	35235
Total, independent, R_{int}	0.0475
Final R_1, wR_2 [b,c]	0.1197, 0.0448

[a] Bruker Apex Duo diffractometer equipped with graphite monochromated Mo(Kα) radiation source and a cold stream of N_2 gas; temperature of date collection 100K.

[b] Structure was refined on F_0^2 using all data; the value of R_1 is given for comparison with older refinements based on F_0 with typical threshold of $F \geq 4\sigma(F)$.

[c] $wR_2 = [\Sigma[w(F_0^2-F_c^2)^2]/\Sigma\, w(F_0^2)^2]^{1/2}$ where $w^{-1} = \sigma^2(F_0^2) + (aP)^2 + (bP)$ and $P = [\max(F_0^2, 0) + 2F_c^2]/3$.

Table A3. Crystallographic data of L^4 complex $[Cd_2(L^4)_2]^{4+}$.[a]

Compound	$[Cd_2(\mathbf{L^4})_2]^{4+}$
Formula	$C_{66}H_{44}Cd_2Cl_8N_{12}O_{16}S_4$
M	1897.77
System, space group	Monoclinic *C*2/*c*
a / Å	24.3339(8)
b / Å	12.1082(4)
c / Å	28.274(1)
α / °	90
β / °	112.789(1)
γ / °	90
U / Å^3	7680.3(5)
Z	4
μ /mm^{-1}	1.641
Reflections collected:	27701
Total, independent, R_{int}	0.0318
Final R_1, wR_2 [b,c]	0.1606, 0.0586

[a] Bruker Apex Duo diffractometer equipped with graphite monochromated Mo(Kα) radiation source and a cold stream of N_2 gas; temperature of date collection 100K.

[b] Structure was refined on F_0^2 using all data; the value of R_1 is given for comparison with older refinements based on F_0 with typical threshold of $F \geq 4\sigma(F)$.

[c] $wR_2 = [\Sigma[w(F_0^2-F_c^2)^2]/\Sigma\, w(F_0^2)^2]^{1/2}$ where $w^{-1} = \sigma^2(F_0^2) + (aP)^2 + (bP)$ and $P = [\max(F_0^2, 0) + 2F_c^2]/3$.

Table A4. Crystallographic data of L^4 complex $[Zn_5(L^4)_5]^{10+}$.[a]

Compound	$[Zn_5(\mathbf{L^4})_5]^{10+}$
Formula	$C_{184}H_{121}F_{30}N_{37}O_{30}S_{20}Zn_5$
M	4868.23
System, space group	Monoclinic *C*2/*c*
a / Å	22.517(2)
b / Å	24.756(2)
c / Å	36.000(3)
α / °	90
β / °	96.827(2)
γ / °	90
U / Å^3	19925(3)
Z	4
μ /mm^{-1}	1.623
Reflections collected:	72997
Total, independent, R_{int}	0.0416
Final R_1, wR_2 [b,c]	0.3120, 0.1183

[a] Bruker Apex Duo diffractometer equipped with graphite monochromated Mo(Kα) radiation source and a cold stream of N_2 gas; temperature of date collection 100K.

[b] Structure was refined on F_0^2 using all data; the value of R_1 is given for comparison with older refinements based on F_0 with typical threshold of $F \geq 4\sigma(F)$.

[c] $wR_2 = [\Sigma[w(F_0^2-F_c^2)^2]/\Sigma\, w(F_0^2)^2]^{1/2}$ where $w^{-1} = \sigma^2(F_0^2) + (aP)^2 + (bP)$ and $P = [\max(F_0^2, 0) + 2F_c^2]/3$.

Table A5. Crystallographic data of L^5 complex $[Cu_5(L^5)_5]^{10+}$.[a]

Compound	$[Cu_5(\mathbf{L^5})_5]^{10+}$
Formula	$C_{137.9}H_{88.4}Cl_{16}Cu_5N_{25.5}O_{41.5}S_{10}$
M	3972.46
System, space group	Triclinic P $\bar{1}$
a / Å	17.2058(8)
b / Å	20.4431(10)
c / Å	25.9847(12)
α / °	87.9110(10)
β / °	85.8010(10)
γ / °	81.7440(10)
U / Å^3	9017.7(7)
Z	2
μ /mm^{-1}	1.010
Reflections collected:	68110
Total, independent, R_{int}	0.0526
Final R_1, wR_2 [b,c]	0.2369, 0.0844,

[a] Bruker Apex Duo diffractometer equipped with graphite monochromated Mo(Kα) radiation source and a cold stream of N_2 gas; temperature of date collection 100K.

[b] Structure was refined on F_0^2 using all data; the value of R_1 is given for comparison with older refinements based on F_0 with typical threshold of $F \geq 4\sigma(F)$.

[c] $wR_2 = [\Sigma[w(F_0^2-F_c^2)^2]/\Sigma\, w(F_0^2)^2]^{1/2}$ where $w^{-1} = \sigma^2(F_0^2) + (aP)^2 + (bP)$ and $P = [\max(F_0^2, 0) + 2F_c^2]/3$.

Table A6. Crystallographic data of L^6 complex $[Cu_5(L^4)_3(L^6)_2]^{10+}$.[a]

Compound	$[Cu_5(\mathbf{L^4})(\mathbf{L^6})_2]^{10+}$.
Formula	$C_{150}H_{88}F_{30}N_{26}O_{30}S_{29}$
M	4263.36
System, space group	Triclinic P $\bar{1}$
a / Å	21.0573(13)
b / Å	21.0816(13)
c / Å	22.4884(14)
α / °	92.2160(10)
β / °	100.0820(10)
γ / °	109.2860(10)
U / Å^3	9227.2(10)
Z	2
μ /mm^{-1}	0.896
Reflections collected:	68246
Total, independent, R_{int}	0.0506
Final R_1, wR_2 [b,c]	0.2619, 0.0919

[a] Bruker Apex Duo diffractometer equipped with graphite monochromated Mo(Kα) radiation source and a cold stream of N_2 gas; temperature of date collection 100K.

[b] Structure was refined on F_0^2 using all data; the value of R_1 is given for comparison with older refinements based on F_0 with typical threshold of $F \geq 4\sigma(F)$.

[c] $wR_2 = [\Sigma[w(F_0^2-F_c^2)^2]/\Sigma\, w(F_0^2)^2]^{1/2}$ where $w^{-1} = \sigma^2(F_0^2) + (aP)^2 + (bP)$ and $P = [\max(F_0^2, 0) + 2F_c^2]/3$.

Table A7. Crystallographic data of L^7 complex $[Zn_4(L^7)_4]^{8+}$.[a]

Compound	$[Zn_4(\mathbf{L^7})_4]^{8+}$.
Formula	$C_{206}H_{147}F_{24}N_{33}O_{33}S_{16}Zn_4$
M	4423.56
System, space group	I222
a / Å	21.1329(10)
b / Å	22.0547(10)
c / Å	22.6598(10)
α / °	90
β / °	90
γ / °	90
U / Å^3	10561.3
Z	2
μ /mm^{-1}	0.706
Reflections collected:	77162
Total, independent, R_{int}	0.0609
Final R_1, wR_2 [b,c]	0.1704, 0.0912

[a] Bruker Apex Duo diffractometer equipped with graphite monochromated Mo(Kα) radiation source and a cold stream of N_2 gas; temperature of date collection 100K.

[b] Structure was refined on F_0^2 using all data; the value of R_1 is given for comparison with older refinements based on F_0 with typical threshold of $F \geq 4\sigma(F)$.

[c] $wR_2 = [\Sigma[w(F_0^2-F_c^2)^2]/\Sigma\, w(F_0^2)^2]^{1/2}$ where $w^{-1} = \sigma^2(F_0^2) + (aP)^2 + (bP)$ and $P = [\max(F_0^2, 0) + 2F_c^2]/3$.

Appendix 2: Publications